


Fall 2014

Nano-engineered polymers in drug delivery: Potential approaches for attenuation of secondary injury after spinal cord trauma

Wen Gao
Purdue University

Follow this and additional works at: https://docs.lib.purdue.edu/open_access_dissertations

 Part of the [Biology Commons](#), [Nanoscience and Nanotechnology Commons](#), and the [Neuroscience and Neurobiology Commons](#)

Recommended Citation

Gao, Wen, "Nano-engineered polymers in drug delivery: Potential approaches for attenuation of secondary injury after spinal cord trauma" (2014). *Open Access Dissertations*. 457.
https://docs.lib.purdue.edu/open_access_dissertations/457

This document has been made available through Purdue e-Pubs, a service of the Purdue University Libraries. Please contact epubs@purdue.edu for additional information.

PURDUE UNIVERSITY
GRADUATE SCHOOL
Thesis/Dissertation Acceptance

This is to certify that the thesis/dissertation prepared

By Wen Gao

Entitled

NANO-ENGINEERED POLYMERS IN DRUG DELIVERY: POTENTIAL APPROACHES FOR
ATTENUATION OF SECONDARY INJURY AFTER SPINAL CORD TRAUMA

For the degree of Doctor of Philosophy

Is approved by the final examining committee:

Richard B. Borgens

Jianming Li

Stephen R. Byrn

Linjie Pan

Youngnam Cho

To the best of my knowledge and as understood by the student in the Thesis/Dissertation Agreement, Publication Delay, and Certification/Disclaimer (Graduate School Form 32), this thesis/dissertation adheres to the provisions of Purdue University's "Policy on Integrity in Research" and the use of copyrighted material.

Richard B. Borgens

Approved by Major Professor(s): _____

Approved by: Laurie A. Jaeger

12/08/2014

Head of the Department Graduate Program

Date

NANO-ENGINEERED POLYMERS IN DRUG DELIVERY:
POTENTIAL APPROACHES FOR ATTENUATION OF SECONDARY INJURY
AFTER SPINAL CORD TRAUMA

A Dissertation

Submitted to the Faculty

of

Purdue University

by

Wen Gao

In Partial Fulfillment of the

Requirements for the Degree

of

Doctor of Philosophy

December 2014

Purdue University

West Lafayette, Indiana

To my lovely parents and husband,

With all the love and support there could possibly be.

ACKNOWLEDGMENTS

I gratefully appreciate the greatest opportunity that Dr. Richard Borgens offered to me. His encouragement and support allow me to become an independent thinker and researcher. Also, I would like to thank Dr. Jianming Li for the guidance and great help during my graduate study and Dr. Youngnam Cho for the inspiration of my earlier experiment design. I also want to thank John Cirillo for all the technical assistance on generator design, Michel Schweinsberg for the amazing figures, and especially Judy Grimmer and Jennifer Danaher for their continuous help. At last, I want to give my appreciation to Purdue University Birck Nanotechnology Center and many their engineering staff and staff scientists as well as Chia-Ping Huang from Life Science Microscopy Facility.

TABLE OF CONTENTS

	Page
LIST OF TABLES	ix
LIST OF FIGURES	x
ABSTRACT	xii
CHAPTER 1. SPINAL CORD INJURY AND ITS POTENTIAL TREATMENTS AT A GLANCE.....	1
1.1 Spinal Cord Injury and Animal Models in Experimental Study	1
1.2 Secondary Injury in Spinal Cord Trauma	3
1.3 Possible Treatments for Secondary Injury	6
1.4 Biomaterials in Spinal Cord Injury Studies.....	11
1.5 Goal of Current Study	13
CHAPTER 2. POLYPYRROLE DRUG RELEASE VIA NON-INVASIVE ELECTROMAGNETIC STIMULATION	14
2.1 Introduction	14
2.1.1 Overview of Conductive Polymers in Neuroscience Study	14
2.1.2 Electrochemistry for Polypyrrole	16
2.1.2.1 Electropolymerization of Polypyrrole	16
2.1.2.2 Doping and Releasing Processes of Polypyrrole	18
2.1.2.3 The Effects of Different Parameters During Eletropolymerization.....	20
2.1.3 Conductive Polymer Based Drug Delivery System.....	22
2.1.4 Synthesis Techniques for 3D Nanostructure	24
2.2 Method and Materials.....	25
2.2.1 Template Preparation for Polypyrrole Polymerization.....	25
2.2.2 Fabrication of Dexamethasone Doped Polypyrrole Carriers.....	25

	Page
2.2.3 Morphology of Polypyrrole Nanowires Imaged by Scanning and Transmission Electron Microscopy	27
2.2.4 Electromagnetic Stimulation	28
2.2.5 Drug Release.....	30
2.2.6 On-Demand Dexamethasone Release.....	31
2.2.7 Temperature Effect on Drug Release	31
2.2.8 XPS Analysis	31
2.2.9 Statistical Analysis.....	32
2.3 Results	32
2.3.1 Structure of Polypyrrole Nanowires	32
2.3.2 Comparisons of Drug release.....	34
2.3.3 The Influence of Temperature Elevation on Drug Release	37
2.3.4 XPS Confirmation of Dexamethasone Release	38
2.4 Discussion	40
CHAPTER 3. DESIGN AND SELECTION OF ELECTROMAGNETIC FIELD GENERATOR	44
3.1 Introduction	44
3.1.1 Time-Varying Electromagnetic Fields	44
3.1.2 Electrochemical Techniques Used for Polypyrrole Based Drug Release.....	46
3.1.3 Electromagnetic Field in Biological and Medical Studies	51
3.2 Methods and Materials	53
3.2.1 Configuration of the Electromagnetic Field Stimulator	53
3.2.2 Electromagnetic Field Measurements.....	54
3.2.3 Antenna Gain Equations	55
3.3 Results	57
3.3.1 Electromagnetic Field Characteristics	57
3.3.2 Drug Release by Square Waveform Stimulation	59
3.3.3 Drug Release Using Sawtooth Waveform.....	60
3.4 Discussion	62

	Page
CHAPTER 4. ATTENUATION OF SECONDARY INJURY BY ELECTROMAGNETIC RESPONSIVE POLYPYRROLE DRUG DELIVERY	64
4.1 Introduction	64
4.1.1 Cellular, Molecular, and Biochemical Cascades in Spinal Cord Injury	64
4.1.1.1 ROS and RNS	64
4.1.1.2 ROS and RNS Associated Mitogen-activated Protein Kinases Signaling Pathways.....	66
4.1.2 Evidence of Neuronal Recovery by Inhibition of iNOS and ROS	68
4.1.3 Glial Cells in Spinal Cord Injury	71
4.1.4 In Vivo Applications.....	73
4.2 Materials and Methods	75
4.2.1 ROS Production in Challenged and Treated Microglial Cells.....	75
4.2.2 Immunofluorescence Labeling Assay.....	77
4.2.3 Surgical and Treatment Procedures	77
4.2.4 Whole Animal Bioluminescent Imaging	79
4.2.5 Statistical Analysis.....	79
4.3 Results	80
4.3.1 ROS Detection	80
4.3.2 iNOS Suppression by Dexamethasone Release.....	82
4.3.3 Selection of Animal Injury Model	85
4.3.4 Neuroinflammation Attenuation by Drug Loaded Polypyrrole Implant	87
4.4 Discussion	92
CHAPTER 5. SYNTHESIS AND CHARACTERISTICS OF SIRNAS CONJUGATED CHITOSAN NANOPARTICLES	99
5.1 Introduction	99
5.1.1 Evolution of Post-transcriptional Gene Silencing	99
5.1.2 Pros and Cons of SiRNAs Therapeutic Strategies.....	101
5.1.3 SiRNAs Inhibition in Spinal Cord Trauma	103
5.1.4 SiRNAs Delivery Strategies	104

	Page
5.1.5 Types and Modification of Chitosan for SiRNAs Delivery	107
5.2 Material and Methods.....	109
5.2.1 Synthesis of SiRNAs Conjugated Chitosan Nanoparticles	109
5.2.2 Transmission Electron Microscopy	111
5.2.3 Size and Surface Charge of Nanoparticles	111
5.2.4 Gel Retardation Assay	111
5.2.5 Toxicity Studies	112
5.3 Results	112
5.3.1 Chitosan Nanoparticles Morphology.....	112
5.3.2 Particle Size and Surface Charge.....	115
5.3.3 Binding Affinity Between SiRNAs and Chitosan Nanoparticles	117
5.3.4 Low Cytotoxicity of Chitosan Nanoparticles	118
5.4 Discussion	121
CHAPTER 6. PREVENTING CELL DEATH AFTER SPINAL CORD INJURY VIA TARGETED SIRNAS DELIVERY	127
6.1 Introduction	127
6.1.1 Macrophages Polarization and Their Role in Spinal Cord Injury	127
6.1.2 Route of Administration for SiRNAs Delivery	129
6.1.3 Nanoparticles Targeting Strategies to Macrophages via Fc Receptor.....	130
6.1.4 Targeting Macrophages in Spinal Cord.....	135
6.2 Materials and Methods	136
6.2.1 Cell Culture.....	136
6.2.2 Light Microscopic Studies on M1 and M2 Macrophages Morphology	137
6.2.3 In Vitro Experiment.....	137
6.2.4 Transfection Efficiency	138
6.2.5 Western Blot Analysis of Gene Silencing	138
6.2.6 NO Assay.....	139
6.2.7 In Vivo Experiment	140
6.2.8 Western Blot Analysis for Spinal Cord Extracts	140

	Page
6.2.10 Statistical Analysis.....	141
6.3 Results.....	142
6.3.1 Divergent Morphologies of M1 and M2 Macrophages.....	142
6.3.2 Efficient Transfection of SiRNA Conjugated Chitosan Nanoparticles.....	143
6.3.3 Protein Knockdown.....	146
6.3.4 NO Recudtion.....	150
6.3.5 Inhibition of Apoptosis Pathway After Spinal Cord Injury.....	152
6.4 Discussion.....	154
CHAPTER 7. FUTURE STUDIES.....	163
BIBLIOGRAPHY.....	167
VITA.....	193

LIST OF TABLES

Table	Page
1.1 Spinal cord stimulators development in clinical trails.....	10
3.1 Polypyrrole based drug release	47
4.1 iNOS inhibitors and their neuroprotective results	70
4.2 Glial responses after SCI	72
5.1 Size distribution and surface charge of different siRNAs conjugated chitosan nanoparticles	116
6.1 Summary of human and mouse Fc Receptors.....	134

LIST OF FIGURES

Figure	Page
2.1 Polymerization of Ppy.....	17
2.2 Neutral, Polaron, and Bipolaron state of Ppy	17
2.3 Redox reaction and overoxidation of Ppy.....	20
2.4 PpyNWs fabrication processes	27
2.5 Stimulation scheme for the application of EMFs	29
2.6 Scanning electron micrograph of PpyNWs.....	33
2.7 Transmission electron micrograph of PpyNWs with inclusion of AuNps	34
2.8 DEX release using various Ppy platforms and stimulation methods.....	35
2.9 DEX release profiles of flat Ppy as a function of temperature and its comparison to that of with and without EMF stimulation.....	37
2.10 XPS spectra for surface analysis of DEX presence on Ppy templates before and after EMF stimulation.....	39
2.11 High magnification of TEM image depicts the successful fabrication of PpyNWs through entire film	41
3.1 Ampere's Law and Faraday's Law	45
3.2 Illustration of Cyclic Voltammetry and Potential Step techniques.....	50
3.3 Schematic figure for three-way square waveform generator	56
3.4 Schematic figure for sawtooth generator	57
3.5 The input signal generated by asymmetric square waveform.....	58
3.6 Illustration of input signals in the case of pulse train (left) and symmetric waveform (right).....	59
3.7 Comparison of DEX release from flat Ppy – AuNps film using pulse train, asymmetric, and symmetric waveforms	60

Figure	Page
3.8 Illustrations of the input signal of magnetic field (right) and electrical field (left) for sawtooth waveform	61
3.9 DEX release comparison between EMF stimulator with sawtooth waveform (blue) and with pulsed square waveform configuration (green)	61
4.1 Composite fluorescence signals and quantitative measurement of ROS.....	81
4.2 Confocal images of the iNOS expression after LPS induction and DEX treatment in BV-2 cells	84
4.3 Illustration of spinal cord injury procedures and EMF stimulation set-up	86
4.4 Luciferin and luciferase reaction based bioluminescence imaging	88
4.5 Bioluminescent images of mice in control, Ppy control, and Ppy treatment groups	90
4.6 Quantitative data of GFAP expression based on bioluminescent results	91
5.1 Transmission electron microscopy images of different siRNAs conjugated chitosan Nanoparticles	114
5.2 Gel retardation assay indicating the integrity of Chitosan Nanoparticles.....	118
5.3 Morphology images of macrophages after treatment of siRNAs and different siRNA conjugated chitosan Nanoparticles	120
6.1 Macrophage morphology of inactivated macrophages (control), activated M2 macrophages, and activated M1 macrophages.....	143
6.2 Illustration of transfection efficiency of siRNAs and siRNA conjugated Ab-chitosan Nanoparticles	145
6.3 Screening of siRNAs for silencing of iNOS mRNA expression	147
6.4 Knockdown of iNOS protein activity	149
6.5 NO production of macrophages.....	151
6.6 NO production using scrambled siRNAs.....	151
6.7 Different proteins expression level after SCI with and without treatment of different chitosan Nanoparticles carried siRNAs	153
7.1 SEM image of single cell on Ppy nanotube structure	164
7.2 SEM images of cell adhesion on flat Ppy and PpyNWs.....	165

ABSTRACT

Gao, Wen. Ph.D., Purdue University, December 2014. Nano-engineered Polymers in Drug Delivery: Potential Approaches for Attenuation of Secondary Injury After Spinal Cord Trauma. Major Professor: Dr. Richard B. Borgens.

Secondary injury elicits a complex series of pathophysiological events after the primary spinal cord trauma and even after its implantation treatment for neural functional recovery. These secondary injuries include an up-regulation of glial cells associated reactive oxygen species, nitrogen species, and reactive astrogliosis, and they can result in various levels of cellular and tissue damage. The inhibition of them has been proved to lead to functional recovery of the spinal cord. In this study, we concentrated on developing polymers and nano-techniques based drug delivery strategies to eliminate these secondary injuries.

To maintain and improve the performance of the implants during treatment, we exploited the polypyrrole as a suitable material to carry and locally release the drug at the injured spinal cord based on its conductive characteristics. We focused on the geometric modulation of implants materials on a nano-size scale and developed a polypyrrole nanowire platform that can served as a high capacity drug reservoir and can release drugs in a relatively longer time. Most importantly, we introduced the electromagnetic responsive feature of polypyrrole for drug delivery. This valuable technique can help us

to achieve a non-invasive and remotely controlled drug release in deep tissues and avoid the physical contacts commonly required during traditional electrical stimulation. We used dexamethasone as a drug cargo, since this drug is commonly used for anti-inflammation treatment and has been successfully delivered from polypyrrole using conventional electrical stimulation methods in earlier studies. According to the results, we showed successful and long lasting polypyrrole mediated drug release under electromagnetic stimulation and the released drugs remained bioactivity and can be used for the treatment of secondary injury.

We also introduced a gene silencing strategies by delivering siRNA conjugated chitosan nanoparticles to the spinal cord lesion. These siRNAs can specifically knockdown inducible nitric oxide synthase and subsequently eliminate nitric oxide induced secondary injury. This drug delivery system were designed to discriminate different macrophages which have divergent effects to spinal cord recovery and to target the specific pro-inflammatory macrophages (M1 macrophages) instead of anti-inflammatory macrophages (M2 macrophages). The targeting effect allowed us more efficiently destruct the negatively impacted mRNA in targeted cells to improve therapeutic effects after spinal cord injury.

CHAPTER ONE

SPINAL CORD INJURY AND ITS POTENTIAL TREATMENTS AT A GLANCE

1.1 Spinal Cord Injury and Animal Models in Experimental Study

Spinal cord injury (SCI) results in a temporary/permanent motor and sensory impairment, also can be destructive to other organs, such as bone fracture, abnormal bladder and bowel movement, and cardiorespiration and cardiovascular risk. It is not only physically but also spiritually affecting the livelihood of injured patients. Main causes of spinal cord injury usually lies in the motor vehicle accident, falls, violence, recreational sports, and some are diseases related. There are approximately 2.5 million patients who are suffering from the chronic paralysis. Apart from this, estimated 130,000 newly injured individuals occurred each year worldwide and approximately 12,000 from United State. Spinal cord injuries symptoms can vary depend on the type and the level of the injury. SCI usually can categorize into 1) complete and incomplete type of the injury based on functional behavior and 2) tetraplegia and paraplegia based on if the level of the injury is above or below the first thoracic spinal nerve. A complete injury refers to the complete sensation and movement loss at the lowest sacral segments of both sides of the body. The individuals with incomplete injury is characterized by some functions below the level of the injury including the lowest sacral segments. In this case, individuals might have one side of body function in a better condition than other.

The database in regarding to the injury conditions after hospital discharges since 2010 shown that there are 40.6% of incomplete tetraplegia, 18.7% of incomplete paraplegia, 18.0% of complete paraplegia, and 11.6% of complete tetraplegia, and only less than 1% of patients shown a complete neurological recovery. [1] In the laboratory researches, many animal SCI models were developed based on the experimental needs to mimic the condition of the human injury. SCI models can be categorized to contusion, laceration, compression, and chemical mediated injury. Contusion model usually conducted by the various impactor devices, such as Multicenter Animal Spinal Cord Injury Study (MASCIS) contusion model, Infinite Horizon (IH) contusion model, and the Ohio State University (OSU) Electromagnetic Spinal Cord Injury Device (ESCID) contusion model. The MASCIS impactor is a device using a rod to drop onto certain level of the spinal cord and tracks the trajectory of the falling rod. Therefore, the same velocity, compression distance, and falling rate can be duplicated in each of the experiment in order to achieve same desired injury. Other impactors also can results in reproducible injury outcomes. IH contusion model is also a force based device which can displace the exposed spinal cord to induce the injury. The impactor produced from OSU is based on a slightly different technique. The main components of this device are sensitive electromagnetic shaker and interactive software which can control the force, slope, duration, and amplitude of peak displacement applied to the cord. Laceration injury is also frequently used in many SCI researches although it is rarely observed in the clinical case of human SCI. It includes partial spinal cord laceration injuries, such as focal myelotomy, dorsal or lateral hemisection, and complete laceration injuries, such as complete transaction, resection, and aspiration lesions. The ascending and descending

axonal pathways can be successfully disconnected using these methods. The most common human SCI is combination of acute impact followed by the persistent or transient compression to spinal cord. Many compression models using aneurysm clip or calibrated forceps are also developed showing a reliable, reproducible injury model especially with economical benefits. [2] These injury methods can successfully initiate certain level of locomotors and sensory loss such that we can investigate 1) the therapeutic efficiency of pharmaceutical agents and 2) intraspinal circuit improvement after grafting neural tissues or implanting biomaterial based guidance channels. The chemical-mediated injuries models can be induced by N-methyl-D-aspartate receptor (NMDA) agonists to study its associated secondary injury cascade, but may not fully express all the condition that may be encountered in the case of human SCI.

Therefore, our proposing therapeutic approaches developed for SCI can based on the condition of compression technique initiated incomplete injuries to recreate the similar injury conditions in human SCI.

1.2 Secondary Injury in Spinal Cord Trauma

The primary injury is usually considered as the initial mechanical damage. It can implicit a complicated cascade of the pathophysiological events in a spatial and temporal manner mainly due to vascular and biochemical effects, and this is considered as the secondary injury. These changes results in a propagating detrimental cycles and jeopardize the potential neuronal recovery after primary injury.

The secondary injury is mainly characterized by apoptotic and necrotic cell death associated events. SCI triggers the resting and infiltration of immune cells to release free radicals. It eventually leads to lipid peroxidation, oxidative stress, and excessive production of nitrous oxide causing cell death. These immune cells also can produce different cytokines and protease, such as tumor necrosis factor- α (TNF- α), interleukin (IL)-1 β , IL-6, caspase, and calpain at the injured sites. These can also initiate and regulate the cell death through different signaling pathways. [3,4] The inflammation combining with deleterious effects of ischemia and hemorrhage by SCI can lead to a progressive scar formation and central cavitations (enlarged scar-encapsulated cavity). Also, excessive intracellular level of Ca^{2+} immediately occurred after the induction of SCI could leads to mitochondrial damage. [5] It also further degrade local axoplasm and results in the membrane breakdown. Not only the direct mechanical invasion but also the production of free radical, inflammatory cytokines, and protease can cause destroy or deteriate the integrity of the plasma membrane. It subsequently results in increased membrane permeability and ionic and molecules homeostasis. Moreover, oligodendrocytes/myelin assoicated neurite growth-inhibitory factor, such as Nogo-A, Rho-A, myelin-associated glycoprotein (MAG), and oligodendrocyte myelin glycoprotein (OMgp), and astrocytes / oligodendrocytes precursor produced various inhibitory proteoglycans, such as chondroitin sulfate proteoglycans (CSPG), brevican, ND-2, and DSD-1, are all showed also deleteriously effects to the axonal regeneration and neuronal recovery after trauma. Glutamatergic excitotoxicity excreted after injury can directly or indirectly via reactive oxygen species (ROS) or nitrogen species (RNS) damage the cord tissue, especially to vulnerable neuron and oligodendrocytes which containing many glutamate receptors.

Therefore, this excitotoxicity is most responsible for the demyelination of the axons. In addition, decreased sympathetic tone and parasympathetic myocardial effects after acute injury can cause various systematic changes. Vasoconstriction of spasm in blood vessel and irregularity of blood flow can potentially result in an ischemic environment. Systematic effects of hypotension and hypothermia induced neurogenic shock, conduction block, and spinal shock were also the primary features during the secondary phases [6].

Immune system mediated secondary injury draws most of our attention due to the controversial role of immune cells and their regulatory proteins in SCI and their potential developments. These include major types of immune cells which are microglia, monocytes, and neutrophils. Resident microglia and some innate immune cells exist in a healthy environment of the central nervous system (CNS). After injury, neutrophils first respond to the intrusion and immigrate to the site of injury, then, perivascular monocytes infiltrate into the damaged region and differentiate into macrophages. Activated resident microglia and infiltrating macrophages, as well as neutrophils secrete various proinflammatory cytokines and neurotoxins and can lead to the exacerbation of the spinal cord. These secondary injuries begin within hours and last for several weeks to months after the initial physical injury, it allowed us to have time windows to apply the potential treatment to enhance neuroprotection and restore the neuronal function after SCI.

1.3 Possible Treatments for Secondary Injury

Overall, the possible treatment approaches for secondary injury can be accomplished by inhibiting the inflammatory responses and neural death, regulating the inhibitory factors on demyelination and scar formation, applying neuroregeneration factors to support neuron growth and spinal tracts, as well as cell or tissue based transplantation. Many pharmaceutical agents for SCI treatment had undergone the clinical practice since 1980's. Inhibition of inflammation responses and oxidative stress was extensively developed. NASCIS II and Japan MPSS trial based on the earlier treatment (within 8 hours post-SCI) of glucocorticosteroid Methylprednisolone Sodium Succinate (MPSS) unveiled the improved neurological and sensor recovery. Other pharmacological compounds with antioxidant properties and neuroprotective functions were also developed including lazaroic acid, cyclosporine A, and EPC-K1. [7]

Maryland GM-1 (Monosialotetrahexosylganglioside, a major component of the cell membrane) trial also achieved the similar outcomes and indicated an improved neurological recovery after injury, but Sygen GM-1 trial which is combination of MPSS and GM-1 treatment did not show the beneficial outcomes. These strategies are focused on controlling cell membrane disruption induced cell death in secondary injury. Other approaches were also revealed similar therapeutic potentials toward delayed cell death for SCI treatment, for example, inhibiting proteases caspases via enforcing the anti-apoptotic protein Bcl-2 expression and reducing proteases calpains by suppressing the cytoskeletal degradation of damaged cells. [8]

Glutamate receptor antagonists (NMDA blocker MK-801 and AMPA/KA receptor antagonist NBQX) have also been shown to have neuroprotective function after SCI. [9,10,11] However, the trial based on the treatment of NMDA antagonists Gacyclidine (GK-11) for suppressing glutamate excitotoxicity did not show any clinical improvement. Since the overactivation of these receptors were responsible for abnormal action potentials and, they can further result in a large amount of transmitter substances and accompanied with electrolytic shifts, and eventually lead to the cell death or spinal shock after SCI. These changes usually indicated by an increased intracellular Na^+ and Ca^+ and extracellular K^+ . Balancing the action potentials by inhibiting the voltage-dependent channels could also be the potential approaches to limit the neural dysfunction and its damages. Sodium channel blocker Tetrodotoxin have shown a functional recovery after SCI, but riluzole did not have a significant clinical improvement. Calcium blocker Nimodipine can reduce SCI initiated ischemia. [12] 4-aminopyridine (4-AP), as potassium channel blocker, aims to restore the conduction properties of demyelinated axons. It has been shown promising outcomes for motor and sensory improvement as well as voluntary bowel controls. [13,14]

Many investigations also focused on enhancing the axonal regeneration and neurite promoting by either applying exogenous neurotrophic factors or limiting the inhibitory factors and unpermissive extracellular matrix that responsible for inhibition of neurite outgrowth. Nerve growth factors (NGF), [15] neurotrophin -3, [16] and 4/5 (NT-3, NT-4/5), brain-derived neurotrophic factor (BDNF), [17] glial cell line-derived neurotrophic factor (GDNF), ciliary neurotrophic factor (CNTF), and basic fibroblast growth factor (BFGF) were the most common neurotrophic factors used for sprouting and regeneration

in different cell type and locations. Many growth inhibitory signals occurred in SCI has been proved to associated with the Rho signaling pathway and Rho associated protein kinase (ROCK). The activation of Rho signaling pathway can disrupt or collapse the cytoskeleton structure of the nerve fiber growth cone. ROCK-inhibitor Y-27632, fasudil (HA-1077) , the protein p21CIP1/WAF1, or genetic deletion of the ROCK isoform were various approaches developed to eliminate the ROCK production and to promote corticospinal tract regeneration and locomotors improvement. A growing strength on targeting protein kinases are developed as treatment in many preclinical studies. Apart from Y-27632, SB203580 and TDZD-8, as potential therapeutics to inhibit p38 α -MAPK and glycogen synthase kinase 3 (GSK-3), were also investigated in clinical study for SCI. [18] Moreover, directly targeting Rho pathways using Rho specific siRNAs, C3 transferase treatment, and Rho pathway antagonists Cethrin also addressed the similar results. Many myelin/ oligodendrocyte -derived growth-inhibitory proteins (Nogo-66, amino-Nogo, MAG, and OMgp) were also received the attention during the SCI treatment since they can activate Rho signalling to inhibit the neurite growth. The blockage of other Rho activator, for example CSPG, versican, and NG2 via chondroitinase ABC, ibuprofen, and indomethacin treatment can also promote neural regeneration. Suppression of the inhibitory protein activity of NoGo by using IN-1 antibody or siRNAs strategies has been shown to support the outgrowth of axonal tracts. [19] However, genetic deletion of myelin-associated glycoprotein (MAG) did not shown the significant regeneration of retinal ganglion cell fibers and corticospinal tract.

Some naturally occurring molecules, such as cyclic adenosine 3'5'-monophosphate (cAMP), [20] inosine, [21] purine nucleoside, [22] and hypoxanthine derivative leteprinim (AIT-082) were also shown their neuroprotective capability.

In many pre-clinical cases, the strategies using various stem cells, such as neural stem cells, schwann cells, embryonic stem cells, olfactory ensheathing cells, and bone-marrow mesenchymal stem cells were developed in SCI study as well. These cells were either implanted or transplanted to the spinal cord for tissue sparing, axonal regeneration, remyelination, and functional recovery and showed improvements at various levels. However, only few investigate the inflammation responses after SCI and treatment.

Computer-controlled functional electrical stimulation (FES) for SCI also extensively developed for strengthening the motor and sensory function of upper and lower extremities and limiting associated dysfunction and issues following with SCI. In addition, these stimulators combined with other physical therapy approaches has also been shown the potentials on improvement of bone health, bladder and bowel movement, reducing neuropathic pain, cardiorespiration and cardiovascular dysfunction which are intimately related with post-SCI. Several stimulators and their applications are summarized in the Table 1.1.

Table 1.1 Spinal cord stimulators development in clinical trails.

Device	Sponsor	Indication	Status
Compex Motion or HEWHS stimulator	Toronto Rehabilitation Institute	Focus on study of upper limb intervention for tetraplegic patient to generate the palmer functions and the lateral grasp.	Phase III
FES cycling (RT300-SL) /FES Stepping (RT-600)	Hugo W. Moser Research Institute at Kennedy Krieger, Inc.	Low level electrical currents is applied to the leg and buttock muscles to initiate muscles contract and produce the motion of the legs. Also, to improve CNS growth factors release and reduce the inflammatory at spinal cord. /To increase motor, pin prick, and light touch score.	Phase II/III; /Phase I/II;
FIRSTHAND System	Department of Veterans Affairs (VA)	Somatosensory stimulation to generate functional movements, such as enhancing pinch strength and upper extremity acitivity.	Phase I/ II
IST-16 (16 channel implanted stimulator-telemeter)	Case Western Reserve University; NIH; VA	Surgical implant multiple contact peripheral nerve electrodes to to excite muscles in order to move paralyzed muscles, facilitate standing duration, stepping, and balance.	
Transcranial Direct Current Stimulator	Beth Israel Deaconess Medical Center	Relieve migraine pain.	Phase II
Ness H200	University of Pittsburgh	To aid movement and stimulate the nerves that supply paralyzed muscles, to improve the arm function.	
Home-based ankle continuous passive motion machine	Chang Gung University	To study the effect of fast continuous passive motion on the reversing adaptation of human paralyzed muscle after SCI.	
Neural Prosthetic System 2 (NPS2)	Richard A. Andersen, PhD	Brain- controlled medical device, any movement plans can be sent to specific region of brain and execute the actual movements.	

1.4 Biomaterials in Spinal Cord Injury Studies

Many biocompatible natural and synthetic materials based platforms were developed not only as a nerve guidance channels or structure supports, but also can be used for drug delivery tools for SCI repair. Due to the complexity of spinal cord bioenvironment, the spinal-blood barriers cause the challenge for nanoparticle (Np) based systematic delivery. Therefore, more therapeutic investments are focused on using implantable platforms for long lasting medication therapy in SCI studies. [23] The platforms mainly include hydrogels, electrospun fiber mesh, and porous scaffolds and can be made of either degradable or non-degradable materials. The most common degradable natural materials used in spinal cord are collagen, hyaluronic acid, chitosan, agarose, fibrin, fibroin, and poly (β -hydroxybutyrate), and degradable synthetic materials are poly (lactide) and glycolide (poly (glycolide-co-lactide)) (PLA-PGLA), poly (ϵ - caprolactone) (PCL). They are characterized by less cytotoxic effects and well supporting to the cell adhesion and connection. They also featured of a lower risk of nerve compression if their degradation rate is at similar pace of the regeneration of the nerves. However, unpredicted inflammation initiated by the debris of these materials could jeopardize the therapeutic effects. When the integrity of the matrices is highly demanded, non-degradable synthetic materials, such as poly (2-hydroxyethyl methacrylate) (PHEMA), poly (3,4-ethylenedioxythiophene) (PEDOT), and poly[N-(2-hydroxypropyl methacrylamide)](PHPMA) are more appropriated to use when safety of these materials were established. The special properties of synthetic material are that they can be simply modified and utilized varying to the application requirements. One special electrical sensitive polymers were also received many attentions. Polymer poly(tetrafluoroethylene)

(PTFE), polyvinylidene fluoride (PVDF), PEDOT, and polypyrrole (Ppy) are commonly investigated because they are compatible to neural tissues and can enhance the neural growth and drug release when expose to electrical stimulation. [24] See more details in chapter 2.1.1.

The nanoparticles mediated systemical drug delivery were also developed althrough under the challenge of spinal-blood barriers. Delivery strategies by enhancing drug targeting showed promising outcomes to solve this issue. Ferulic acid and glycol chitosan synthesized Nps can be delivered to lesioned spinal cord through systemical administration and result in neuroprotection. [25] The direct injection of nanoparticle suspension into the injury site of spinal cord can also be used to bypass the spinal-blood barriers and efficiently deliver the drugs. Directly inject glial cell line-derived neurotrophic factor loaded PLGA Nps to the damadged spinal cord can promote neural survival and functional recovery.[26] In addition, some material itself in a nanoscales, such as self-assembled monomethoxy poly(ethylene glycol) -poly(D,L-lactic acid) diblock copolymer and poly(ethylene glycol), also showed beneficial results to reduce lesion and inflammation, or repair damadged nerve membrane. [27,28] During this nanoparticle administration, the size, shape, and surface charge of the nanoparticles can significant influence its drug delivery outcomes.

1.5 Goal of Current Study

Broad and brief review of existing issues and solutions of SCI described above allow us to have a general understanding during SCI, especially for secondary injury studies. Our goal and primary contribution in this work is to focus on exploiting the potential approaches based on polymer materials drug delivery strategies to eliminate the noxious molecules initiated by various glial cells after SCI. We included microglial cells and macrophages in vitro study, and reactive astrocytes in vivo study. First, we modulated the Ppy platform based on structure and synthesis to optimize the local drug delivery by maximizing the drug loading capacities of Ppy. Especially, we are firstly introduce the non-invasive electromagnetic generator to initiate the chemical and mechanical alternation of conductive polymer Ppy for remotely controlled drug release (details described in Chapter 2, 3, and 4). Second, we developed a chitosan Nps associated siRNA gene silencing strategies with specific targeting effects to pro-inflammation macrophages (M1). This targeting strategy is the first time to discriminate different macrophages subsets during drug delivery for neuroinflammation inhibition efficiency after SCI (details described in Chapter 5 and 6).

CHAPTER TWO
POLYPYRROLE DRUG RELEASE
VIA NON-INVASIVE ELECTROMAGNETIC STIMULATION

2.1 Introduction

2.1.1 Overview of Conductive Polymers in Neuroscience Study

Conducting polymers characterized by high electronic conductivity, electrochromism, charge storage capacity, and electrochemically controllable ion exchange capacities have been exploited in various engineering applications such as high-power supercapacitors, [29] batteries, [30] fuel cell, [31] anti-corrosion coatings, antistatic coatings, [32] shielding interferences, [33] sensors, actuators, and synthetic receptor. [34] In neuroscience study, many conductive polymers, for example, polyaniline, polythiophene, especially PEDOT and Ppy are primarily used for nerve guidance conduits due to their biocompatibility and high conductivity properties. Ppy, as the archetype of electronically conducting organic polymers, have especially been exploited due to: 1) the fabrication of Ppy is simple and can be accomplished in both aqueous and non-aqueous conditions; 2) Redox activity of Ppy can be potentially used for various application, especially for drug delivery of our interests; 3) Ppy in the oxidized state is inherently stable for long storage times as long as the material is keep away from oxygen and humidity; 4) Most

importantly, different nature of Ppy dopant or counterions can influence Ppy characteristics and further expanded or improved its applications.

Conductive Ppy has especially been used as a substrate to support the interaction and connection of nerve cells in many studies. [35] Polycaprolactone (PCL) fumarate synthesized with Ppy enhanced cell attachment, proliferation, and neurite extension. [36] This result also supported by Paul Geoge et al where neurons and glial cells become enveloped and grew through the implants of polystyrene sulfonate (PSS) or sodium dodecylbenzenesulfonate (NaDBS) doped Ppy. [37] Neurites outgrowths from PC-12 cells have also been observed when NGF electrically released from its originally conjugated Ppy scaffold. [38] Electrical stimulation to Ppy films in PC-12 cells, Dorsal Root Ganglia, and Schwann cells culture results in a significant increased neurite lengths compared to the ones without stimulation.[39,40] In vivo studies, Ppy implants showed its connection to the spinal cord tissue without increased inflammation responses; [41] and also suggest motor recovery and improved somatosensory evoked potential conduction after implantation of Iodine doped Ppy into transected rats spinal cord. [42]

In neurology, many medical devices have been developed to record electrophysiological activity in neural circuit and/or to support nerve conductance by neurostimulation. Developing biocompatible electrodes are very important because these electrode component in many of these devices can result in invasion to the tissues during recording and stimulation. Conducting polymer coating as neural tissue-electrode interface has been a promising tool to offer effective long-term performance of electrode implants. They are

featured of relatively high charge storage densities but low impedance, therefore, can optimize the electrode-tissue communication.

2.1.2 Electrochemistry for Polypyrrole

2.1.2.1 Electropolymerization of Polypyrrole

The proposed mechanism of Ppy polymerization starts with a slow neutral monomer oxidation to form a pyrrole cation radical. The reaction then followed by the coupling of radical cations that generate different resonance forms, fast deprotonation, and aromatization process to form a dimer. The chain growth then propagates by preferential coupling with monomers and/or dimers and continues until the charge on the polymer's backbone is incorporated with counterions. These counterions can maintain electroneutrality of the polymers when positive charges accrue along the polymer backbones. This electropolymerization process is based on the radical-radical coupling mechanism and illustrated in Figure 2.1. [43]

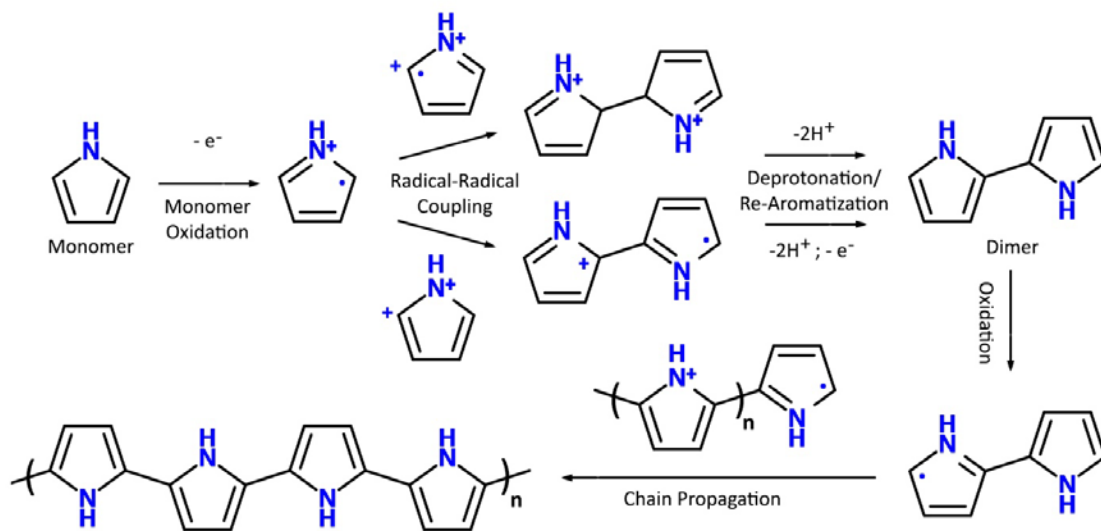


Figure 2.1 Polymerization of Ppy.

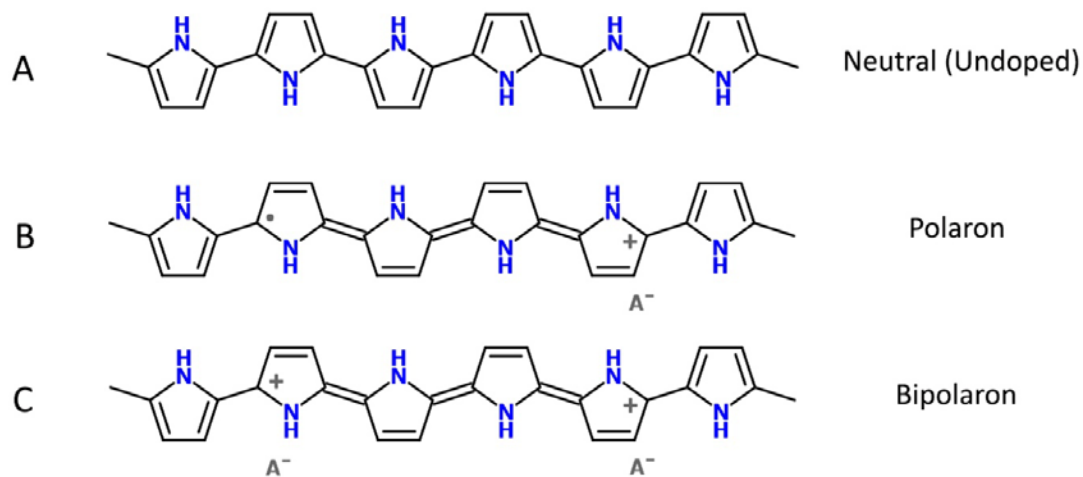


Figure 2.2 Neutral, Polaron, and Bipolaron state of Ppy.

2.1.2.2 Doping and Releasing Processes of Polypyrrole

How does the Ppy conducting organic polymer become conductive? First, we need to understand that how hundreds of inorganic substances can become conductive. This is through a process called electronic doping: the substances can be conducted by addition of impurities, that can be accomplished by giving electrons to or accepting electrons from the nonconducting form of the substances. Conductivity in the conducting organic polymer Ppy is related to the configuration of alternative single and double bond along the polymer backbone (See Figure 2.2). Every bond contains “s” bond and every double bond contains “p” bond. The introduction of voltage potentials and dopant ions to the Ppy allows the displacement of the weakly bonded electrons in between the stronger double bonds, resulting in the conductivity of this material. Therefore, we can say, Ppy need to be “oxidatively” or “reductively” doped in order to be conductive.

In our study, we conducted drug incorporation experiment based on the characteristics of Ppy oxidation as it is the most common mechanism in many drug delivery studies. The oxidation process develops cation along with the polypyrrole backbone, and concomitantly yields a local deformation which due to a geometrical change in every four pyrrole units. These processes constitute a “polaron” (Figure 2.2 B) and combinations of polarons pair can form “bipolarons” (Figure 2.2 C) during further oxidation process with higher charging levels. Polarons and bipolarons are the dominant charge carriers by transport charges along the segment of conducting polymer chain. The conductivity of Ppy can be reflected not only by charge migration but also the hopping charges of the

carriers from chain to chain. In sum, the mobility of charge carriers and the amount of charges in polymer chain are important for Ppy become conductive. [44,45,46]

Here, I need to point out that redox activity of conductive polymers Ppy not only involve mass and resistance charges but also electron transitions, and Ppy electrochemistry processes can be accomplished by only involving electrons. During oxidation of Ppy, when certain level of positive potential is applied, electrons are removed from the backbone of the Ppy, thus negatively charged dopants or counterions are taken up and can be incorporated to the Ppy structure. These dopants compensated with the positive charged sites on the polymer backbone and reach electroneutrality of Ppy. On the other hand, when a negative potential is applied and reducing it, the anions or anionic molecules can be expelled (or “undoping”) as there is a loss of electrostatic attraction to the Ppy. (See Figure 2.3 A) Apart from the expulsion of these anions, reduction process can also involve the incorporation of cations. Therefore, both negative or positive charged drugs can be ingress or expelled to compensate the resulting charges along the polymer chains. In our case, an anionic drug DEX can synthesize with Ppy at the oxidated state and released at the reduced state of Ppy.

Additionally, the oxidation-reduction action of Ppy can provoke mechanical effects such as swelling and de-swelling of the conductive polymer materials along with the ionic or small molecules fluxing in or out of the polymer structures. [47]

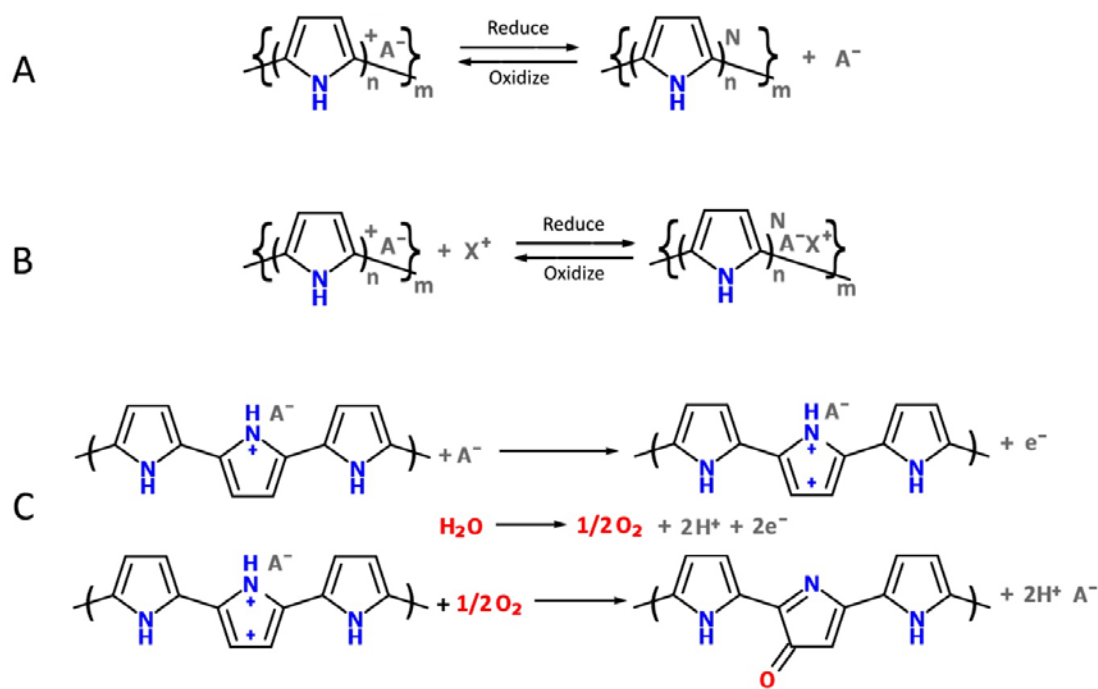


Figure 2.3 Redox reaction and overoxidation of Ppy. Redox reaction of Ppy for conjugation and releasing of Anionic (A) and Cationic (B) molecules and overoxidation of Ppy (C).

2.1.2.3 The Effects of Different Parameters During Eletropolymerization

The electrochemical approach for making electroactive materials depends on many parameters. For example, applied potentials, current densities, substrates, dopant, doping level, solvent, electrolyte, concentration of polymers, electrodes, even temperature and pH can influence the outcomes of polymerization of polypyrrole.

Doping level represents the average positive charge per pyrrole ring. In general, the oxidation level of Ppy is at 0.25-0.32 per pyrrole unit which is one anion for every 3 to 4 pyrrole units, which can be influenced anion types and its charges. [48] However, at high

doping levels which might be caused by the application of an excessive level of anodic electrode potential, Ppy can be overoxidized due to trace water or other nucleophiles, such as OH⁻ attack causing irreversible changes in the polymer's chemical structure. (See Figure 2.3 C) This interruption of Ppy structure could lower the intrinsic conductivity of the polymer and make Ppy lose the capability of electrochemical activity. Thus, Ppy would not be able to release the drugs as described in 2.1.2.2. Since conductivity of Ppy at high doping levels is dramatically decreased, we control the level of potential at range of 0.8-1mV during Ppy synthesis, and -0.1mV for Ppy drug releasing.

The substrates of where Ppy will be deposited during electropolymerization also determine the characteristics of Ppy. Many materials can be used as the substrates, such as glassy carbon, gold, indium-tin oxide coated glass, platinum, titanium, and aluminum. [49] Some substrate materials work less efficient than others, for example, when Ti, Fe, and Al are used as substrate, it results in an increased oxidation potential of pyrrole. In our experiment, we select the indium-tin oxide coated glass as substrate for flat Ppy due to its strong structure support and its conductivity. Also, since gold materials feature high conductivity and non-toxicity, evaporated gold base was used as substrate for Ppy nanowire synthesis.

The resulting electrochemical properties of Ppy also depend strongly on the synthesis medium where polymer prepared during electropolymerization. One study indicated that interaction of counterions melanin in Ppy and various components in the synthesis medium. It also indicated that medium containing sulfate, phosphate, or chloride can be responsible for ion dynamics in Ppy films.[50]

The dopant used for Ppy electropolymerisation can highly influence the characteristics of Ppy film and have been widely discussed in different literatures. In summary, the counterions should be chemically inert, very soluble in the monomer contained synthesis solution, and electrochemically more stable during oxidation-reduction process than the monomer itself (in our case is pyrrole). Curtin et al indicate that the anion preference of Ppy is I⁻>Cl⁻>Br⁻>ClO₄⁻, [51] which could arise from the buffer salts, such as I₂, BF₄, FeCl₃, and perchlorates. Much of research also reported aromatic sulfonate variants are good candidate as dopant for Ppy polymerization, especially for application as neural interfaces. These include PSS, sodium benzenesulfonates (BS), and para-toluenesulfonate (pTS) dopants. Moreover, various biological dopants, such as laminin peptide sequences, neurotrophins, hyaluronic acid, fibronectin fragments, human serum albumin, and polysaccharides, can also be immobilized into the Ppy to enhance cell proliferation and differentiation in biomaterial tissue engineering studies. [52]

2.1.3 Conductive Polymer Based Drug Delivery System

To successfully deliver the drugs using a Ppy platform, the characteristics of the drugs themselves are also critical for the application. To design an efficient drug delivery system, the size of the dopants can influence the incorporation of the drug into Ppy or their release from Ppy. Maria Hepellet et al reported that melanin (a bulky molecule) is irreversible after incorporation into polypyrrole, whereas the small chloride ions can be easily released from polypyrrole after conjugation. [50] However, one study described that despite the fact that nicotine has a lower molecular weight compared to

naproxen, it cannot be released during the potential cycling of Ppy. This result indicates that size is not the only parameter that should be considered during the selection of the drugs for Ppy based drug delivery system.[23]

The charge of the drug molecules is usually associated with its pKa value and it is especially important to Ppy mediated drug delivery. This drug delivery system is not only able to release the anionic drugs, but also can successfully achieve the delivery of cationic and neutral drugs. As described previously, anions are incorporated into the polymer to balance out positive charges initiated during oxidation. When immobilised larger sized anionic dopants (e.g. melanin, PSS, pTS) with Ppy, cations or cationic drugs can be incorporated into Ppy, but during reduction instead of oxidation, and then released during oxidation. The study of chlorpromazine conjugated Ppy/melanin films has provided more insight. The mass of chlorpromazine in Ppy was increased during reduction and decreased in concomitant with the oxidation when evaluated by electrochemical quartz crystal microbalance, indicating the egress and release of cationic drug, chlorpromazine. [50] Many studies of dopamine release used immobilized PSS with Ppy and also successfully accomplished the cationic small molecules delivery. Similar mechanisms also applied to incorporation and release of NT-3 and BDNF with immobilized molecules pTS in Ppy. The detailed mechanism of cationic drug delivery is the same as that of anionic drugs by using electrostatic forces with slight differences as shown in Figure 2.3 A and B. Novel strategies have also been developed to help incorporation of neutral drugs, such as N-methylphenothiazine by using anionic dopant β -cyclodextrins prepared Ppy films and achieved by encapsulation drugs into the hydrophobic interior of β -cyclodextrins. [53]

2.1.4 Synthesis Techniques for 3D Nanostructure

Compared to 2D structure, 3D structured polymers showed promising results to load larger amounts of therapeutic agents, especially useful in the treatment of chronic medical conditions. Many polymer nanostructures are well developed, such as nanowires, nanotubes, opal structures, and inverted opal structures. The template method is considered to be the most convenient for nanostructure development. For example, porous polycarbonate and porous anodic alumina membrane are typically used as templates for nanowire growth. The formation of pores in the template is related to either 1) dissolution of the oxide to form pores or 2) self-organized anodization which generally performed by different strong acidic electrolytes. Unlike PANI nanotubes which formed along with phenazine-based aniline oligomers spontaneously produced internal template, Ppy nanotubular growth need an external template. It could be generated using coating on hard template method, that is, placing insoluble inorganic nanofibres, such as manganese (IV) oxide, titanium (IV) oxide into the synthesis solutions during oxidation process, then dissolving the template to form nanotubes. [54] Its formation also can based on the self-assembling of some dyes, such as MO, acid blue AS, rhodamine B, Prussian blue, or methylene blue. The surfactant characteristics which combine both hydrophilic and hydrophobic moieties in these dyes, allows them to form supramolecular structures. Other 3D geometric structure of Ppy are also exploited, for example, Luo and Cui synthesize Ppy over polystyrene beads deposited electrode, and formed a 3D structured polymer porous film after removal the beads. [55]

In our study, polypyrrole nanowires (PpyNWs) were manufactured based on the simple template technique using anodic alumina membrane. The modulation of the geometric structures of Ppy to nanowire shape can maximize the drug incorporation and can release drugs in relatively longer time.

2.2 Method and Materials

2.2.1 Template Preparation for Polypyrrole Polymerization

Indium tin oxide (ITO) glass slides with 5-15 ohms resistivity (Delta Technologies, CO) were used for fabrication of flat Ppy. They were washed with acetone, ethanol, and then Milli-Q water by incubating glasses with each solution for 30 mins at an ultrasonic bath. For PpyNWs experiments, anopore inorganic aluminum oxide membrane (AAO) with 0.2 μ m pore size and 60 μ m thickness (Whatman) were used. The AAO templates were coated with gold at thickness of 100 nm on one side using a Varian E-beam Evaporator. Then, they were stored in a dry oven prior to use.

2.2.2 Fabrication of Dexamethasone Doped Polypyrrole Carriers

One synthesis solution was prepared by mixing 0.2M pyrrole (Py, Sigma), 0.025M dexamethasone 21-phosphate disodium salt (DEX, Sigma), 0.05 M 10 nm NanoXact spherical gold nanoparticles (AuNps, NanoComposix, CA) together. For comparison, 0.2M pyrrole, 0.025M DEX, 0.1M Poly (3,4-ethylenedioxythiophene)-poly(styrenesulfonate) (PSS, Sigma) was also prepared by gentle mixing. Prepared AAO

templates were subsequently incubated into each of solution mixtures for 30 minutes before PpyNWs electropolymerization. This procedure allow the Pyrrole monomers, drugs, and other sytheis components (either AuNps or PSS) diffuse into the pores of the template. Cleaned ITO slides or AAO templates were connected to the working electrode from a CH Instrument model 604 electrochemical workstation with a platinum counter electrode and a Ag/AgCl reference electrode placed in the synthesis solution. The electropolymerization of DEX doped Ppy was then performed using a constant potential at 1V. This constant potential is cotrolled by potentiostat device in the electrochemical workstation, it will be briefly called potentiostat stimulation in the later content. Following polymerization, the final films were rinsed thoroughly with Milli-Q water. At end, the AAO templates will be removed by incubation in 3M sodium hydroxide. The whole synthesis procedure is indicated in Figure 2.4.

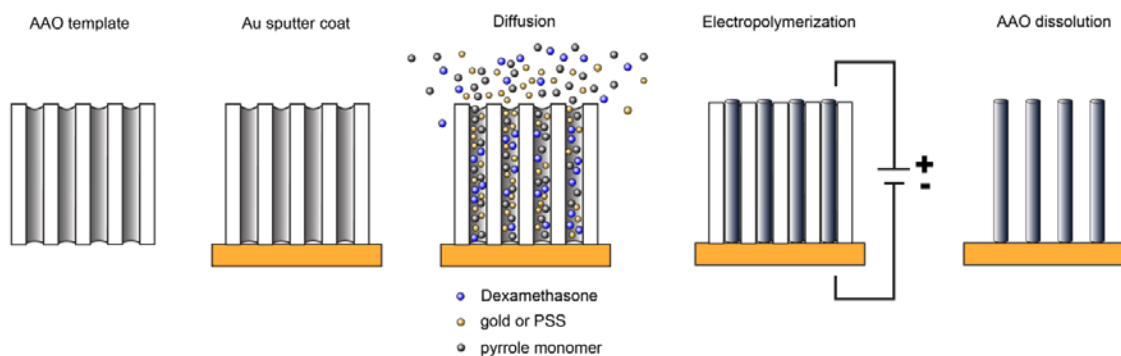


Figure 2.4 PpyNWs fabrication processes. The figure at far left is an illustration of the AAO template. Next step showed one-side gold coated template. The third step demonstrate the diffusion of pyrrole monomer, AuNps or PSS, and DEX into the porous column of the template. The fourth step is formation of DEX doped Ppy after electropolymerization process. The far right figure indicate the removal of AAO templates and free standing PpyNWs structure.

2.2.3 Morphology of Polypyrrole Nanowires

Imaged by Scanning and Transmission Electron Microscopy

Ppy samples were prepared by first sputter coating with platinum for 60 seconds. SEM images were taken with a FEI NOVA nano SEM field emission scanning using ET and TLD at high vacuum at an accelerating voltage of 5 kilovolts. TEM images were taken using a FEI/Philips CM-10 Transmission Electron Microscope, operated at 100 kilovolts; A 200 μ m condenser aperture; and 70 μ m objective aperture. TEM images were captured by a SIA L3-C digital camera.

2.2.4 Electromagnetic Stimulation

The set up of electromagnetic stimulation was illustrated in Figure 2.5. More details are described in CHAPTER THREE: Method and Materials and Results sections.

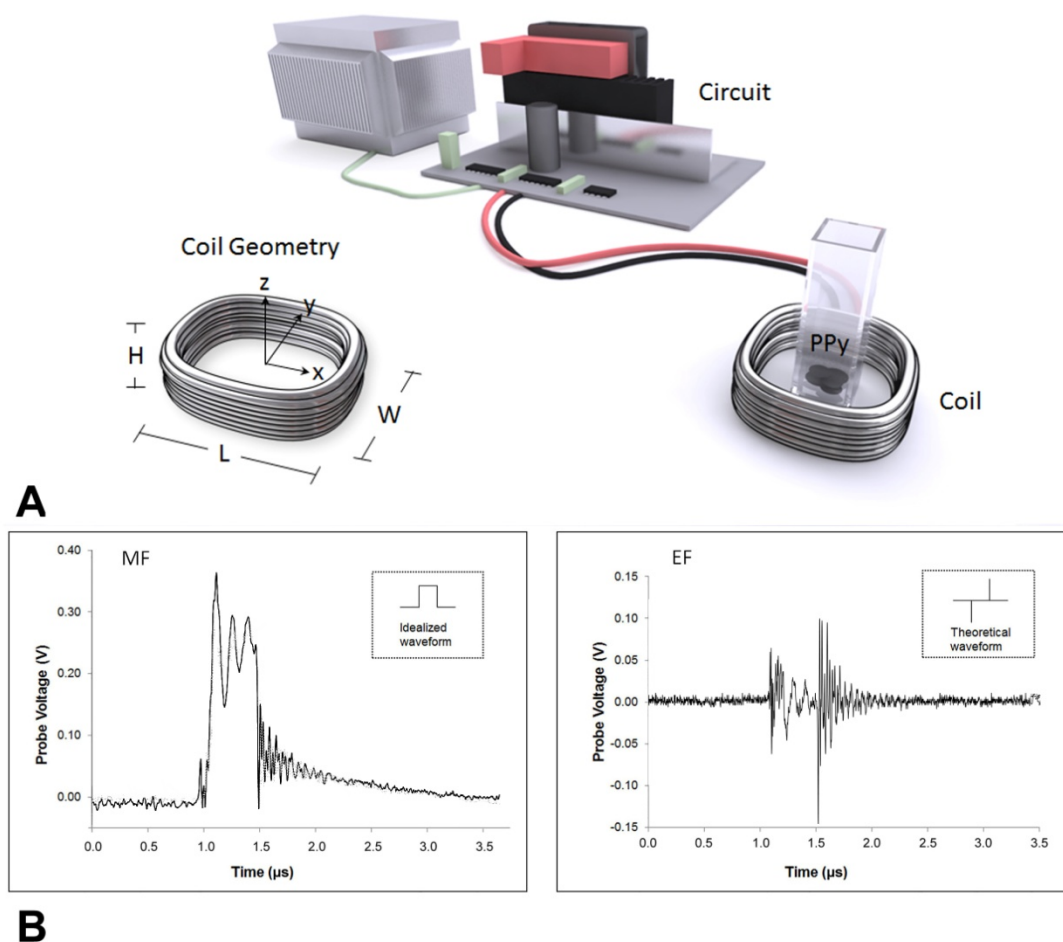


Figure 2.5 Stimulation scheme for the application of EMFs. (A) The top illustration shows the setup of EMF generator during the stimulation. The stimulator is connected to a circular wire-wound coil. A standard cuvette containing DEX doped Ppy film was placed in the center of the coil. Left inset describes the dimensions of the coil, where Height(H) is 1.2cm, Length(L) is 3.8cm, and Width(W) is 3.0cm. The recordings in B are probe measurements of the magnetic fields (MF) and electric fields (EF) at the center of the coil, with ~ 36 Gauss and ~ 4000 V/m respectively. The insets demonstrate the idealized waveforms for both MF and EF based on the input square pulse stimulation regime.

2.2.5 Drug Release

Both potentiostat electrical stimulation and EMF stimulation were used to release DEX and these two methods are described in more details in CHAPTER THREE. In former cases, the procedure is similar to the electropolymerization process with three electrodes. The stimulation is potentiostat device controlled constant potentials and the DEX conjugated Ppy films was linked to a working electrode and emerged in PBS solution. Then, a constant voltage of - 0.1V was applied for five hours using electrochemical workstation. The DEX conjugated Ppy platforms were also stimulated by EMF generator illustrated as Figure 2.5 which depicts the experimental set-up and the essential components of the EMF stimulation system. Before conducting the drug releasing, the Ppy samples were placed into PBS contained cuvette and this cuvette was then positioned in the center of the coil without any physical contact. The coil was energized with an asymmetrical square wave pulses and remotely trigger drug release from Ppy. The supernatants were subsequently collected after 1, 3, and 5 hours of stimulation.

In addition, different Ppy compositions used for polymer synthesis were also tested and compared. All experiment were last for 16 days with EMF stimulation. The sample solutions were collected at 1, 3, 5, 7, 10, 13, and 16 days after continuous EMF stimulation.

All collected aliquot samples were analyzed by a UV-Vis Spectrometer at 242nm wavelength. A calibration curve of DEX ($y(\text{OD})=23.8x-0.04$) was used to calculate the amount of released drugs.

2.2.6 On-Demand Dexamethasone Release

To determine the controllability of EMF stimulation to Ppy drug release, “on and off” experiments were performed on PpyNWs with AuNps components. The recordings were begun after 10 hours of stimulation by the EMF to avoid the robust release at first couple of hours. Pulsed EMF stimulation was turned on for 2 hours and turn off for 2 hours. This regimen was continued for four cycles for each sample.

2.2.7 Temperature Effects on Drug Release

To test if the release of DEX might be influenced by the heating during the stimulation, we placed the DEX doped flat polypyrrole templates within a incubator at 37°C. This temperature was slightly higher than the ambient temperature in the vicinity of the active coil, which was measured to be about 30°C.

2.2.8 XPS Analysis

Ppy samples about 0.5-1.0cm² were prepared and submitted for XPS analysis. The surface chemical composition of the samples was analyzed by X-ray photoelectron spectroscopy (XPS) using a Kratos Axix Ultra DLD spectrometer. The spectra were collected using monochromatic Al K α radiation (1486.6 eV). The survey and high resolution spectra were obtained at the constant Pass Energy mode with the pass energy of 160 eV and 20 eV respectively (survey 1 eV/step; high resolution spectra 0.05

eV/step). A built-in Kratos charge neutralizer was used. Data analysis was performed with CasaXPS software version 2.3.12.

2.2.9 Statistical Analysis

All data are shown with standard error of the mean (\pm SEM). Independent Student's t-test and one way ANOVA followed by Tukey Post Hoc test were used to determine statistical significance. Significance was determined by a P-value ≤ 0.05 .

2.3 Results

2.3.1 Structure of Polypyrrole Nanowires

Nanowire architecture was imaged by SEM and TEM and illustrated in Figure 2.6 and 2.7. Since polymers thickness can be easily controlled during electropolymerization, the growth of (or length of) PpyNWs can be vary with the deposition time during synthesis. 1300-1400 seconds of deposition time can achieve approximately 10 μ m long PpyNWs (Figure 2.6 A) while shorter lengths were completed in a faster deposition times. The commonly used deposition time in our study is at 200-300 sec and it can form PpyNWs structure as showed in Figure 2.6 B. All the PpyNWs showed as free-standing vertically aligned conformation. For PpyNWs with AuNps composition, the distribution of the AuNps within the polymer bulk were indicated in Figure 2.7 A and B.

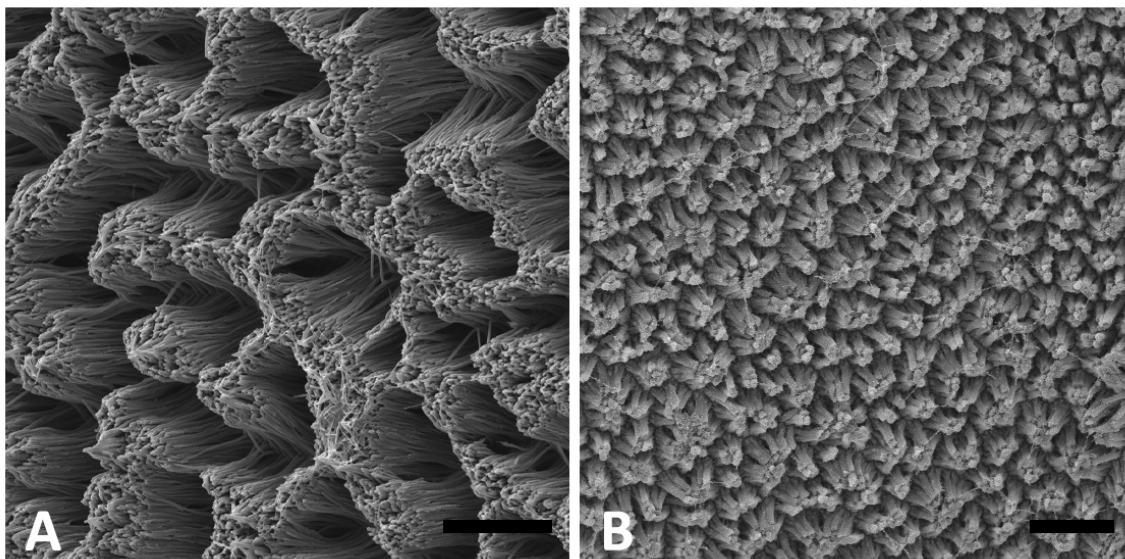


Figure 2.6 Scanning Electron Micrograph of PpyNWs. (A) Scanning Electron Micrograph showing a top view of polypyrrole nanowires (200nm diameter and $\sim 10\mu\text{m}$ length) with longer deposition time. (B) A similar micrograph where showed a 200nm diameter and $\sim 500\text{nm}$ long PpyNWs synthesized in a shorter time. Scale bar in A= $10\mu\text{m}$; in B= $2\mu\text{m}$,

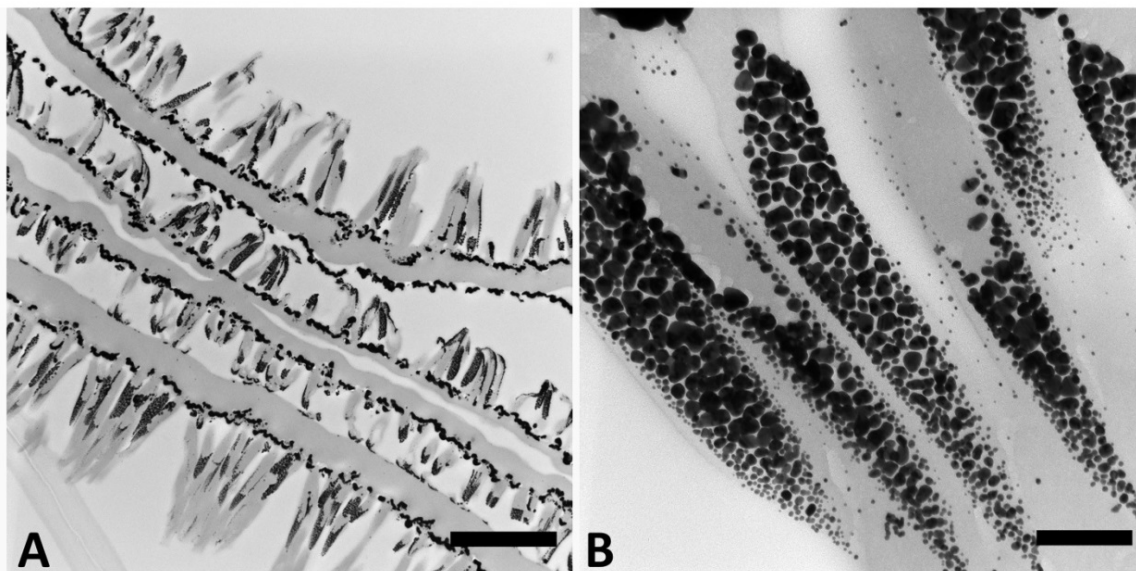


Figure 2.7 Transmission electron micrograph of PpyNWs with inclusion of gold nanopartilces. (A) Transmission electron micrograph of PpyNWs. The dark regions are the accumulation of AuNps in the Ppy. (B) showed details of gold nanopartilces in each individual PpyNWs. These wires range from approximately 500nm to 2000 nm in length, and ~200 nm in diameter. Scale bar in A=2 μm ; and in B = 0.2 μm .

2.3.2 Comparisons of Drug Release

Drug release profile of the PpyNWs compare to conventional flat Ppy films are shown in Figure 2.8 A, B, and C.

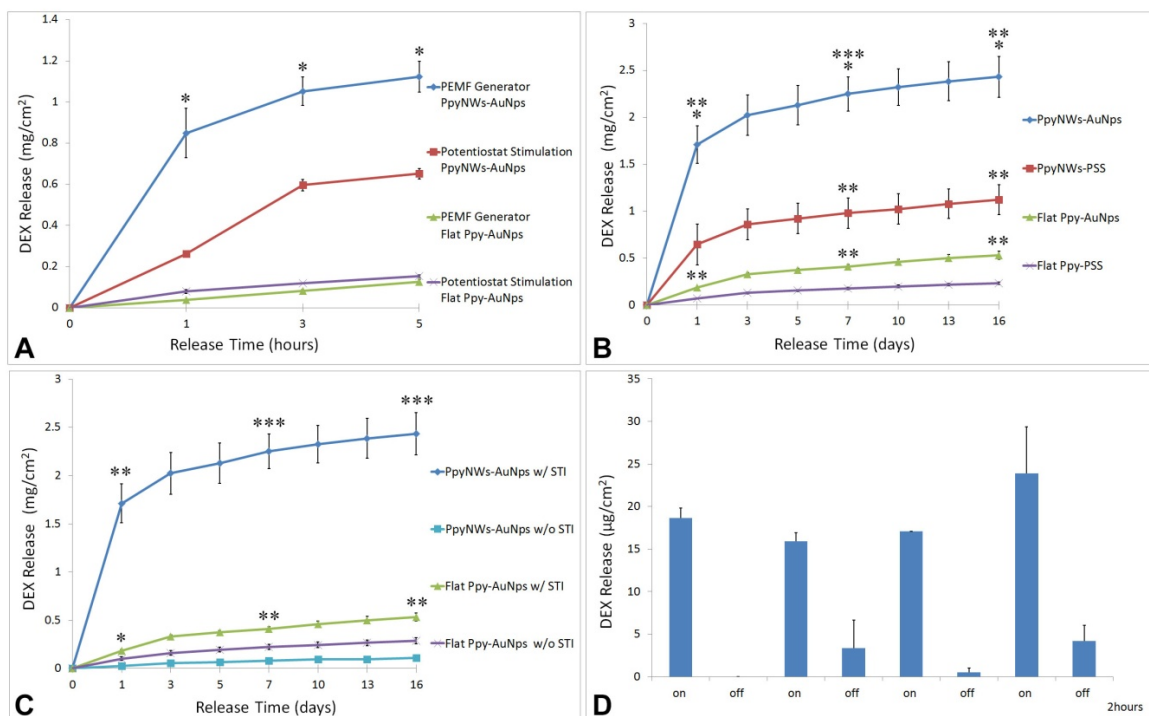


Figure 2.8. DEX release using various Ppy platforms and stimulation methods. (A) The DEX release using either constant potentials (potentiostat stimulation) or EMF stimulation from both flat Ppy film and PpyNWs. The releasing time were tested for five hours. (B) Comparison of DEX release with different synthesis compositions (AuNps vs. PSS dopant). All experiments were applied with EMF stimulation for 16 days. (C) Active (EMF stimulation) vs. Passive (no stimulation) for both flat Ppy films and PpyNWs. (D) "on" and "off" EMF experiment to test the DEX release from PpyNWs-AuNps when response to the stimulation. Higher concentrations of DEX were generated with EMF stimulation whereas a smaller amount of DEX was detected at the absent of EMF stimulation. * $p \leq 0.05$; ** $p \leq 0.01$; and *** $p \leq 0.001$.

Figure 2.8 A reveals the results of DEX release over a five hour period of stimulation. For flat Ppy, potentiostat mediated stimulation was not significantly different from that of EMF stimulation. Although there is no statistical difference between EMF stimulation and potentiostat mediated stimulation in the case of PpyNWs, there was more apparent DEX release when using EMF stimulation. Also, upon the exposure to EMF stimulation, there was a statistically significant increase in the DEX release of PpyNWs compared to flat Ppy film ($*p \leq 0.05$).

AuNps embedded Ppy either in flat Ppy films or PpyNWs also showed increased DEX release when compare to the PSS doped Ppy films. At 1, 7, and 16 days, these differences were by almost double for both Ppy platforms ($*p \leq 0.05$ between PpyNWs and $**p \leq 0.01$ between Flat Ppy). Also, the results of flat Ppys only showed marginal release of DEX ($<0.5\text{mg}/\text{cm}^2$) from flat Ppy films. In contrast, PpyNWs showed a very significant enhancement of DEX release. (At day 1 and 16, $**p \leq 0.01$, and at day 7, $***p \leq 0.001$ between AuNPs; At day 7 and 16, $**p \leq 0.01$ between PSS study; Figure 2.8 B). The groups without EMF showed relatively small amount of DEX diffusion, and it was below $0.11\text{ mg}/\text{cm}^2$ for PpyNWs and $0.3\text{mg}/\text{cm}^2$ for flat Ppy films on the last day of recording. This reveals a extrodinary DEX release occurred after EMF stimulation compared to without EMF stimulation. (At day 1, $**p \leq 0.01$, and at day 7 and 16, $***p \leq 0.001$ between PpyNWs; At day1, $*p \leq 0.05$, and at day 7 and 16, $** p \leq 0.01$ between Flat Ppy films; Figure 2.8 C). Further "on" and "off" switching stimulation performed by EMF was used to test the control of DEX release as shown in Figure 2.8 D. In such cases, DEX release fell off precipitously at absence of EMF stimulation, and was regained when

EMF coupling was applied. Such consistency over several cycles demonstrated the potentials to controlled drug release using this drug delivery strategies.

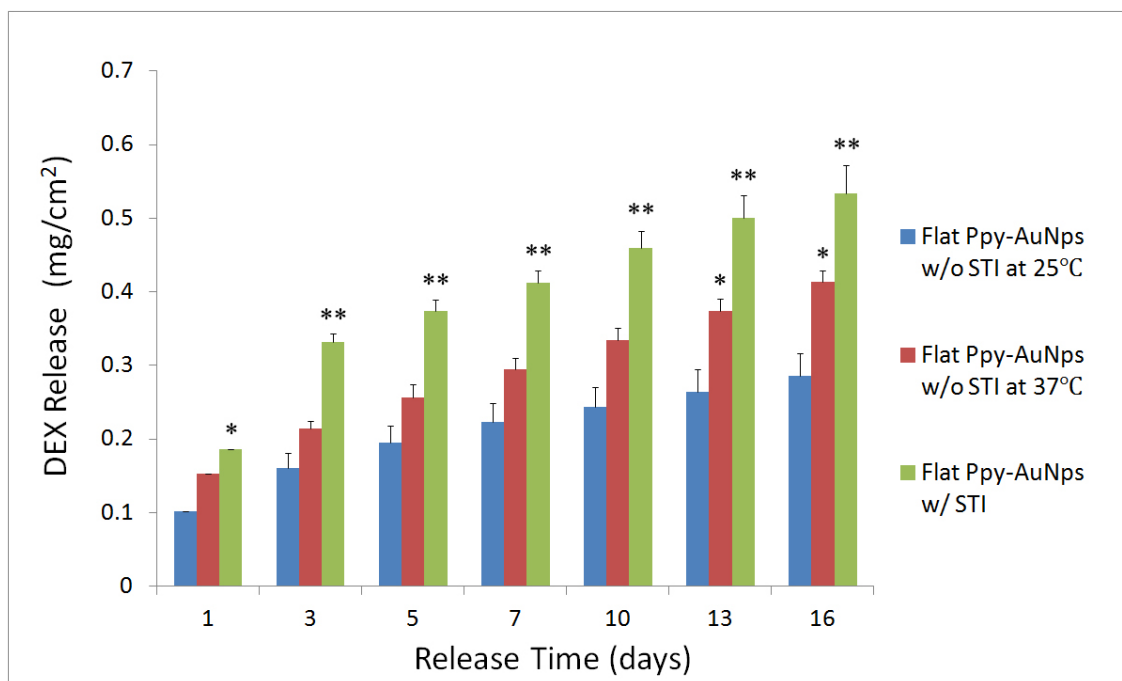


Figure 2.9 DEX release profiles of flat Ppy as a function of temperature and its comparison to that of with and without EMF stimulation. * $p \leq 0.05$, ** $p \leq 0.01$.

2.3.3 The Influence of Temperature Elevation on Drug Release

According to the results from Figure 2.9, there is some increased level of DEX passive release under the elevation of temperature (37°C) compare to the samples at room temperture without EMF stimulation. However, no statistical difference was observed until 13th day whereas the significant statistical difference occurred from day 1 when using EMF stimulation compared to without stimulation . Therefore, we conclude that the

DEX release result from increased temperature did not reach the levels of active EMF stimulation during the entire experiment, and are not the driving force for DEX release.

2.3.4 XPS Confirmation of Dexamethasone Release

X-ray photoelectron Spectroscopy (XPS) was used to verify the existence of DEX after loading with Ppy and the escape of these loaded DEX after EMF stimulation (See Figure 2.10). XPS surface analysis was conducted on the PpyNWs before and after (16 days) EMF stimulation. High-resolution spectra of F 1s (fluorine) and P 2p (phosphorous) elements in the DEX molecule can reveal the elemental components in PpyNWs before and after stimulation. It can denote the presence and absence of DEX upon exposure to the EMF. These two elements were vanished after EMF stimulation indicating the DEX release after EMF stimulation. For PpyNWs-AuNps, the pre-stimulation F 1s and P 2p atomic percentages were 1.53% and 1.54%, respectively while the post-stimulations results were 0.00% and 0.17%. For PpyNWs-PSS, the pre-stimulation F 1s and P 2p atomic percentages were 0.60% and 1.31%, respectively while the post-stimulations results were 0.00% and 0.15%.

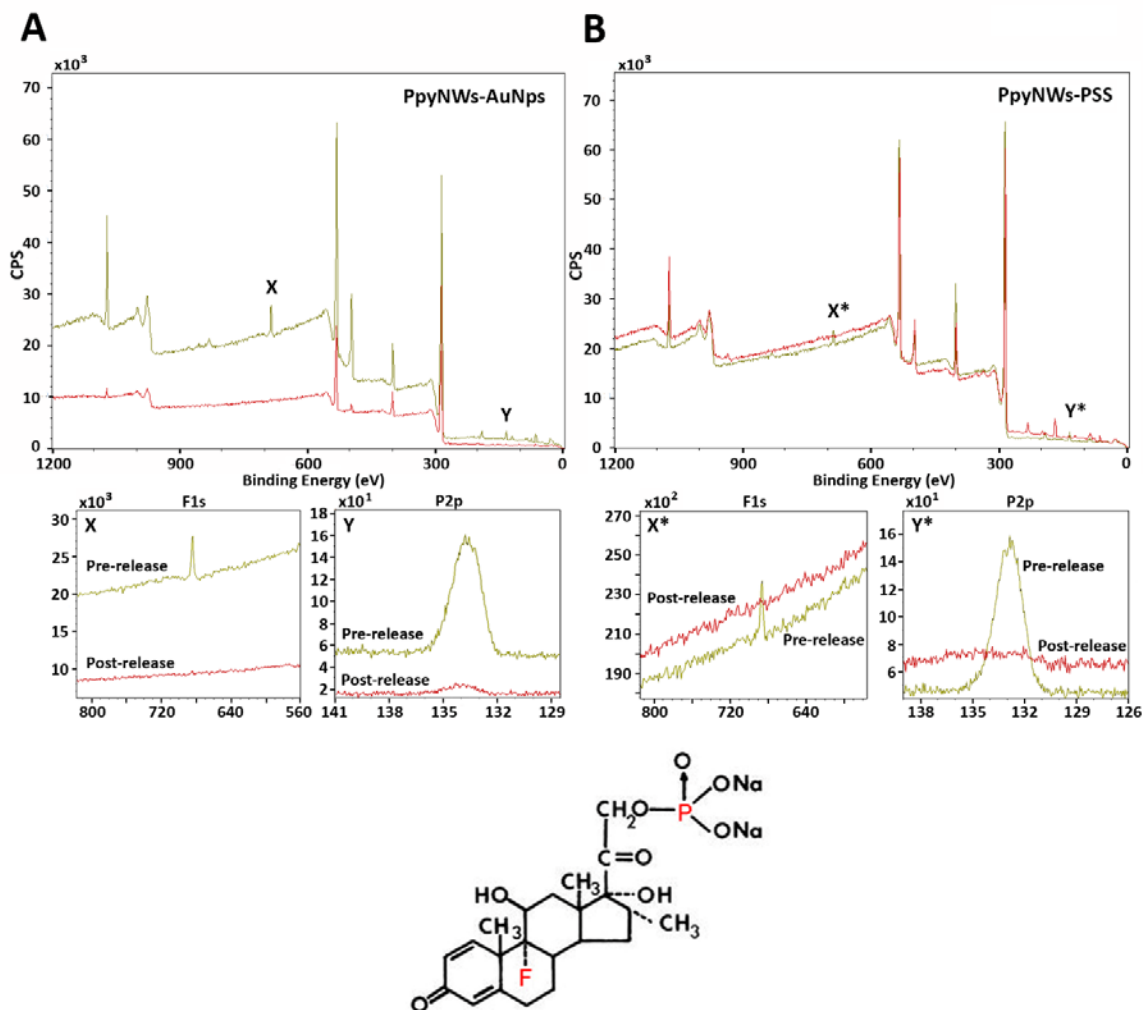


Figure 2.10. XPS spectra for surface analysis of DEX presence on Ppy templates before and after EMF stimulation. (A) Elements identification on the surface of DEX doped PpyNW-AuNps before (Green) and after (Red) EMF stimulation. Characteristic peaks are shown in this spectrograph. (B) Same recording for DEX doped PpyNWs-PSS before (Green) and after (Red) 16 days of EMF stimulation. Below A and B are expanded views. These show details of signature fluorine and phosphorous elements indicating DEX molecule. Note that apparent elemental signatures were observed before EMF stimulation and vanished after EMF stimulation, indicative of DEX release from the surface of

PPyfilms. The very bottom graph shows the molecular structure of DEX, with fluorine (F) and phosphorous (P) highlighted in red.

2.4 Discussion

In this study, we investigate the potential of polymer implantation for local drug delivery strategies based on the nature of implantation. We focused on the Ppy mediated drug delivery system from three aspects: structure, synthesis, and releasing profile in order to non-invasively administrate the drugs over a relative long-term. A geometrical modification of Ppy to 3D structure increased both surface areas and overall volume of the Ppy, and enhanced the possible payload capacity of these carriers. It has been proved that dramatically increased NGF were indicated in a inverted opal structure (porous) of Ppy compare to the flat Ppy. [56] In addition, the template assisted manufacture of PpyNWs is simple and highly reproducible. A large area of PpyNWs film showed consistency of vertical nanowires through entire film (See Figure 2.11). The embedded AuNps enhanced the strength of Ppy structure and improved its electrochemical activity with increased DEX release. Most important, we are the first to introduce Ppy responses to non-invasive electromagnetic fields and its potential use for drug delivery. This approach was designed to optimize the performance of many medical devices and implants which require relatively long-term and stable amount of drug administration to very local sites.

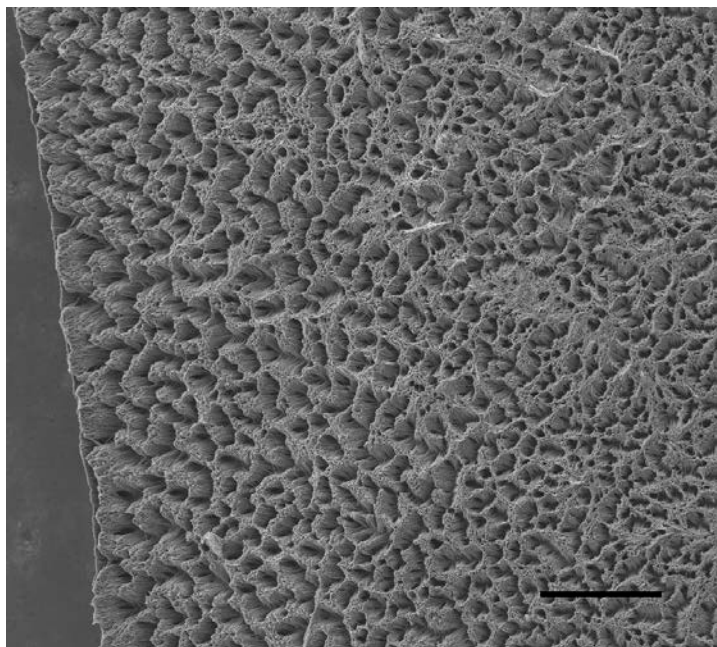


Figure 2.11 High magnification of TEM image depicts the successful fabrication of PpyNWs through entire film. Scale bar is 50 μ m.

The mechanism of DEX release from Ppy when it responded to EMF exposure could be the result of single or multiple phenomenon. As we mentioned in the Introduction, Ppy films undergo a reduction when sufficient negative potential is applied, therefore, anionic drugs DEX can be expelled to the surrounding solutions. The other potential cycling methods, such as cyclic voltometry and bipolar (pulsed) current stimulation (See details in 3.1.2), applying both cathodic and anodic current which is similar to EMF stimulation have been reported and indicated that they can also successfully release drugs out of Ppy matrix.[57,58,59,60] Ppy conducting polymers swell during oxidation along with the entry of counterions into the polymers and results in a mechanical change and volume enlargement of the polymer. Conversely, Ppy shrinks during the expulsion of counterions at the reduction process. This electromechanical property is commonly used as the basis

of actuator, such as polymer based artificial muscles, and also existed during drug incorporation and releasing. In our case, the Ppy with high conductivity has more mobile charge carriers that can interact with the EMF. The switching of the polarity of the EMF produces a very short-lived, but bipolar electric field. This transitory alternative electrical field potentially provide the conditions for undoping of the anionic drugs from the Ppy at the concomitant of polymer de-swelling. According to the results, drug release amount dramatically increased at the first day of release and was reduced after 5 days. This is possibly due to doped Ppy films possess high conductivity and mechanical strength, but this decrease during the undoping process.

We are not excluded the possibility of the anions in aqueous solutions might move into the interstices of the Ppy polymer coil and exchange small sized anions or anionic drugs out of the Ppy films during the potential sweeping. This effect has been used to develop electrically switchable ion-exchanger for purification of water. [61] Bipolar current or heating can cause the movement or relative rapid movement of ions in the solution, providing the potential exchanges between anions. In this situation, certain anions in aqueous solution such as Cl^- with a stronger electrostatic interaction might be more vulnerable to exchange with other anions. This ion exchange action of Ppy could potentially play a role during DEX release.

pH values can also be responsible for the ion exchange abilities of Ppy. During the low pH, protonation of the nitrogen increase the capacity of ion exchange, in contrast, deprotonation in a higher pH environment can result in reduced or even devanished electronic conductivity and eventually lead to the expulsion of anions. [62,63] This is not

likely the reason in our case since all the solutions in which Ppy placed remain a neutral pH value. However, the possible disruption to the weak electrostatic interaction between DEX and polymer because of a changing EMF field should be under the consideration.

CHAPTER THREE

DESIGN AND SELECTION OF ELECTROMAGNETIC FIELD GENERATOR

3.1 Introduction

3.1.1 Time-Varying Electromagnetic Fields

A time-changing electric field can produce a magnetic field, and conversely, a time-changing magnetic field can produce an electric field. The former statement is the experimental basis of Ampere's law and the latter for Faraday's law in a time-varying conditions. Ampere's Law (See Figure 3.1) indicates that a magnetic field is produced by a changing electric field and a current. For time-varying magnetic field, it includes conduction current (for static (dc) conditions) and the displacement current. It means that either true conduction current density J (A/m²) or by a time-varying of electric flux density D (C/m²) through the enclosed surface can generate magnetomotive force (H).

Ampere's Law :

$$\oint_c \mathbf{H} \cdot d\mathbf{l} = \int_s \mathbf{J} \cdot d\mathbf{s} + d/dt \int_s \mathbf{D} \cdot d\mathbf{s}$$

Faraday's Law:

$$\oint_c \mathbf{E} \cdot d\mathbf{l} = - d/dt \int_s \mathbf{B} \cdot d\mathbf{s}$$

Figure 3.1 Ampere's Law and Faraday's Law.

In the equation of faraday's law (See Figure 3.1), left side indicates that a voltage is induced in the closed loop considered as electromotive force. Right side is the time-changing magnetic flux penetrating the surface whose perimeter refer as contour. Here needs to be clarified is that Faraday's law gives the same results for different surfaces as long as the contour size does not change, that is, only those magnetic field lines that penetrate the contour of surface contributes to flux. In sum, the faraday's law refers to time-varying magnetic flux (the average of magnetic field over the area of the loop) that penetrates a surface bounded by contour will induce an electromagnetic force (emf) which is very similar to a voltage source in that contour. The minus sign in Faraday's law is related to Lenz's law providing that the direction of that induced emf will produce a current in contour whose magnetic field will oppose changes in the original magnetic field.

In our study, we based on this physics pheomenon of electromagnetic induction and custermized a electromagnetic generator where an alternating current flowing through the coil at a certain frequency and generates an oscillating magnetic field around the coil. When the coil is closely positioned to an electrically conductive material, it also induced

a current known as eddy current in the conductive materials. We hypothesized that this current can initiate the drug release from conductive polymer Ppy.

3.1.2 Electrochemical Techniques Used for Polypyrrole Based Drug Release

The most frequently used electrochemical techniques in the Ppy based drug releasing system are summarized in the Table 3.1 with released compound and stimulation conditions

Table 3.1. Polypyrrole based drug release.

Dopant	Released Compound (anion+/cation-)	Stimulation Condition	Ref
Galvanostatic:			
	(DEX)(-)	Galvanic Mg alloy	[64]
Cathodic Potential:			
Ppy/Cl	Glutamate (-)	-1.0V vs SCE	[65]
	Sulfosalicylic acid (-)	-0.5,-0.8,-1V	[66]
	Fluorescein (-)	-2V	[55]
Ppy	ATP(-)	-0.6V	[67]
	Salicylate and Naproxene (-)	-0.7,-0.4V	[68]
	Hexacyanoferrate (-)	-0.4,<-0.6V	[69]
	DEX (-)	<-0.6V	[70]
Anodic Potential:			
Ppy/biotin/streptavidin	NGF	+3V	[71]
Poly(N-methylpyrrole) /PSS	Dopamine (+)	+0.5V	[72]
Cyclic Voltometry:			
	DEX (-)	-0.8~+0.9V/+1.4V	[73,74]
	ATP (-)	+0.6~-0.6V	[75,76]
	Acetylsalicylate or salicylate (-)	-1V	[77]
Ppy/ pTS	NT-3	-0.8~+1.0V	[78]
Biphasic Pulsed Potential or Current:			
Ppy/ pTS	NT-3 and BDNF(+)	+/-0.5 and +/-20 mA at 5 Hz; -0.6~+0.6V at 5Hz; +/-1mA/cm ² ;	[58-60, 78,79]
Stepped Potentials:			
Ppy/pTS	ATP(-)	-0.6~+0.6V	[80]
Ppy/melamin and Ppy/Cl	Chlorpromazine (+)	-0.8~+0.2V	[50]
Poly(N-methylpyrrole) /PSS	Dimethyldopamine (+)	+0.4~+0.6V	[81]

The potentiostat is an electronic device controlling constant potential difference between the working and reference electrodes. Chemically, it refers to the flow of required electrons in order to maintain voltage potentials at a fixed level. In some of controlled-potential techniques, such as cathodic potential and anodic potential listed in Table 3.1, bulk electrolysis coulometry is usually the most common and desirable method used to achieve the constant potential. On the other hand, a galvanostat is a device to measure and control the constant current flowing through the system, instead of the constant potential.

Cyclic voltammetry is a potential cycling technique by changing the potentials of stationary working electrode linearly with time from no reaction occurred to potentials where reduction or oxidation of a analyt occurred. It scans potential negatively (reduction process) before reaching to the switching potential, and the scan reversed where scan potential positively (oxidation process), the voltage then swept back to original point. (shown in Figure 3.2 A and B) During this potential sweeping, the current is measured by potentiostat device and display to a cyclic voltammogram plotted as current vs. potential (See Figure 3.2 B). As the summary Table 3.1 shows, there also are many investigations on the potential step techniques for Ppy drug delivery. In the potential step measurement, the applied voltage is instantaneously jumped from one level to another, and corresponding current were measured as a function of time. It could include either single potential step (Figure 3.2 C and D) or double potential step (Figure 3.2 E and F). The former one is related to only the potential with forward step, and latter case is with addition of the potential that returned to a final value following a time period. Many stimulation methods, such as galvanostatic, cathodic potential, and cyclic

voltammetry, have been successfully used to release DEX from Ppy platforms. (Bolted in Table 3.1) (These can provide as useful reference to understand the mechanism of DEX release.

In our study, we focus on a special stimulation technique: pulsed current stimulation. The electrical field induced by our electromagnetic field generator (See Figure 2.5) shares a similar pattern to that of biphasic pulsed current. The pattern of this bipolar current is similar to double potential step shown in Figure 3.2F) with an alternative polarity of potentials and current. The exact illustration was indicated at Rachael T. Richardson et al. [58]

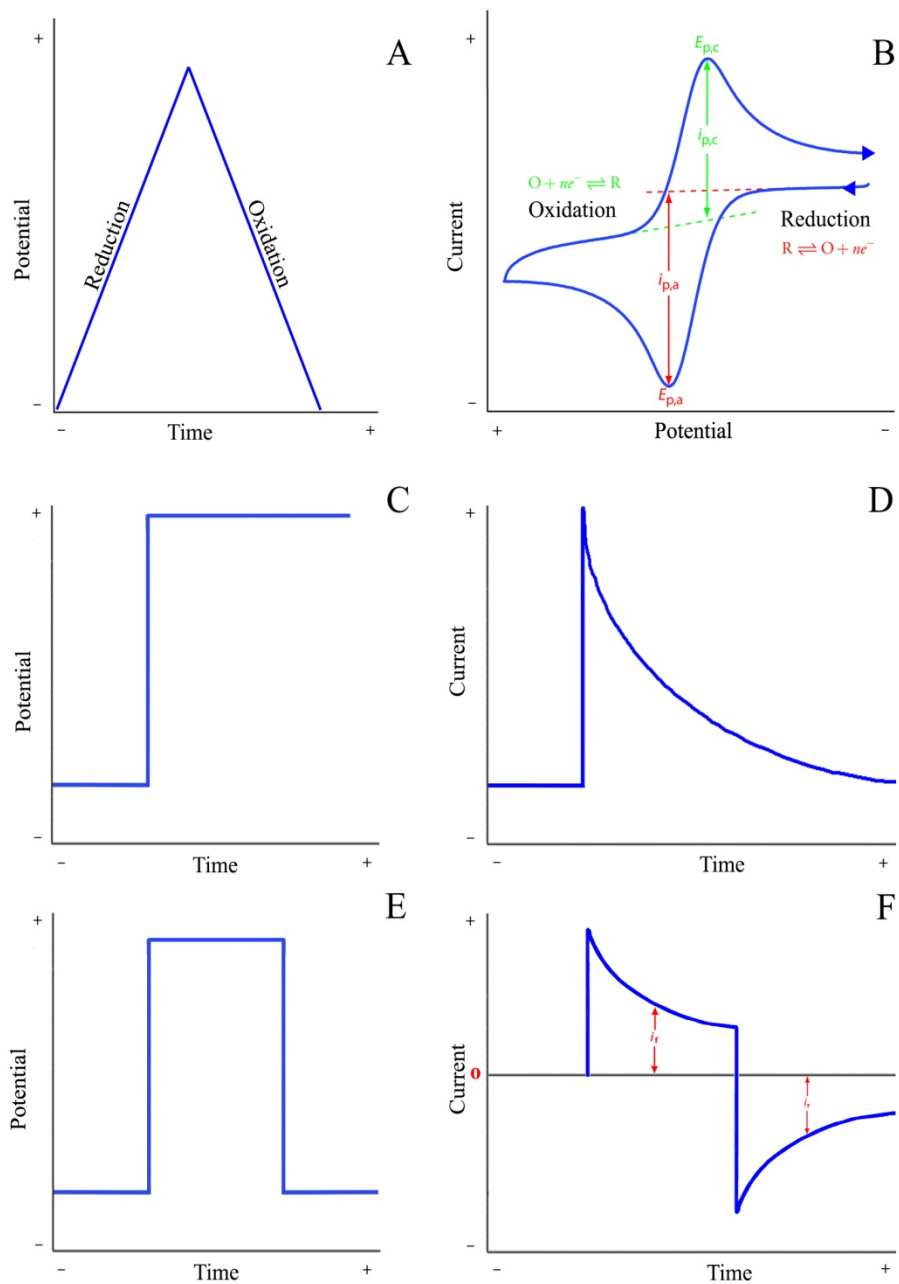


Figure 3.2 Illustration of Cyclic Voltammetry and Potential Step techniques.

This biphasic pulsed current generator with +/- 0.5mA current amplitude and frequency of 5Hz has shown a successful NT-3 release for 7 days. [78] The same generator with +/- 1mA and frequency at 250 Hz has also indicated the potential application to produce a long- term releasing profile by Ppy conductive polymer. [58,59,60] The most significant drawback of biphasic pulsed current stimulation is that it requires the direct contact of the electrode with the drug-doped polymer. This is not required in our EMF method. Our electromagnetic generator was designed to simulate the drug release without any physical contact to avoid any potential invasion to tissues during clinical application.

3.1.4 Electromagnetic Field in Biological and Medical Studies.

The inductive coupling of pulsed EMF technique has revealed an emerging and substantial clinical application in tissue repair, dominantly in orthopedic application and wound healing. A large number of studies had shown the physiological efficiency of electromagnetic-based clinical devices. The majority of these investigations used extremely low frequency electromagnetic device exposure. Moreover, these devices have been shown to be physiologically effective usually up to 20 Gauss peak time-changing magnetic fields and up to a 150mV/cm for peak induced electric field at the treatment sites. For example, some studies have suggested that the combined application of alternating and static magnetic fields with low frequencies might alter the binding kinetics and result in the changes of ion or ligand movement in the binding site. [82] Pulsed EMF also has shown the potentials to exert an anti-inflammatory action, alleviate pain in arthritis and degenerative joint injuries. [83]

Not only extremely low frequency electromagnetic devices used in biological study, pulsed radio frequency devices were also exploited in some application. The induced electric field from a pulsed radio frequency devices at orders of magnitude larger, which is approximately between 10 and 40 MHz. Among many biological therapeutic strategies, cancer treatment commonly associated with radiofrequency devices because it can raise the local body or tissue temperature to a desired level (effective temperature range would be 42-45°C) to cause hyperthermia and destroy the tumors. The application of electromagnetic field in drug delivery system was commonly conducted with magnetic nanoparticles, or many temperature- sensitive materials. [84] These earlier studies did not investigate the response of conductive polymers to EMF, therefore, in our work, we concentrated on the action of Ppy EMF exposure and its potential applications.

Concerns regarding the safety of EMF exposure to human body were also arised as the developing the EMF associated medical application. The available data from IITRI(US), IAF(Canada) and MKI(Japan) showed no evidence regarding to EMF related general toxicity, including epidemiologic studies for occupational EMF exposures and experimental studies for both animals and humans. In teratology studies, there has no results indicating decreased in fertility in male or female animals that receiving EMF exposures. The possible role of EMF in immunotoxicity studies and carcinogenesis have also been thoroughly investigated. The results of these studies reveal that there are no observable deficits in lymphoid organ cellularity or histology and T or B cell function after exposed to the EMF field. There are few studies indicated the significant suppression of NK cell function, but only in female mice, not in the case of male mice or female and male rats. In some biochemical based experiment, extremely low frequency

magnetic field (60Hz, 50 Gauss) combining with 100 μ m H₂O₂ showed a decreased number of viable cells after 24 hours exposure time, however, there is no Bax and Bcl-2 protein level or activation of caspase-3 apoptosis signaling were observed. [85] Combination of other noxious element (such as H₂O₂, FeCl₂, or UVA) together with a long-term EMF exposure could generate ROS, [86,87] but not for a short time exposure. Zmyslony and others tested the effects of EMF with radiofrequency to the production of ROS and showed that the 15mins of radiofrequency exposure did not alter the production of ROS.[88]

3.2 Methods and Materials

3.2.1 Configuration of the Electromagnetic Field Stimulator

Multiple factors must be considered when designing the EMF stimulation system and pulse conditions. These parameters include waveform shape, pulse duration, pulse magnitude, duty cycle, etc. Three-way switchable magnetic field stimulator was custom made for the purpose of this study. This device is an integrated system with asymmetric, symmetric, and pulse train three different waveform conformations (Illustrated in Figure 3.5 and 3.6), and a professional electronics schematic is provided in Figure 3.3. We chose square waveform to maximize the induced electric fields within the Ppy since that is the hypothesized stimulus for drug release. The coil was made of AWG 16 copper wire with 15 turns, and its geometry of the coil was build at the size of 3.0cm (W) x 3.8cm (L) x 1.2cm (H) (See Figure 2.5). The coil was then stimulated with a pulsing regime using a custom made circuit. Each input pulse was only “on” long enough to saturate the coil

(pulse width at 500ns), and then turned off for the duration required to completely unload the coil ($\sim 10\mu\text{S}$) (See Figure 3.6). Therefore, the duty cycle was approximately 4.8%, and other two stimulation patterns are also maintained a $\sim 5\%$ duty cycle. For comparison, sawtooth waveform shown in Figure 3.8 is also studied. This generator can be designed by various ways, in our case, it composes of NPN and PNP transistors show in Figure 3.4.

3.2.2 Electromagnetic Field Measurements

Using the waveform patterns shown in Figure 3.5 as the input signal, the real time magnetic and electric field output from the stimulation coil were measured using high frequency EMC 100B (magnetic) and 100D (electric) probes (Beehive Electronics, CA). Probes were connected to a Tektronics TDS 2012B oscilloscope and terminated with a 50Ω resistor. For data collection, each probe was positioned and oriented in the stimulation coil center for maximum expected reading. This value was taken to be the output probe value and converted to dBm. The recorded data points from the oscilloscope were imported into MS Excel in which the Fast Fourier Transform (FFT) of the waveforms was calculated. From the FFTs, the fundamental frequency, along with the output dBm power value was used with the antenna gain equation provided for each probe to estimate AC field magnitudes.

3.2.3 Antenna Gain Equations

The antenna gain equations used to convert EMF probe voltage into the corresponding magnetic and electric fields are as described:

For magnetic field (100B) probe:

$$P_{out} = 42.2 + 20\log(B) + 20\log(F)$$

Where

B is the magnetic flux density, in tesla

F is the frequency of the received signal, in megahertz

P_{out} is the probe output power into 50 ohms, in dBm

For electric field (100D) probe:

$$P_{out} = -113.2 + 20\log(E) + 20\log(F),$$

Where

E is the electric field strength, in volts/meter

F is the frequency of the received signal, in Megahertz

P_{out} is the probe output power into 50 ohms, in dBm

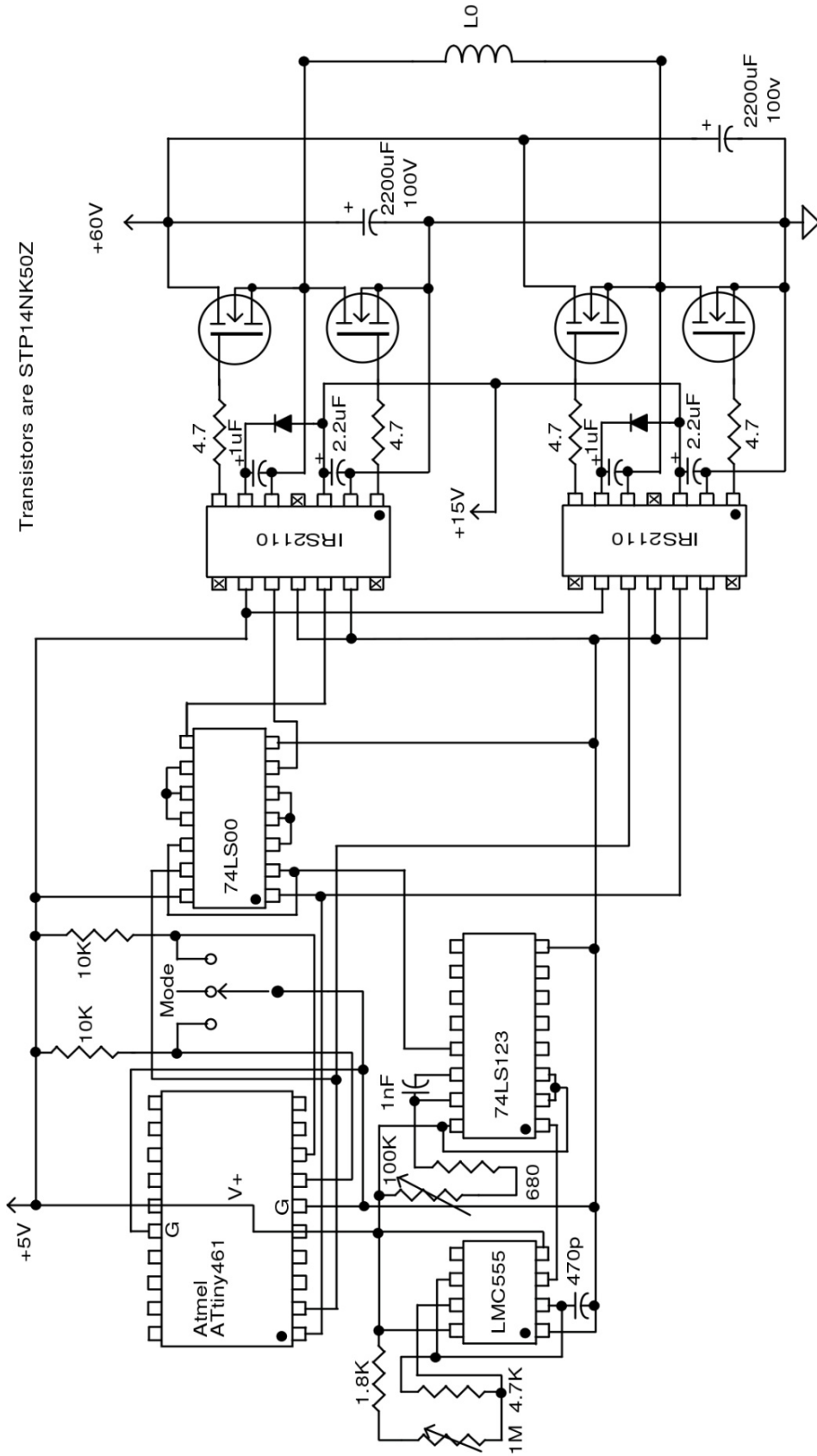


Figure 3.3 Schematic figure for three-way square waveform generator.

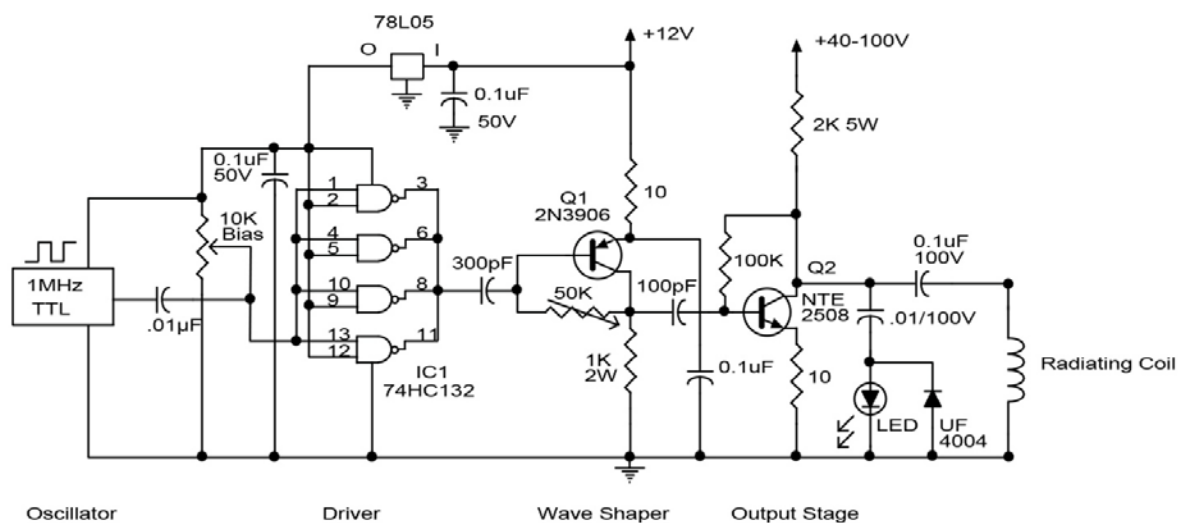


Figure 3.4 Schematic figure for sawtooth generator.

3.3 Results

3.3.1 Electromagnetic Field Characteristics.

The real-time magnetic and electric field output waveforms at the coil center were plotted in Figure 2.5. The measurements revealed that the magnetic field output was similar to the input field, with some oscillation noise present in the square waveform. FFT decomposition of the measured signal showed the fundamental frequency of the magnetic field was to be 3.2MHz. This converts to average peak amplitude of 36 Gauss when using the antenna gain equation. Moreover, the amplitude of the magnetic field did not vary by more than 20% within the coil. The highest field amplitudes were in the x-y plane at the center level of z-axis. Along the z-axis, there was a small drop-off in intensity as the probe was moved away from the coil center. Overall, the magnetic field surrounding outside the coils has weaker signals at a order of cubic decay. Therefore, all

Ppy drug release experiments were applied within the coil and exposed to peak magnetic fields roughly within the range of 25-40 Gauss.

Similarly, the raw electric field data is also depicted in Figure 2.5. Note that the measured electric field corresponded to the measured magnetic field, as expected by Faraday's law. The electric field waveform exhibited oscillatory behavior with sharp peaks primarily concentrated at the "ramp-up" and "switch off" phases of the EMF. The peak E-field of was measured at 4700V/m with a fundamental frequency of 65MHz. Thus, the estimated electric field magnitude in which the Ppy film positioned is in the 3000-5000V/m range. The time-averaged EMF values are lower when considering the duty cycle, and would be less than 5% of these values. The distance dependence of the electric field from the coil center is similar to that of the magnetic field.

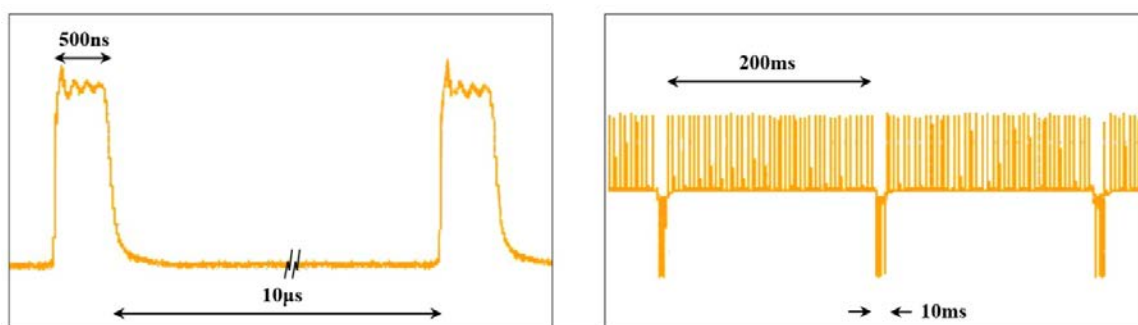


Figure 3.5 The input signal generated by asymmetric waveform stimulation. 500ns pulse duration were spaced 10µs apart. These pulses were in the positive direction for 200ms and then alternated to the reverse polarity for 10ms.

3.3.2 Drug Release by Square Waveform Stimulation

The geometry of the signal can highly influence how effective they create the biological, chemical, or physical responses. In our study, to compare the efficiency of drug releasing, the releasing profile of DEX conjugated flat Ppy – AuNps films using train waveform and symmetric waveform were also performed (See Figure 3.6). In both cases, pulses of duration were spaced $10\mu\text{s}$ apart which is the same as that of asymmetric waveform. The difference is that there is no reversed stimulation in the case of train waveform. For symmetric waveform, the pulses are in the positive direction for 200ms and then alternated to the reverse polarity for another 200 ms. EMF measurements for these two waveforms were conducted as the study of asymmetric waveform. To define the most effective electromagnetic fields, we compared the DEX release using these two square waveform configurations to the results of asymmetric waveform. (See Figure 3.7).

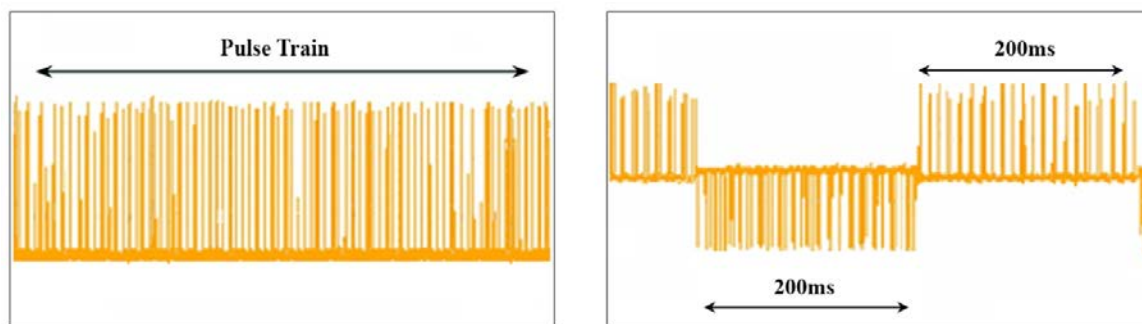


Figure 3.6 Illustration of input signals in the case of pulse train (left) and symmetric waveform (right). There is no reversed stimulation for pulse train waveform. The pulses in symmetric waveform have same stimulation duration (200ms) in both positive and negative direction.

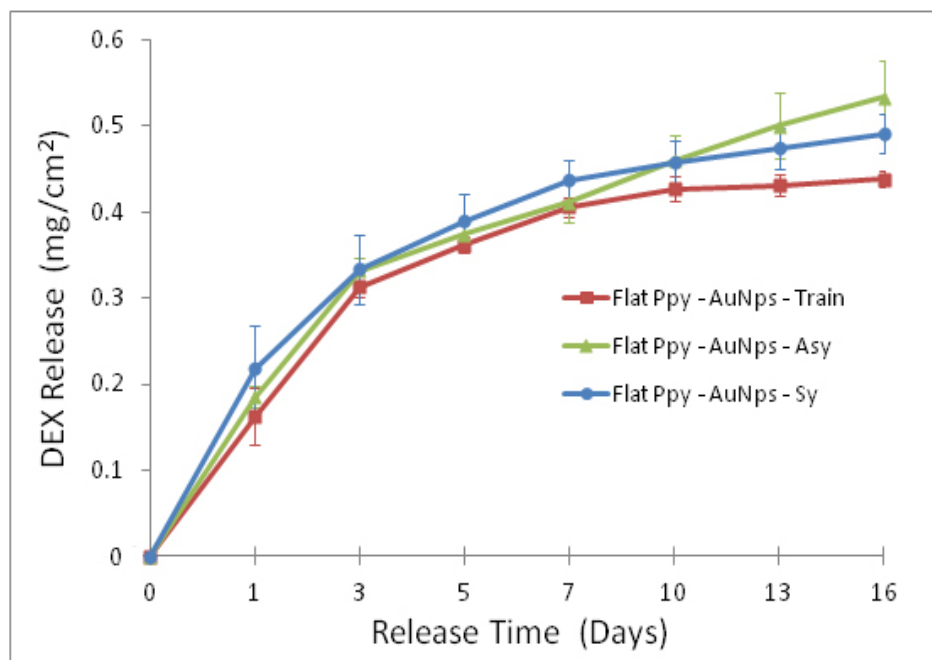


Figure 3.7 Comparison of DEX release from flat Ppy–AuNps films using pulse train, asymmetric, and symmetric waveforms.

According to the results, there is no statistical difference between these three cases. It could be due to the magnitude of peak magnetic field and electrical field of these two waveforms were similar to that of asymmetric waveform.

3.3.2 Drug Release Using Sawtooth Waveform

To optimize the drug release, we also developed an electromagnetic field generator that could produce a sawtooth waveform. The sawtooth waveform can be considered as an extreme case of asymmetric triangle waveform. The magnetic field produced on the wave's ramp and collapses on the wave's cliff (Shown in Figure 3.8 left) where induced

the maximum level of electrical field. Since the magnitude of saw tooth pattern increase very sharply, it can produce a strong electromotive forces (Figure 3.8 right), but the polarization of electric field cannot be determined using sawtooth potential.[89]

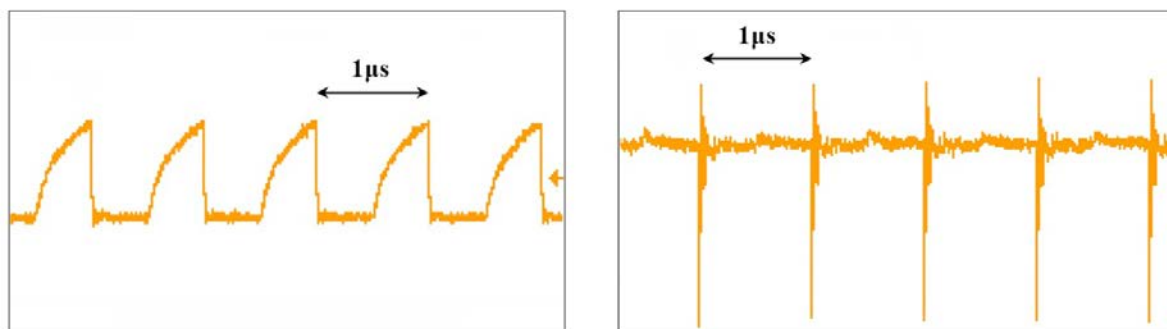


Figure 3.8 Illustrations of the input signal of magnetic field (right) and electrical field (left) for sawtooth waveform.

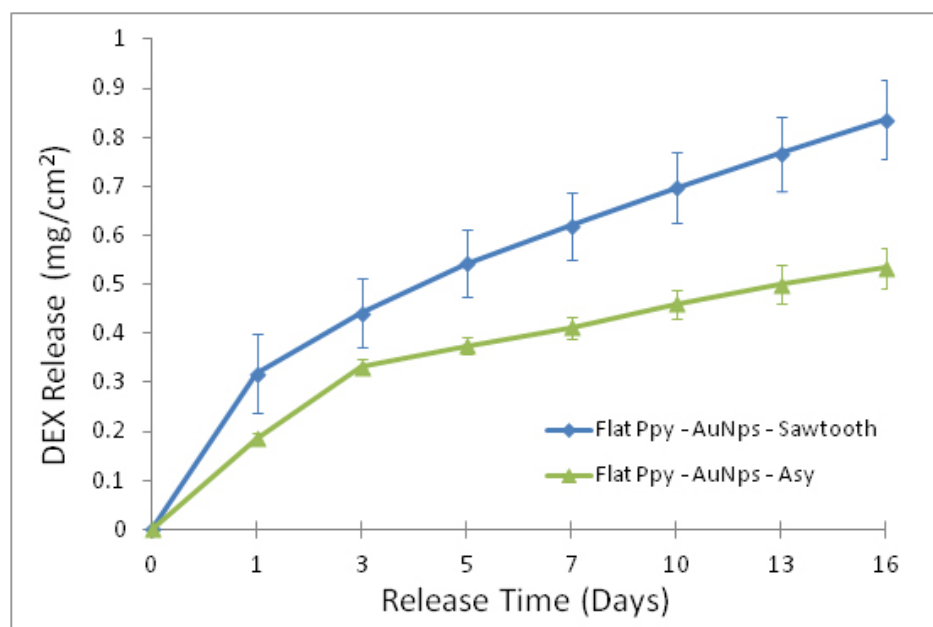


Figure 3.9 DEX release comparison between EMF stimulator with sawtooth waveform (blue) and with pulsed square waveform configuration (green).

Increased amount of DEX release was clearly observed using sawtooth wave stimulator from day 1 to the end of the experiment (See Figure 3.9). However, there was no statistical significant difference between the square wave and the sawtooth wave at any point of the experiment. At day 16, the p value for statistical analysis was calculated as 0.06 using independent student t-test with assumption of normal distribution. A increased trend of the DEX released using sawtooth waveform was observed compared to that of the square waveform. It kept a the constant increasing level during the testing, indicating the excessive DEX release of each sample under sawtooth wave based stimulation.

3.4 Discussion

Since the cells usually are at a condition of highly conducting ionic medium, it has been proven that they can response to the electrical field and their biological effects are greatly influenced by ion displacement in the body. In general, this ion displacement occurred due to the peak voltage value also represented as the electromotive forces. This electromotive forces can be initiate at abrupt "falling " time in a given pulsed signal, depending on the electrical characteristics of the coil employed, the shape or waveform of the electromagnetic signals, and how fast the rising and falling time changes. Among various waveforms, both sawtooth and square signals are far more abrupt than the simple sine waveform. The advantage of sawtooth pulse form is that it simultaneously contains various individual sine vibrations with broadest frequency and amplitude. These can composed of the similar frequency and amplitude of oscillating wave from cell

membrane. In this case, cell membrane can respond to the resonate frequency which similar to the cell's natural frequency. This waveform is first introduced by Dr. C.A.L.Bassett and proved by FDA for the treatment of non-union fractures and assist spinal fusion operations. This is based on Faradays' law we described earlier, that is: changes in the electromagnetic signals can induce an electrical current, and the maximum current induces when the magnetic flux changes most abruptly. Since the intensity of electric field is dissipating from the center of the coil in our case, the higher level of induced electrical field generated from alternating magnetic field may compensate the negative impacts of the distance. In this case, the actual penetration capability of the induced current can be critical for this drug delivery system to be used in clinical applications, and it usually refers to the standard depth of penetration equation. This penetration involves with several parameters. The penetration decreases when eddy current at a higher frequencies travelling through a materials with high conductivity and permeability. Since redox property of Ppy requires highr conductivity in order to release the drugs, we need to adjust the stimulator to larger coil size and lower pulse frequencies in order to achieve an increased penetration of both magnetic field and current flow. Therefore, we would not be limited during in vivo application because of the larger tissue depth.

CHAPTER FOUR
ATTENUATION OF SECONDARY INJURY
BY ELECTROMAGNETIC RESPONSIVE POLYPYRROLE DRUG DELIVERY

4.1 Introduction

4.1.1 Cellular, Molecular, and Biochemical Cascades in Spinal Cord Injury

4.1.1.1 ROS and RNS

Collected evidences have identified that the activation and accumulation of resident microglia and infiltrating macrophages after spinal cord trauma can cause inflammatory and immune responses which can amplify the destruction. Macrophage and microglial cells can be activated by different endotoxins or cytokines, such as TNF- α , lipopolysaccharide (LPS, a component of the wall of Gram-negative bacteria), and a combination of interferon γ (IFN- γ) and LPS, or H₂O₂. Then, they can trigger various inhibitory molecules, such as IL-1 β , TNF- α , nuclear factor-kappa B (NF- κ B), nitric oxide (NO), and ROS which initiates a cascade of neuropathological events and results in the cellular death via necrotic or apoptotic pathways. In our study, we focused on the RNS and ROS production due to the suppressive ability of DEX to them (See details at 4.1.2) and their detrimental effects to SCI. These can be used to test drug delivery efficiency in vitro and in vivo studies.

During the activation of macrophages, inducible nitric oxide synthase (iNOS) utilizes oxygen and electrons from nicotinamide adenine dinucleotide phosphate (NADPH) to oxidize the catalytic substrate L-Arginine into NO. NO and superoxide ($\bullet\text{O}_2^-$) are radical effectors of the innate immune system that helps to inhibit the growth of invading microorganisms. Although NO is an anti-bacterial and anti-viral effector and can protect the brain and spinal cord from certain infectious diseases, excessive levels of NO can also be toxic to neurons and could cause neuroinflammatory conditions after SCI. Many studies have suggested that synergistic reaction of NO and superoxide can produce cytotoxic molecules peroxynitrite (ONOO^-) which can readily oxidize nucleic acids, proteins, and unsaturated lipids [90,91] causing neuronal cell death in SCI. [92,93,94,95] Furthermore, reactive intermediates of over-expressed iNOS are mutagenic and would not only lead to DNA impairment but also results in the growth of tumors in CNS.

Suppressing ROS production also critical in SCI because they contribute to lipid peroxidation by attacking the cellular membranes, especially to polyunsaturated fatty acid, and many other macromolecules, such as protein and nucleic acid, leading to the neuron death. ROS usually refers to small molecules $\bullet\text{O}_2^-$, hydrogen peroxide (H_2O_2), and hydroxyl radical ($\bullet\text{OH}$) that are generated during the electron transfer process of mitochondria as well as the unstable intermediates during the lipids peroxidation. The hydrogen peroxide is generated from superoxide via superoxide dismutates. Hydrogen peroxide can either be converted to a strong toxic oxidant hypochlorous acid by myeloperoxidase (MPO) or converted to highly reactive hydroxyl radical during the Fenton reaction, or converted to water and oxygen becoming non-toxic when catalyzed by catalase and glutathione (GSH) peroxidase. Aerobic organisms can reduce molecular

oxygen (O_2) in water to create energy. During this process, partially reduced oxygen species are inevitably generated, such as superoxide, which is not detrimental in low concentrations. However, an abnormally excessive production of various ROS causing an imbalance between radical generation and scavenging which will actually cause damage. This imbalance is represented as oxidative stress and always occurs after SCI. Since radicals have an unpaired electron, they can become highly reactive with any macromolecules and damage them by modifying their structures and/or functions.

4.1.1.2 ROS and RNS

Associated Mitogen-activated Protein Kinases Signaling Pathways

It has also been implicated that the cascade of secondary damages in SCI is closely involved with the regulation of mitogen-activated protein kinases (MAPKs) signaling pathways. [96] Phosphorylation of MAPKs on a specific activation loop which contains a characteristic threonine-x-tyrosine motif active three principal subfamilies of MAPKs signaling pathway: extracellular signal-regulated kinases (ERKs), p38*mapks*, and c-Jun NH₂-terminal kinases (JNKs) or stress-activated protein kinases (SAPKs). Thus, the initiation of the subfamily of MAPKs in the study of secondary injury after SCI was critical. [97,98] They especially play an important role in NO associated deterioration of neuronal activity in the SCI. [99] Therefore, the inhibition of MAPKs family signaling pathway implies the physiological importance to neuronal recovery after traumatic injury. In a microglia-neuron co-culture condition, p38 and JNK inhibitors can partially rescue neurons from death after LPS challenge. [100] Also, inhibiting ERK1/2 pathway may

eliminate cortical neuron damage after IL-1 insults. Administration of the specific inhibitor of MAPK3/MAPK1 (PD98059) significantly improved motor functional recovery. These evidences demonstrate that the activation of MAPK highly influence the secondary injury after spinal cord trauma. [96]

The activation of MAPK can be initiated by the ROS related oxidative stress, and ROS blocking approaches have showed the inactivation of this MAPK signaling pathway.[101,102] This ROS mediated activation can be due to oxidation of growth factors, oxidative modification of intracellular kinases, such as thioredoxin, and down-regulation of inactive members in MAPK pathways, such as mitogen-activated protein kinase phosphatase 1 (MKP-1). [102,103,104,105,106,107] There is an abundance of literatures reporting that the activation of several MAPK families signaling pathways including ERK1/2, ERK 5, JNK, and p38 can be initiated by H₂O₂ and then generates ROS.

The MAPKs have also been shown to be involved in activating many transcription factors and directing cellular responses to various noxious stimuli, for example, proinflammatory cytokines. The transcription regulation of iNOS has been reported to involve with JNK pathway by IFN- γ +TNF- α . [108,109] Further studies have indicated that the LPS or combination of IFN- γ and LPS stimulated ERK and p38 mapk cascades of signaling molecules regulate the induction of iNOS in glial cells. [110] Thus, we designed our experiment using LPS and H₂O₂ as stimuli to initiate iNOS and ROS via MAPK signaling pathway.

Dexamethasone, as a well-known anti-inflammation drug, has shown its successful regulatory effects on inflammatory responses. It has also been known to antagonize LPS-induced JNK/SAPK pathway via inhibits the production of cytokines, TNF- α , [111] and partially limit the pro-inflammatory gene expression by inducing the expression of MKP-1.[112] Suppression of NF- κ B activation by glucocorticoids can result in iNOS down regulation in some cells line .[113] Further results indicate that the suppression of LPS activated MAPKs by dexamethasone blocks the iNOS expression and ROS production. [114] The different concentration of dexamethasone between 0.1 to 10 μ M has been proved to inhibit the expression of iNOS in a dose-dependent manner when applied to primary cultured rat hepatocytes, [115] vascular smooth muscle cells, [116] murine macrophages, [117,118] and activated microglia. [114] In primary microglia culture, the NO production can be suppressed to 50% and iNOS protein and mRNA expression can be downregulated to 70% by administration of DEX. [119] All the supportive evidences showed a well-established in vitro model for testing the DEX release from Ppy using our non-invasive EMF stimulator.

4.1.2 Evidence of Neuronal Recovery by Inhibition of iNOS and ROS

The enhanced production of ROS and NO has been reported to associate with neuronal death after SCI. Among the ROSs, H₂O₂ and OH \cdot are known detrimental effectors for oxidative damage. Antioxidants and antioxidant enzyme can inhibit ROS and ameliorate motor neuron damage and dysfunction after SCI. [120,121] The potential pathophysiological role of elevated iNOS level in SCI has been investigated in many

studies and many experimental models indicate that the inhibition of over-expressed iNOSs during earlier phase of SCI leads to a modest functional recovery. (See Table 4.1)

Table 4.1 iNOS inhibitors and their neuroprotective results.

iNOS inhibitor	Charateristics	Results	Ref.
Cyclosporin-A (CsA)	Protect damage tissue from lipid peroxidation (initiated by free radicals) and reduce the formation of RNS, such as peroxynitrile.	A significantly better myelination index, motor recovery, red nuclei neurons survival, and axon growth.	[122]
Aminoguanidine (AG)	Nucleophilic hydrazine compound, selective inhibitor, more effective at inhibiting the enzymatic activity of iNOS than eNOS and nNOS.	Decreased lesion volume and significant recovery of rat hindlimb motor function after spinal cord injury.	[123]
Flavokawain A	Significantly inhibited LPS-induced activation of JNK and p38 MAPK signaling pathway via NF- κ B and AP-1.	Reduce iNOS expression and many pro-inflammatory cytokines in macrophages, such as TNF- α , IL-1 β , and IL-6.	[124]
Nomega Nitro-L-arginine-methyl ester(L-NAME)	Non-selective competitive inhibitor of NOS, associate to the L-Arg binding sites, usually as L-Arg analogues.	Results in reduction of necrotic volume and damaged cells in the lesioned area.	[125]
3-bromo-7-nitroindazole	Selective nNOS inhibitor and potent against iNOS	Significantly decrease contusion volume after traumatic brain injury.	[126]
Pyrroloquinoline quinone (PQQ)	Oxidized the redox modulatory site of N-methyl-D-aspartic acid receptor. The production of NO complicate this receptor mediated neurotoxicity.	Significantly decreased lesion size and increase axon density and promote the functional recovery of SCI.	[127]
NOS knock out mice	iNOS gene deficient.	A gradual improvement of motor function and no observation of delayed neuron damage.	[128]
ASOs	iNOS antisense oligonucleotides.	Significantly decreased iNOS positive immunoreactive cells and retard neuronal cell death at the injury site.	[129, 130]
N-[3(Aminomethyl) benzyl] acetamidine (1400W)	Selective iNOS inhibitor.	As the results as ASOs treatment, but less effective. Negatively regulate the LPS activated macrophages.	[131]

4.1.3 Glial Cells in Spinal Cord Injury

The spatial and temporal glial activation can further complicate and intensify the detrimental effects after initial physical damage at spinal cord, resulting in secondary sensory and motor impairment. Many previous studies reported a variety of astrocyte and microglial activation patterns in regards to different injury models, locations, and methods.

[132] The summary is illustrated in Table 4.2.

Table 4.2 Glial responses after SCI.

Sites	Animal	Injury Methods	Glial Response After SCI	Ref.
Spinal Contusion Injury				
T10	Rat	NYU-MASCIS	Astrocytes: start day2 and decreased till day30	[133]
T10	Rat	IH Imapctor	Glial:persistent activation for 2hrs-3months	[134]
T12	Rat	Metal Rod (2mm in diameter, weight 30g)	Microglial:1-12wks	[135]
Spinal Cord Compression Injury				
T11	Rat	Clip Compression	Astrocytes and microglial: start at day1	[136, 137]
T8	Mice	OSU-ESCID (Eelectromagnetic Device)	Astrocytes: day2-1month	[138]
Spinal Hemisection/Hemitransection Injury				
T13	Rat	Adjustable wire knife, right lateral hemisection	Astrocytes and microglial: day7 persistent to 3months	[139]
T12	Rat	Micro-scissor, left lateral hemisection	Microglial: start at day 1; Astrocytes: day3-over 4wks	[140]
T8/9	Rat	Micro-scissor, right dorsolventral hemisection	Microglial: day2- over 3wks	[141]
Spinal Ischemic Injury				
T8	Rat	Argon laser beam with 560nm wavelengths after rose bengal injection	Astrocytes and microglial: start at day2	[142]
T8	Rat	8kLux illumination with halogen lamp after rose bengal injection	Astrocytes: <1hr-2wks	[143]
T8	Rabbit	Argon laser beam with 560nm wavelengths after rose bengal injection	Astrocytes and microglial: start at 2hrs	[144]
Spinal Excitotoxic Injury				
T7	Rat	NMDA-induced	Astrocytes and microglial: start at day1	[145]
Right striatum	Rat	Quinolinic Acid (NMDA Receptor agonist)	Astrocytes and microglial: start at day1 and developed from day 7 to 1month	[146]

4.1.4 In Vivo Applications

In neuroscience study, various prosthetics and medical devices are commonly used to assist the patient with traumatic injury or other neurodegeneration diseases and neurologic disorder. Recording/stimulating electrode arrays often accompanied with these devices either to stimulate the neural connection and muscle movement or to analyze the encoded information from neuronal tissues. Because these devices can be invasive to the tissue and causes negative impacts on patients, the local delivery of anti-inflammation drug could be an appropriate approach to optimize the conditions. The local drug delivery generally can be used to achieve high concentration drug administration at targeted site while minimizing risk of side effects. Many studies have shown the anti-inflammation treatment of DEX in many implantation cases. DEX released from nitrocellulose-based coating materials on silicon neural probes can facilitate a long-term recording without accelerating the glial scar formation around the recording sites. [147] Other researches also have unveiled the potentials of DEX local delivery to eliminate the activation of microglia, macrophages (stained by ED-1), and CSPG expression (stained by CS56) one week after implantation. In addition, the number and density of reactive astrocytes evidenced by glial fibrillary acidic protein (GFAP) staining were also remarkably reduced by DEX release at both 1 week and 4 weeks after probes invasions to brain, indicating local treatment of DEX can reduce astroglial over-responses.[147]

In addition to microglial and macrophages, astrocytes are indispensable component to modulate the inflammatory processes of neurological disease and neurotrauma.

Astrocytes produce many inflammatory chemokines, such as KC (also known as CXCL1), and MIP-2 (CCL2), immediately after injury and responsible for the early neuroinflammation.. The over-activation of astrocytes was also contribute to the inhibitory molecules, including of tenascin, semaphoring 3, ephrin-B2, slit proteins, and a CSPG after SCI. Especially for proteoglycans, it is believed that it creates the nonpermissive environment for axonal regeneration. Under the presence of these inhibitory molecules, the axons from peripheral regions are unable to reach to the damage site of spinal cord and end up to a dystrophic state causing the regeneration failures. [148] We can say, the neuronal activity are mostly likely to be interrupted or inhibited not only by mechanical boundary but also by the production of inhibitory molecules induced from activated astrocytes. [149,150] Manipulating the environment of the extracellular matrix and attenuating the production of inhibitory molecules would provide an opportunity for a successful neuronal recovery.

Astrocytes reactivity and reactive astrogliosis were usually characterized as increases in GFAP level which occur rapidly after CNS injury, GFAP was generally considered as an indicator of alternations in astrocyte phenotype. The severity of astrogliosis is classically determined based on the morphology, numbers, and levels of GFAP and vimentin expression. [151] Therefore, the massive up regulation of GFAP was associated with the increased spread of inflammation in response to all CNS injuries and disease. One previous study described that the proliferation of immunoreactive GFAP expressed reactive astrocytes increased as the motor neurons in lower spinal cord of mice progressively deteriorated. [152] Inhibition of over-activated GFAP positive astrocytes can promote white matter preservation and axonal sparing, allowing an improved

functional recovery after SCI.[153] The actual role of GFAP was also exploited along with astrocytes study in CNS. It is believed that GFAP, as intermediate filament in astrocytes, contributes to the maintenance of myelination and structuration of white matter,[154] but also glia scar formation with vimentin. One study based on cultured neonatal astrocytes which are believed to have similar characteristics of reactive astrocytes unveiled that the inhibitory function of GFAP on neurite growth. The study using a GFAP null mice models response to direct injuries didn't suggest the different degree of scar tissue formation or improved neuron production compared to wild type mice, but showed the poor scar formation in the case of neurotoxins application, infection, Alzheimer's disease, and multiple sclerosis.[155]

Since activation and reactive gliosis indicated by increased GFAP intermediate filament proteins proliferation, we used a GFAP-luc mice as animal model, which can express upregulated GFAP signals after SCI, to detect the release of DEX in vivo studies as well as its therapeutic effects for neuroinflammation treatment.

4.2 Materials and Methods

4.2.1 ROS Production in Challenged and Treated Microglial Cells.

The microglial BV-2 cells were maintained in Dulbecco's modified Eagle's medium (Sigma-Aldrich) containing 10% fetal bovine serum, 100 IU/ml penicillin, and 100 µg/ml streptomycin at 37°C in a humidified incubator with 5% CO₂. Cells were harvested by trypsinizing and reseeded in 12-well plate for 24 hours at cell density of 1*10⁶. They were then incubated with 1µg/ml Lipopolysaccharides (LPS; Escherichia coli 026:B6

from Sigma-Aldrich) for 6 hours, and followed by 1 μ g/ml DEX treatment for 1 hour. In addition, approximately 30-40 mm² size of PpyNWs-AuNps films were placed in cell culture and stimulated for 30 minutes or 1 hour by pulsed EMF after LPS challenge. The similar procedures were also applied to another group at exception of no stimulation of EMF. For control groups, cells were only received six hours of LPS challenge. Then all cells were trypsinized, centrifuged, and resuspended in PBS containing 10 μ M oxidative stress indicator (CM-H₂DCFDA, Molecular Probes). Suspended cells were then placed into the incubator for 1 hour, then the production level of ROS was detected using the fluorescence plate reader. ROS expression was also imaged by a fluorescence microscope with an X-Cite series 120PCQ fluorescence illumination source (Olympus IX 81 inverted). Moreover, another strong oxidizing reagent, hydrogen peroxide (H₂O₂) was used to confirm the LPS results. The experiment was based on the company instruction for OxiSelect Intracellular ROS assay kit (Cell Biolabs, Inc.) Briefly, BV-2 cells were seeded in black 96-well plates for 12 hours and then incubated with 1mM DCFH-DA solution for 1 hour. The medium with 20 μ M hydrogen peroxide was then placed in each wells except the ones for control groups and incubated for 30 minutes. DEX treatments were applied for another 15 minutes after discard hydrogen peroxide contained medium. To evaluate DEX release by EMF stimulation, the PpyNWs-AuNps films placed in the wells for a 15 minutes stimulation. The fluorescence signals of all samples was then read using a fluorescence plate reader. In all instances, the coil was placed below the culture plate during the EMF stimulation.

4.2.2 Immunofluorescence Labeling Assay.

BV-2 cells were cultured on Poly-D-lysine (Sigma) pre-coated round cover glass (#1.5 thickness, 12 mm) in 12-well plates for 24 hours. After applying LPS, DEX, and released DEX, BV-2 cells were fixed at room temperature for 30 minutes using 4% paraformaldehyde solution. Then, the cells were incubated in 1% albumin from bovine serum blocking buffer for 1 hour, and subsequently incubated in primary antibody solution containing anti-nitric oxide synthase II antibody (EMD Millipore) (1:400) overnight at 4 °C. Next day, diluted Cy3 conjugated goat anti-rabbit IgG antibody solution (EMD Millipore) (1:100) were applied to cells for 2 hours. Dried cover glasses were mounted on glass slides using vectashield hardset mounting medium with DAPI (Vector Lab). These samples were all imaged with a confocal microscope (Leica SP5 /STED /MP System).

4.2.3 Surgical and Treatment Procedures

The demonstration of surgical and treatment procedures are shown in Figure 4.3. All aspects of animal care and treatment were carried out according to the guidelines of Purdue Animal Care and Use Committee (PACUC). Female GFAP-luc transgenic mice were purchased from Taconic. Surgery began when mice reached the age 9-12 weeks old and their weight was above 22g. Animal anesthesia was applied by intraperitoneal injection with ketamine 90 mg/kg and xylazine 10 mg/kg. All the mice then received a bilateral, hemilaminectomy procedure at low thoracic region. The dorsal surface of the dura mater was exposed at a size of approximately one third of the cord. SCI was induced

by clamping to exposed cord under stereoscopic illumination. For Ppy control and Ppy treatment group, the DEX doped polypyrrole films was lifted on a drop of sterile saline and deposited on the dorsal domain of injured spinal cord. The lesion was surgically closed in layers, and then skin were closed and sutured. Animals were then moved to their individual cage and warmed with incandescent lights until recovery. Also, all mice were received buprenorphine HCl after surgery and the next day.

The control group only received the SCI. Sham-treated animals (Ppy control group) possessed DEX doped PpyNWs, though the polymer was not exposed to the EMF stimulation. For Ppy treatment groups, the first treatment of released DEX by EMF stimulation was conducted within three hours after surgery. During the treatment, the coil was positioned over the arch of the animal's back and brought to the surface of the epicenter of spinal cord lesion site when animal were under isoflurane anesthesia. (See Figure 4.3) The highest intensity of the EMF was roughly at the center of coil. Stimulation of EMF was applied 2 hours daily for seven days. The mice were euthanized and followed by fixation perfusion at seven days after injury. Two animals were euthanized before 7 days due to the condition of animals self-damaging their rear limbs, and they were replaced, prior to the end of the experiment.

4.2.4 Whole Animal Bioluminescent Imaging

At day 1, 3, and 7 after spinal cord injury, mice were imaged using Caliper IVIS Lumina II at the Purdue Multi-scale Imaging Center (MUSIC). One of common luciferase substrates, D-Luciferin - K⁺ Salt Bioluminescent Substrate (Perkin Elmer) at 15mg/ml in DPBS was freshly prepared and all mice received intraperitoneal injection at 10 μ l/g of body weight before imaging. All mice underwent imaging during short period of immobilization under isoflurane anesthesia. Luciferin kinetic study was performed with peak wavelength at 560nm and the maximum signal was determined between 18-22 minutes after luciferin injection. The quantitative data of luminescent density were confined at the region of interest (ROI) around spinal cord region and also analyzed with setting at the range of 9.5e5 to 1.2e7 p/sec/cm²/sr. A automatic ROI measurement methods is used to identify the bioluminescent emission automatically with fixed threshold.

4.2.5 Statistical Analysis

All the data are shown with standard error of the mean \pm SEM. Comparative independent student's *t* test, Tukey's HSC multiple comparisons tests were used for in vitro studies, and one way ANOVA followed up with three Fisher's LSD post hoc were used for in vivo study to detect the statistical significance. Statistical significance were determined by a P-value \leq 0.05. Prior to conducting the ANOVA, the assumption of normality was evaluated and the normality test is determined based on the level of skew and kurtosis less than 2 and 9, respectively.

4.3 Results

4.3.1 ROS Detection

ROS production was detected after challenge murine neonatal microglial cells (BV-2) with two toxins, LPS and H₂O₂. In one group, cells were received the LPS (Figure 4.1 A-G) and in the other, the cells were directly insulted with H₂O₂ (Figure 4.1 H). Additionally, the treatment either by direct apply DEX or release DEX via EMF was also evaluated to determine whether they can reduce ROS generation and rescue damaged cells.

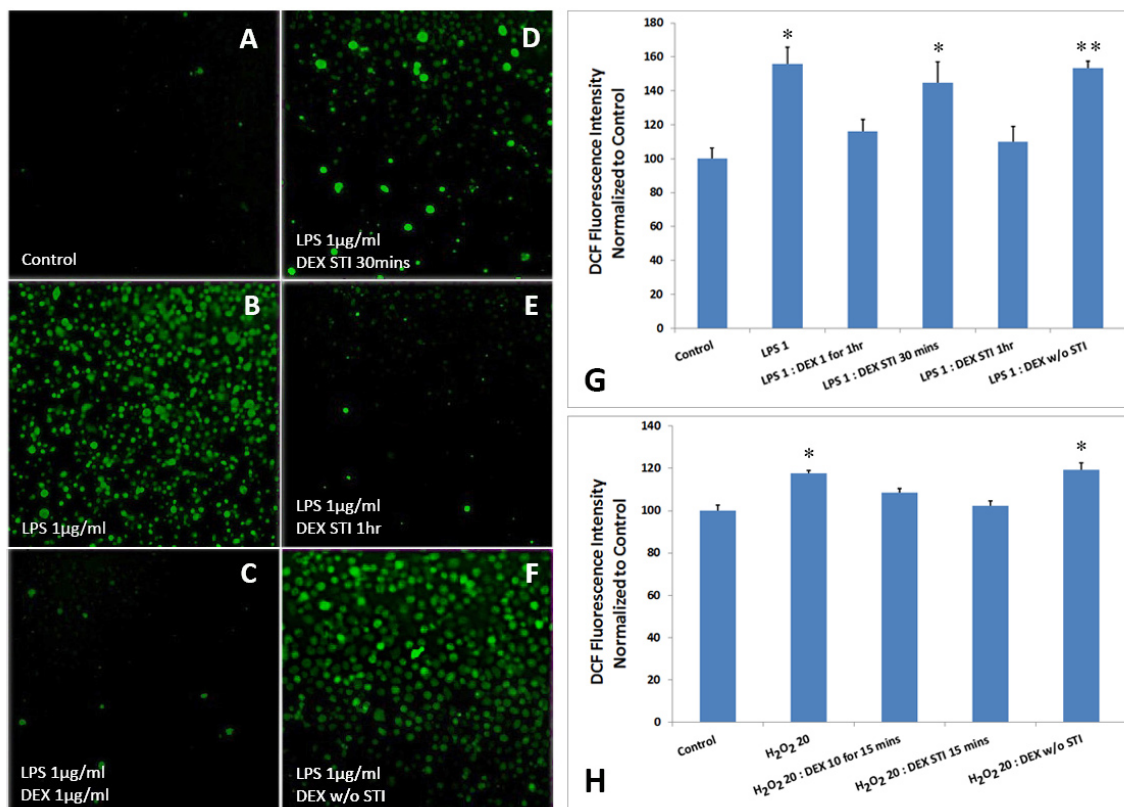


Figure 4.1 Composite fluorescence signals and quantitative measurement of ROS. (A) Control: without LPS insult. (B) BV-2 cells challenged by 1 μ g/ml LPS, showing intense ROS production indicated by green fluorescence signals. (C) Introduction of 1 μ g/ml DEX treatment after LPS insults (D) After LPS incubation, cells were applied with combination of DEX doped PpyNWs-AuNps film and EMF stimulation for 30 minutes (E) for 1 hour stimulation (F) without EMF stimulation. (G) Corresponding graph describes the quantitation of ROS production in panels (A-F). Values shown as percent normalized to control. (H) Quantitative data of ROS production after H₂O₂ insults and DEX treatment. * $P \leq 0.05$, ** $P \leq 0.01$.

CM-H2DCFDA, as ROS indicator, was used to measure the ROS production during this experiment. BV-2 cells treated with LPS (1 μ g/ml) exhibited intense green fluorescence, indicating the enhanced production of oxidative stress (Figure 4.1 B). The addition of DEX (1 μ g/ml) after LPS challenge effectively suppressed ROS production during the inflammatory cascade (Figure 4.1 C). ROS production was nearly undetectable when applied DEX-doped PpyNWs-AuNps platform with EMF stimulation for 1 hour (Figure 4.1 E). A less suppression of ROS activity occurred when shorter stimulation times (30mins) were applied (Figure 4.1 D). In contrast, DEX-doped PpyNWs-AuNps film not subjected to EMF stimulation did not show signs of ROS scavenging. (Figure 4.1 F)

Similarly, more ROS byproducts in BV-2 cells were observed after 20 μ g/ml H₂O₂ exposure. (Figure 4.1H). This increased level of ROS was suppressed either by direct application of 10 μ g/ml DEX for 15 mins or with 15 mins of EMF stimulation to the DEX coupled PpyNWs-AuNps.

4.3.2 iNOS Suppression by Dexamethasone Release

Above findings were further corroborated by the results of iNOS measurements. The iNOS expressions were demonstrated by labeling of Cy3 (red) fluorescence signal. The control group does not show any iNOS expression due to absence of LPS challenge. Microglial cells showed intense fluorescence signals (primarily localized in the cytoplasm regions) when exposed to a higher concentration of LPS (10 μ g/ml) (Figure 4.2), showing significant upregulation of iNOS. A less upregulation of iNOS expression was observed at a reduced LPS concentration while PpyNWs-AuNps not stimulated with

EMF (Figure 4.2 DEX w/o STI) also showed a similar response. In both cases, there is apparent iNOS expression occurred, showing the potentials of NO-mediated cell damage. In contrast, EMF stimulation of DEX conjugated PpyNWs-AuNps resulted in a strong suppression of iNOS as directly applied DEX treatment (Figure 4.2 DEX STI 1hr and DEX 1 μ g/ml), also indicating a reduced level of nitric oxide. These results addressed the successful DEX release using EMF stimulation and also indicated the stimulated DEX remain bioactivity for iNOS suppression. These results are all in agreement with the ROS results showed in Figure 4.1.

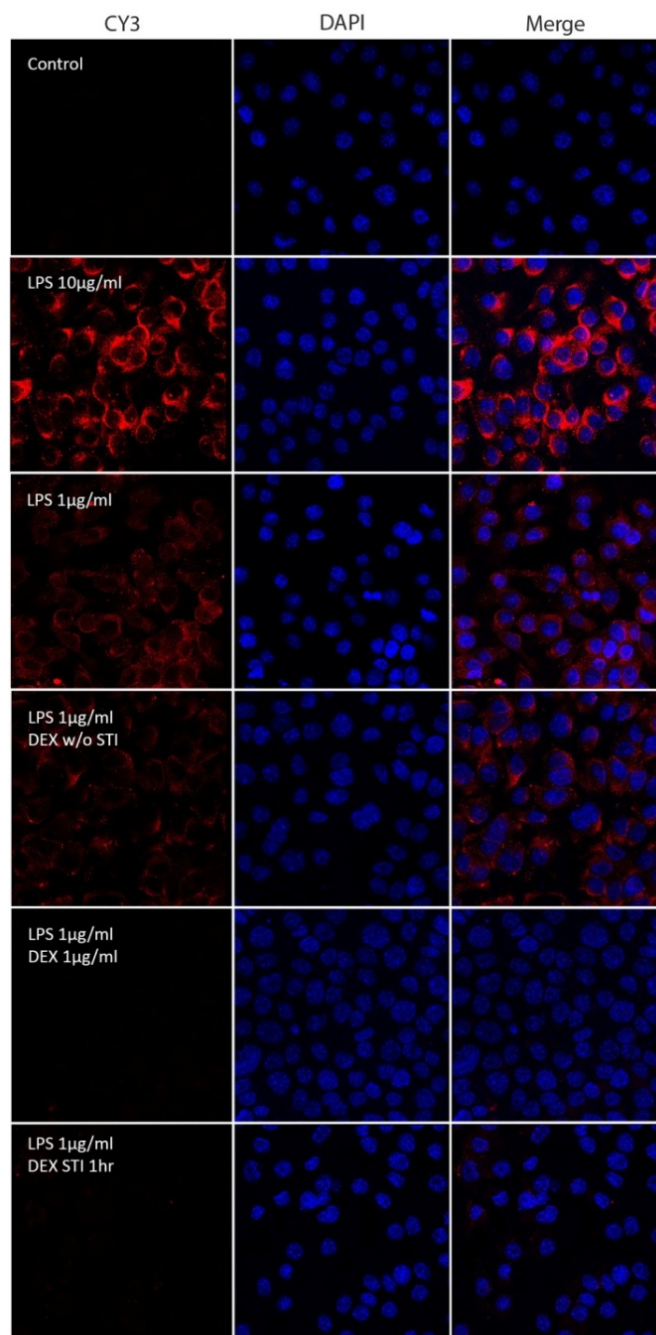


Figure 4.2 Confocal images of the iNOS expression after LPS induction and DEX treatment in BV-2 cells. iNOS expression in BV-2 cells is shown as red fluorescence (CY3 column). Nuclear staining with DAPI is shown as blue signal (DAPI column). The control group didn't receive any LPS challenge and DEX treatment. The row LPS

10 μ g/ml indicate the stimulation of high concentration LPS and high iNOS production. Row LPS 1 μ g/ml showed lower concentration of LPS applied to the tested cell population. DEX doped PpyNWs-AuNps film not stimulated with EMF (DEX w/o STI) showed a similar response as in LPS 1 μ g/ml. Row LPS1 μ g/ml:DEX1 μ g/ml illustrates the results when direct DEX treatment applied while row LPS1 μ g/ml:DEX STI 1hr as comparison indicating the DEX release treatment when PpyNWs-AuNps film was stimulated with EMF for 1 hour.

4.3.3 Selection of Animal Injury Model

GFAP – luc transgenic mice were chosen because they were genetically engineered to express firefly luciferase under the control of the GFAP promoter, so that they can express the level of GFAP protein as feature of astrocyte activation and reactive gliosis when there is alternation of astrocytes occurred in the healthy nerve tissue of CNS. This GFAP expression can be initiated by any insults, such as directly injury, bacterial infection, neurodegenerative disease, ischemic defects, and tumors. This technique combining transgenic mice with bioluminescence imaging system can permit multi-dimensional imaging of GFAP expression and its changing dynamics in the living animal.

The SCI was induced at low thoracic regions with a compression method illustrated in Figure 4.3. This is not a robbing injury and intentionally very mild to ensure the low mortality and not severe behavioral deficits during a week of study. The compression method has been reported to be able to activate the astrocytes starting at day 1 after SCI.

[156,157] Since we focused on the study of neuroinflammation, not behavior testing, the compression method has been considered as suitable for this situation.

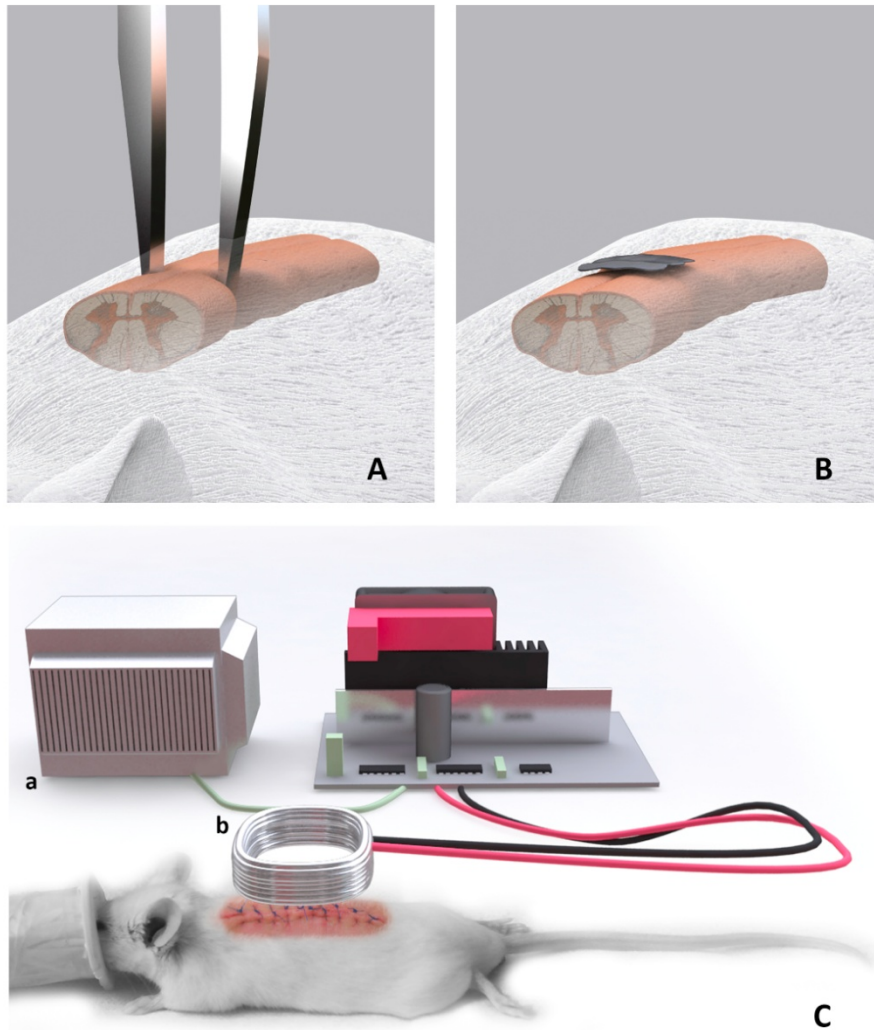


Figure 4.3 Illustration of SCI procedures and EMF stimulation set-up. A) shows a spinal cord compression using blunted forceps. The dimensions are exaggerated for explanatory purposes. The cord was compressed to a depth of approximately 50 % of its diameter. The degree of lateral compression was also approximately $>50\%$ of the cord's diameter, and arrested by a detente built on the inner face of the forceps. B) The PpyNWs thin

film was physically placed on the injured site immediately after compression. C) Experimental setup. This illustration shows the application of the EMF to a spinal cord injured mouse under anesthesia. a) The background shows the integrated system and power supply for the generation of the EMF. b) The coil positioned directly over the spinal cord injury in the mouse.

4.3.4. Neuroinflammation Attenuation by Drug Loaded Polypyrrole Implant

All mice were distributed to three study groups: Control Group: animals only receive SCI; Ppy Control Group: animals received implantation of DEX doped PpyNWs film, though they were not exposed to an externally stimulated electromagnetic field; Ppy Treatment Group (Experimental animals): the identical implantation procedures were applied as Ppy control group with exception to the EMF exposure. An applied EMF is required to induce the release of DEX from the PpyNWs.

Figure 4.5 shown the bioluminescent images of three groups of GFAP-luc transgenic mice at day 1, 3 and 7 after SCI. The data illustrated by bioluminescent imaging system can provide the level and specific sites of GFAP expression and can compare relative GFAP intensity between groups. The quantitative data can be expressed via converting the ROI of the images in relative lights units (CCD camera counts) to a physical units of radiance (photons/sec/cm²/sr). It means that the total flux of photons or radiance in each pixel (photons/sec) was integrated over the ROI area and then multiplied by one steradian (sr). The upregulation of GFAP mRNA or we may say luciferase protein after SCI can be

visualized after injection of the luciferase substrate D-luciferin due to the reaction shown as below Figure 4.4.

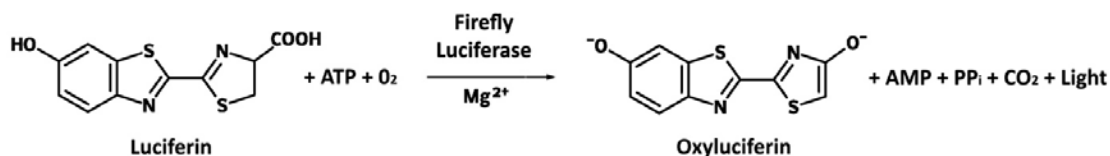


Figure 4.4 Luciferin and luciferase reaction based bioluminescence imaging.

The image and descriptive statistics of the GFAP expression are reported in Figure 4.5 and 4.6. There was a trend for the intensity of GFAP to become reduced in all groups of animals. A statistical difference between two control groups during the entire experiment was not detected. There always had a clear and observable GFAP expression at every time point in these two control groups. It has also been shown that the EMF induced DEX release produced a relatively steep decline of GFAP level. The experimental groups were always associated with numerically smallest mean level during the detection. At the first measurement day post-injury, the mean value of GFAP expression was 60% lower than control values, though this difference did not reach significance given the wide variability of the means 24 hours after surgical injury ($P > 0.05$). By day 3, this radical decline in experimental animals was very significant compare to the control groups both visually and statistically ($P \leq 0.01$). The statistical testing between control and Ppy treatment groups, between Ppy control and Ppy treatment groups also yielded a significant effect ($P \leq 0.05$) at day 7. Moreover, at post-surgery day 7, 2 of 5 experimental animals did not possess a trace of GFAP. The other animals in this group at this time point revealed GFAP expression only at the barest level of detection. It has also been seen that the standard error of the means (SEM) of the experimental group was

significantly smaller compared to both control and Ppy control groups at day 3 and day 7.

(See Figure 4.6)

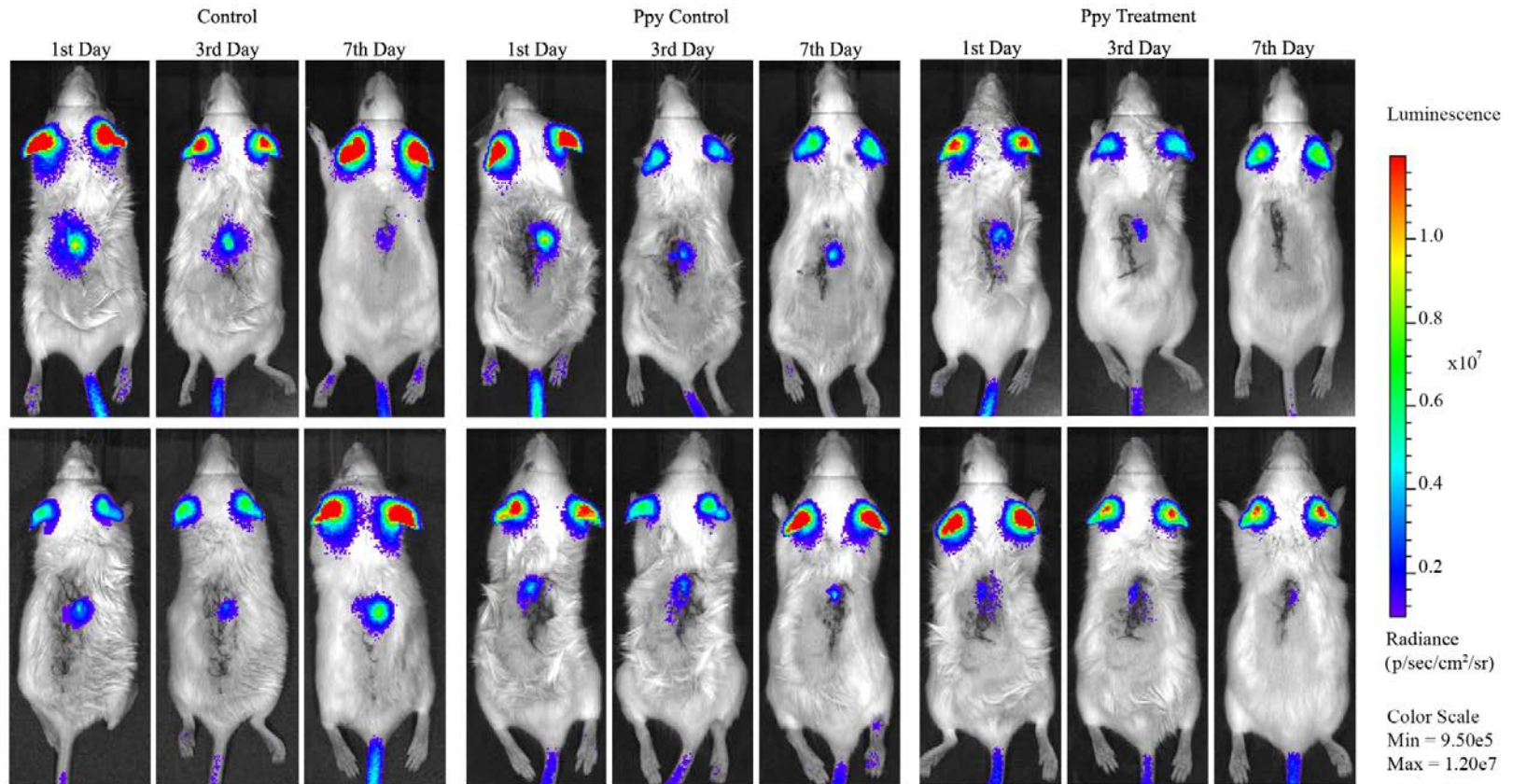


Figure 4.5 Bioluminescent images of mice in control, Ppy control, and Ppy treatment groups. Each row is one individual at 1 day, 3 days, and 7 days post injury. Note that, at day 7, the GFAP signal is at the barest level of detection or completely absent in treated animals. Clear GFAP signal from ear infections, as internal controls, are observed in all animals at all times. The luminescent intensity given in units of radiance is shown at the scale bar at the far right.

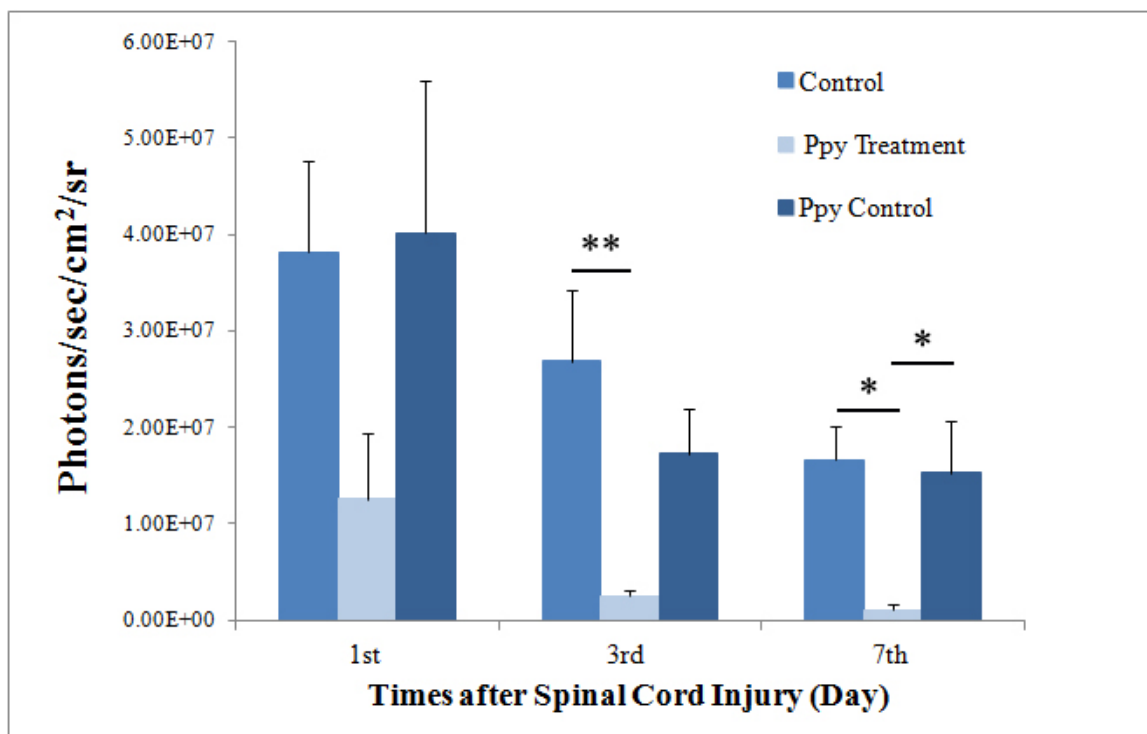


Figure 4.6 Quantitative data of GFAP expression based on bioluminescent results. GFAP expression displayed is given as a function of time at post-injury. Note that EMF - treated animals show striking and statistically significant reduced values compared to controls. * $P \leq 0.05$; ** $P \leq 0.01$.

GFAP signal associated with ear infections was also observed which was present with all received transgenic mice. (Figure 4.5) It is important to point out that GFAP positive ear infections in all animals can be provided as “Internal Control”. This Infection was not reduced or otherwise affected in either control groups or experimental samples. Note that the level of GFAP expression in ear regions (Figure 4.5) did not indicate the strongest signals when figure is captured since the kinetic study of this signal is based on the region of spinal cord. We suggest that the reduction of GFAP level in spinal cord region is explained by the likelihood of released DEX after EMF exposure. This observation

provides formal proof that the local release of DEX by smart PpyNWs was restricted to the spinal cord lesion, where DEX-doped PpyNWs were surgically placed and later exposed to an EMF.

4.4 Discussion

The functionality of glial cells was extensively investigated in SCI studies. Activated microglial cells triggers many pro-inflammatory factors, ROS, and RNS, initiating cell apoptosis cascades. Also, many studies implicate that not only physical barrier of astrocytes mediated scar formation, but also the inhibitory molecules triggered from reactive gliosis contributes to the abortive neuronal regeneration after SCI. Thus, glial cells have been emerged as an attractive target in many CNS related pathological context. In this study, we used LPS and H₂O₂ challenged microglial cells (BV-2) in vitro and spinal cord compression model in vivo to simulate the neuroinflammation conditions and then detect the releasing profile of anti-inflammation drugs DEX using a novel application of EMF-sensitive conductive polymer based drug delivery systems under this neuroinflammation conditions.

Among all the harmful molecules produced from glial cells, we primarily study the ROS and RNS production. It has established that NO primarily produced from macrophages and microglial cells via iNOS expression and act as a neurotoxic agent in spinal cord injury model, brain ischemia, and hypoxia. However, some researches also shown that NO may exerted neuroprotective functions and particularly resistant to neurodegeneration in Huntington's disease. [158] Therefore, balancing the level of NO production is very

important and vary based on different neuronal degeneration disease and neurological deficits. According to many case studies of SCI, the reduction of NO-mediated neurotoxicity showed potentials to achieve the successful neuronal recovery and avoid the functional impairments.

Since the possible ROS and NO reduction of DEX, we deliver the DEX from EMF sensitized conductive polymer Ppy to LPS and H₂O₂ challenged microglial cells, and test the successful delivery of DEX according to the cellular responses. The results showed dramatically suppression of iNOS expression by DEX at 1 μg/ml and moderate reduction to ROS. Many studies also confirmed these outcomes. In the study of hyperglycemia, DEX has been proven to reduce ROS levels in multiple myeloma cells through regulation of thioredoxin activity.[159] Low concentrations of DEX in a range of 10nM to 1 μM substantially inhibition of IL-1 beta, IL-6, and TNF-alpha secretion.[160,161] Lina Ruiz et al also reported that DEX can delay neutrophil apoptosis by inhibiting ROS generation. [162] In addition, DEX suppresses intracellular ROS production in platelets [163] and directly blocks LPS-induced ROS production in microglial cells by up regulation of MKP-1.[114] However, long term administration of DEX can accelerate the oxidation process in some tissues and imbalances the lipid metabolism. [164] One study has shown increased ROS levels of differentiated M2 macrophages induced by DEX when applying DEX for 7 days but not 2 days. [165] Our experiment also addressed similar phenomenon. DEX failed to reduce or , in some situation, initiated production of ROS when a higher concentration of DEX (10 μg/ml) was applied to a low concentration of LPS (1 μg/ml) stimulated microglial cells. Also, we challenge the cells with different concentration of H₂O₂ range from 5 μM to 100 μM with various concentration of DEX at

similar range. The results showed that DEX can eliminate low production of ROS, but not for a high level of ROS. This is indicated by a failure ROS reduction of DEX when H₂O₂ at concentration of 50 μ M or above were applied to the cells. (data not shown here)

Although a clear explanation to the role of GFAP is still under exploration, it is important to realize that the GFAP level that not be expressed under normal circumstances indicate the changes in the function and secretion of the astrocytes and normally due to neuroinflammation related reactive astrogliosis. Many investigations showed that increased oxidatively damaged proteins can also cause the increased GFAP expression in different neurodegeneration cases. [166,167,168] In our SCI study, a GFAP-luc transgenic mice combining with bioluminescent imaging technique were used to trace the spatial and temporal changes of GFAP expression after SCI. We reduced these GFAP signals by releasing DEX via EMF from local Ppy nanosouce which placed at spinal cord lesion. The results from our study indicated a significant statistical difference between treatment and control groups at day 3 and 7, but not the first day after injury although it showed an apparent numerically reduction of mean value in the treatment group. It propably due to the various responses of animals to traumatic injury in spinal cord and treatment. The selection of statistical testing methods is based on the assumption of normal distribution which determined depend on the skew and kurtosis value. Mann-Whitney testing as non-parametric test described a significant difference at day 1 ($P \leq 0.01$). Moreover, there is an obvious reducing tendency of GFAP expression at post-SCI in all three groups, but it quite different. 2 out of 5 control animals appeared GFAP signals at day 1, and decreased at Day 3, but prominent by Day 7, and other control animals showed a prominent GFAP expression from Day 1 up to Day 3, but vanished at

day 7. A similar GFAP expression and proliferation pattern after spinal cord compression injury has been reported using immunohistochemistry testing method. One reports indicated that the reactive astrocytes displaying GFAP signals by Day 1 and reach to the peak level at Day 3 post-SCI. [169] Other studies reported an increased GFAP level at the injured and its adjacent sites at day 1 after traumatic injury. It is then predominant between 3 to 7 days and gradually decreased afterwards. [170] However, in the experimental groups, there was a consistent reduction in GFAP expression after initiation of SCI and showed similarity as described by Theriault et al. [169]

It is also important to understand the plasticity of these astrocytes in CNS injury. There is no absolute detrimental role for them, they also can benefit to the injured tissues to certain level. For example, the proteoglycans produced by astrocytes may be protective for the surrounding viable tissues by limiting the propagation of cavity after SCI. [171,172] It is beyond the scope of this report to critically review the biology of reactive astrogliosis after SCI. Opinions vary significantly in many literatures on the role of reactive astrocytes is detrimental or helpful to biological recovery functions. We emphasize that there are more GFAP positive activated astrocytes accumulate at injury sites as their increased number of hypertrophy and largely increase the glioscars in open injury. These events are considered to be aspects of neuroinflammation in CNS injury. We can say with certainty that the corticosteroids drug DEX has performed anti-inflammation properties which would be useful after SCI. These beneficial effects would be many and vary such as reduction of edema, lipid peroxidation, concomitant with cell survival. Especially, the effects of DEX on astrocytes associated GFAP irradiation have been extensively reported in earlier papers. [147]

The glucocorticoid steroids drugs, such as methylprednisolone, have been commonly used in clinical treatment of brain and spinal cord injury to inhibit post-traumatic lipid peroxidation and other physiological conditions in traumatic injury for more than 30 years. A survey from USA indicated that corticosteroids are widely used for management of traumatic head injury, taking for 64% of treatment centers. However, a randomized CRASH trial unveiled an increased risk of death under methylprednisolone treatment compare to the placebo groups. We need to emphasize that corticosteroids, under debating, but still used in different condition of SCI. Unlike traumatic brain injury, there are many evidences support that corticosteroids treatment can results in beneficial outcomes, especially for motor functional recovery which proved in NASCIS-2 clinical trail. In addition, DEX administration to spinal cord injured cat had proved to have a remarkably functional recovery by eliminating the potassium loss. [178] This beneficial effect was considered to relate to the maintenance of cellular structural integrity offered by the steroid drugs. [179] Our studies also addressed the same results. A LDH (lactate dehydrogenase) assay, as the indicator of cell membrane integrity, was perform for DEX treatment to LPS challenged microglial cells. It showed a decreased level of LDH activity after DEX treatment, indicating the potential protection to cell membrane by DEX. (Data not shown here) However, some reports have shown that there is no statistical difference in the trauma score, average length of hospital stay, mortality, [173,174] and neurological benefit [175] between steroids treatment and without the treatment.

It is noteworthy that the timing and dosages of corticosteroids drugs applied to the patients with acute spinal cord injury plays an key role and have been studied in many trials. For example, "patient who receives methylprednisolone within 3 hours of injury

should be maintained on the treatment regimen for 24 hours. When methylprednisolone is initiated 3 to 8 hours after injury, patients should be maintained on steroid therapy for 48 hours." [176] "Methylprednisolone sodium succinate (MPSS) has been shown to improve neurologic outcome and significant recovery in rodent motor function up to one year post-injury if administered within eight hours of injury and in a dose regimen of: bolus 30mg/kg over 15 minutes, with maintenance infusion of 5.4 mg/kg per hour infused for 23 hours." [177] Therefore, unsuccessful or even detrimental outcomes to patient with SCI could relate to the difference in administration. In our animal studies, we applied the treatment within 3 hours after SCI and locally administrate the drugs to injured region. It could result in a different therapeutic effects compared to the traditional systemically drug delivery.

Many clinical results showed improvement after SCI by modulating inflammatory processes, but the steroid treatment alone is not sufficient enough to get fully recovery for patient with SCI. A combination approaches, often together with pharmacological therapeutics and some of non-pharmacological strategies, such as targeted rehabilitation, individually designed cognitive training and exercise, or multisensory stimulation, could be a more beneficial therapeutics intervention to the patient with SCI.

According to our study, a local steroids treatment might have different impacts for CNS treatment compare to the systematic administration which applied to all earlier studies. The targeting strategies of drug release can simply accomplished by physical placement by coating the drug loaded materials with implants, and not encumbered by side effects. Our technique also can be as simple as placement using a biopsy needle. Moreover,

despite the treatment of corticosteroids drugs DEX are less capable to suppress lipid peroxidation compared to MPSS in spinal cord studies and steroid treatment alone has its limitation in spinal cord injury, this Ppy mediated drug delivery strategies are not limited only for the treatment of SCI. It can broaden the potential application for local treatment to different diseases, such as rheumatic disorders, decubitus ulcerations, and even early tumor formations in breast, lung, prostate. Additionally, this drug delivery system has been proved that it can successfully conjugated different molecules, such as NT-3, NGF, BDGF, ATP etc, such that it can be used in various applications. Especially, the administration of the drugs can be controlled by external stimulation of electromagnetic field without any physical invasive contact to human tissues. This drug delivery system opens the door to many known therapies that cannot be easily or safely applied systemically, but till now, could not be delivered continuously for many days to specific localized tissues.

CHAPTER FIVE
SYNTHESIS AND CHARACTERISTICS OF
SIRNAS CONJUGATED CHITOSAN NANOPARTICLES

5.1 Introduction

5.1.1 Evolution of Post-transcriptional Gene Silencing.

In 1990, the first study of post-transcriptional gene silencing was investigated regarding to the promoter in the gene controlling the color of Petunia flowers. In 1998, Andrew Z. Fire and Craig C. Mello, who later on were awarded the Nobel Prize in Physiology or Medicine 2006, discovered a sufficient gene activity silencing by introducing the double-stranded RNA into animal cells. This discovery of RNA interference introduced a powerful biological and therapeutic tool in medicine. Meanwhile, Alnylam Pharmaceuticals (which mainly focuses on the development of RNA interference (RNAi) based gene therapeutics) first reported data for use of RNAi therapeutics in rodent in 2004 and in primates in 2006. In 2008, RNAi was shown as the potential therapeutics for the use in human.

The strategies of this post-transcriptional silencing of gene expression was rapidly developed in only a decade, but has proven its strong and effective therapeutic effects on genetically oriented disease. Reduction in targeted messenger RNA levels and their

associated gene activity can be initiated by either microRNA (miRNAs), short hairpin RNA (shRNAs), synthetic short interfering RNA (siRNAs), or even single-stranded antisense oligonucleotides (ODNs) and ribozymes. The differences of these mRNA antisense approaches can result in a very different level of cellular uptake, transfection efficiency, and toxicity. Their characteristics can also lead to different procedures for mRNA inhibition. MicroRNAs are considered as an artificial miRNAs and mimics the primary miRNA stem-loops, shRNAs are processed pre-miRNAs and transcribed as sense and antisense sequences connected by a loop of unpaired nucleotides. In contrast, siRNA is a laboratory-made synthetic miRNAs and can be engineered to be perfectly complementary to targeted sequences. In this endogenous pathway, the effects of both microRNAs and shRNAs are initiated at the nucleus, Drosha-DGCR8 process primary miRNAs to pre-miRNAs and followed by the cytoplasm transportation of Exportin-5. The cleaving of Dicer removes loop region and produces the desired mature miRNAs as single strand RNAs. RNA induced silencing complex (RISC) along with this single strand RNAs reach to the targeted specific sequences for silencing and eventually leads to the knockdown of this protein expression. Synthesized siRNAs can be directly transfected into cytoplasm, follow by either directly loaded onto RISC or utilize a Dicer mediated process, and then process the rest of the pathway as that of microRNA and shRNA.

5.1.2 Pros and Cons of SiRNAs Therapeutic Strategies

The success of RNAi based strategies has led to many ongoing clinical trials and developmental pipelines. Of them, siRNAs are shown promising outcomes due to efficient gene silencing and highly specific inhibition of the target of the interest. Another key feature is that, unlike microRNAs and shRNAs, the process of siRNAs occurs inside the cytoplasm instead of the nucleus, therefore it limits the risks of unexpected genome modification. Since shRNAs are endogenously produced, they have long lasting gene-silencing effects whereas the synthetic siRNAs only have short inhibitory effects (generally last for 3-5 days) because of their constant cell division as well as intracellular degradation. But siRNAs were proven relatively more stable in the bloodstream compared to ODNs and ribozymes which only remain stable for up to a few minutes, even though ODNs and ribozymes more easily pass through cell membrane due to less negative charges on them compared to siRNAs. The long duration of inhibitory effects can be used in the condition with highly expressed mRNA levels but could be detrimental. For example, it can induce inappropriate immune response and interference with the endogenous miRNA pathways - both can eventually lead to toxic effects.

From a pharmaceutical industrial perspectives, the low cost and easy synthesis of siRNAs does not need to involve either cellular systems or complicated protein purification procedures, suggesting the promising advantages over other small molecule drugs. Moreover, siRNAs have relatively low toxicity compared to organically synthesized drugs due to their natural nucleotide components. Therefore, siRNAs have promising potential in treatment of various gene oriented diseases. However, there are many

remaining challenges ahead and could affect possible clinical application. The primary biological challenges of siRNAs are described below. [180]

- 1) Off target effects. The major reasons are due to 3' UTR or its homologous sequences are present in siRNAs.
- 2) Non-specific immune response. Certain siRNAs sequences with 5'-UGUGU-3' or 5'-GUCCUCAA-3' motifs have the potential to initiate the inappropriate activation of immune systems by producing interferon and interleukin products. Many researchers have also indicated that the siRNAs with long nucleotides (>30bp) or at a high concentrations could also cause interferon or interleukin responses in certain cell lines by reticuloendothelial system (RES).
- 3) Saturating the RISC. Due to the protein silencing mechanism of siRNA, excessive amounts of siRNAs might influence the normal activity of cellular miRNA.
- 4) Low transfection efficiency/ poor cell penetration. siRNAs are unable to passively diffuse through negatively charged cellular membranes due to their anionic charge and consequent electrostatic repulsion between them. [181]
- 5) Poor cellular uptake. Apart from the reason of inability of siRNAs crossing anionic cell membrane, rapid degradation of siRNAs by nucleases also can limit the cellular uptake. SiRNAs especially through systematic administration into bloodstream can easily undergo a degradation caused by relative larger amount of ribonucleases (RNAses) in the blood, aggregation with serum proteins, or limited blood stability. The lack of a specific delivery system to the target during siRNA delivery is also a particular limitation for siRNAs therapeutic strategies.

- 6) Lysosomal compartmentalization. Endocytic vesicle can entrapped the siRNAs in lysosomes which prevents the efficient release siRNA into the cytoplasm.
- 7) Rapid renal excretion. This is mainly due to the capture of mononuclear phagocytic cells which leads to a rapid clearance from the circulation.

5.1.3 SiRNAs Inhibition in Spinal Cord Trauma

The exploration of siRNA strategies in central nerve system disease are ongoing and involved in an broad applications from neurodegeneration, cancer glioma, pain syndromes, to primary and secondary damages. In the case of SCI, various target proteins were investigated to inhibit using siRNAs strategies. Alnylam/Merck collaboration focused on the development of RNAi therapeutics targeted to Nogo pathway for SCI treatment. Since Nogo receptor is important axonal inhibitor, inhibiting its associated pathway could potentially improve neuronal outgrowth and injury conditions, many other research groups dedicated to the study on the downstream of signaling pathway, such as RhoA and ROCK signaling pathways. [182] Although RhoA specific siRNA treatment did not indicate the recovery of motor function, but controlled tactile hypersensitivity and significant improved white matter and serotonergic axonal regrowth. Also, the accumulation of ED1+macrophages is dramatically reduced which limits inflammation. [183] Pretreatment of ERK2 siRNAs has been reported to improve locomoter performance, so does ephrinB3 siRNA inhibitory strategies which are based on reversal signaling of ephrinB3 promote axonal pruning and regeneration as well as synapse formation. [184]

Other findings also focus on the reduction of scar tissue formation after injury in order to reconstruct neuronal growth conditions by delivering siRNAs to the injured sites. For example, GFAP siRNAs combined with photomechanical wave-driven approach shown a significant locomotive improvement after SCI.[185] SiRNA targeting to telomerase reverse transcriptase (TERT) and CSPG were also developed to control astroglial scar formation and to promote robust axonal regeneration. [186,187] In addition, matrix metalloproteinase-3 (MMP-3) siRNAs can prevent the increased permeability and disruption of blood-spinal cord barrier after SCI and lead to the potential for functional recovery.[188]

Other siRNA applications have been used in other CNS diseases such as stroke or neurodegeneration disease and could be potentially used for SCI treatment. The siRNAs targeting apoptosis mediated protein, such as CCAAT-enhancer-binding protein homologous protein (CHOP) and caspase 3, might be used to control cell death after SCI.

Our study focused on the targeting to the macrophage and its initiated pro-inflammatory molecules which plays a key role in secondary injury after SCI. The hallmark expression of detrimental macrophages is iNOS expression. Therefore, siRNAs targeting of iNOS as a treatment strategy was hypothesized to be able to alleviate NO production and improve injured conditions of spinal cords. More details will be addressed in chapter 6.

5.1.4 SiRNAs Delivery Strategies

The remaining challenges described in chapter 5.1.3 result in a large scale of development of siRNAs based delivery materials and chemical modifications. Many studies have proved that these modulations can solve the existing limitation of siRNAs

and optimize the outcomes of this siRNAs application. Generally, the delivery strategies usually involved viral vectors and non-viral vectors materials. Despite the viral vectors based delivery system shown the successful results of gene silencing, the danger of viral toxicity and relatively strong immune responses from the host still present. Many studies have indicated the possibility of unexpected inflammatory immune reactions, insertional mutagenesis, oversaturation of RNAi pathways, and cellular toxicity that were caused by viral vectors carried siRNAs delivery. These obstacles directed many researchers to pursue safe carriers for siRNA therapeutics. Complexes of siRNAs with various materials, such as polymers, lipids, peptides, antibodies, aptamers and small molecules, as non-viral vector carriers, have been extensively developed. They have been considered to be able to protect the siRNA from the RNase-rich in vivo environment and deliver them to the targeted cells and tissues, showing more efficient silencing outcomes compare to siRNAs alone.

Over many recorded RNAi based clinical trials and commercial products, lipid nanoparticles or lipid based transfection reagents have been widely used to assist the siRNAs crossing the cell membrane. However, they have also been reported to be responsible for cytotoxicity. According to earlier and current studies, the assisted delivery of siRNAs favors the cationic polymer because siRNAs are anionic. Therefore positive charged polymers was vulnerable to synthesis with negative charged phosphate group of siRNAs. This self-assembly formation of inter-polyelectrolyte complexes with drugs is a non-covalent electrostatic complex formation, which is a very simple and reliable approach. Meanwhile, the cationic polymer shares a similar feature as a lipid based material and can easily carry siRNAs crossing cellular membranes.

Chitosan, as a linear binary polysaccharide, comprised of beta linked 2-amino-2deoxy-beta-D-glucose(GlcN; D-unit) and N-acetylated analogue (Glc NAc; A-unit). It can be protonated in slightly acidic conditions, expressing the cationic polymers nature. Chitosan also can process the properties of low costs as well as biocompatible and biodegradable which can minimize the side effects and the possible cytotoxicity. It is currently used as a common dietary supplement and has been classified as generally recognized as safe (GRAS) by the FDA. It is considered to be a promising carrier for the delivery of siRNAs and has been extensively investigated. Moreover, a relatively short transfection time of siRNAs (approximately 4 hours) when assisted with chitosan Nps also provides the possibility in clinical applications.[189]

Many previous findings exploited siRNAs conjugated chitosan Nps were successfully used in various disease and medical conditions, but mainly focus on the anti-tumor effects. Some reports have indicated that the mucoadhesive and permeation features of chitosan can be used to delivery siRNAs to the respiratory sites by intranasal administration or drop wise into the trachea to treat pulmonary cancer. [189,190] The chitosan mediated siRNAs deliverery was also widely developed for other cancer cell lines, such as hepatocellular carcinoma, [191] colorectal cancer cells, [192] cervix, ovary, mammary carcinoma, [193,194] and leukemia. [195] A novel strategy using chitosan Nps to deliver siRNAs to peritoneal macrophages to reduce inflammation in an arthritis model has also been reported.[196] However, in central nervous system study, the chitosan mediated siRNAs strategies is still underdeveloped. P-glycoprotein siRNAs conjugated chitosan complexes were tested to be efficient to penetrate blood-brain barrier by silencing the efflux pumps P-glycoprotein which involved the maintenance of brain

barriers.[197] Efficient neurite growth and spinal cord repair has also been reported by delivering of Rho siRNAs via chitosan Nps. [198] Most importantly, chitosan can limit lipid peroxidation and propagated damage at cell membranes in order to prevent secondary injury after SCI. [199]

Therefore, chitosan can be developed as a good candidate for siRNA carriers based on the nature of the materials and the various supportive and successful studies.

5.1.5 Types and Modification of Chitosan for SiRNAs Delivery

The most important characteristic of chitosan is that it can offer a variety of modification according to the requirement of different applications. The modifications of chitosan can improve siRNAs delivery by enhancing administration efficiency. Trimethyl chitosan with cysteine conjugate has shown an enhanced mucoadhesion and permeation, therefore, it can be successfully used in nasal administration.[200] Encapsulation of (+)-catechin (C) and (-)-epigallocatechin gallate (EGCg) or crosslinking with hydroxypropyl methylcellulose phthalate (HPMCP) with chitosan Nps has also been proved to increase the intestinal adhesion, penetration and absorption in order to optimize oral administrations. Although N-octyl-O-glycol modification of chitosan Nps did not show significant improvement during intravenous administration, it has been reported to have good biocompatibility without signs of cytotoxicity. [201]

Additionally, modified chitosans were especially helpful for transfection efficiency in siRNAs delivery. Gaspar et al. synthesized chitosan-histidine-arginine (CH-H-R) based Nps for plasmid DNA delivery. These demonstrated remarkably higher transfection

efficiency than unmodified chitosan and without leading to any cytotoxic effect. [202] The design of trimethylchitosan/siRNA complexes is through quaternization of amine groups to create the enhanced protonization of chitosan and help its interaction with siRNAs. [203] Chitosan grafted with PEI have increased long-term transfection efficiency and decreased cytotoxicity than PEI alone. Furthermore, the proton-buffering ability of PEI can catalyze the osmolysis of endosomes and help siRNA nanocomplexes easier escape into the cytosol than chitosan alone. [201] The optimization of transfection efficiency can be further supported by the good stability of siRNA conjugated chitosan Nps. Ionic crosslink sodium tripolyphosphate(TPP) with chitosan Nps suggest a new strategy to protect the siRNAs in serum contained conditions and shows a more strong stability with siRNAs. [204] Deoxycholic acid incorporated with chitosan showed good stability during the delivery process due to hydrophobic property of deoxycholic acids. [205] At last, from clinical application perspectives, the conjugation of PEG on chitosan-siRNAs Nps allowed lyophilization for a longer shelf life and avoid aggregation during systematic delivery. [206] In summary, the selection of nanocarriers for siRNAs highly relies on the characteristics of materials and its targeted cells and tissues. Different modification or copolymerization approaches allow chitosan processing much broader applications.

Intriguingly, recent work raises promising results of enhanced transfection efficiency and alleviated side effects when using ligand mediated targeting methods. [207] Our studies focused on this modification of chitosan with ligand conjugation to achieve specific cell targeting and improve therapeutic outcomes. Various chitosan salts, such as chitosan glutamate (CS-Glu) and chitosan hydrochloride (CS-HCl), are also developed for in vitro

siRNA delivery, because of their high solubility at physiological pH. The different types of chitosan salts have much less influence on transfection efficiency of functionally active siRNA in comparison to the molecular weight of chitosan salts and weight ratio or N/P ratio between siRNAs and chitosans. [208] Chitosan hydrochloride is readily soluble in water, and its properties as a siRNA carrier was also investigated in our experiment for conjugating different targeting motifs.

5.2 Material and Methods

5.2.1 Synthesis of SiRNAs Conjugated Chitosan Nanoparticles

Four different Chitosan/siRNA Nps were prepared, three of them conjugated with targeting ligands. Low molecular weight chitosan was purchased from sigma and dissolved in 0.2 M sodium acetate buffer (pH 4.5), and the solution was adjusted to pH5.5. (indicated as Chi) For antibody conjugated siRNA/chitosan, Purified mouse IgG solution was mixed with chitosan solution which dissolved in 0.2 M sodium acetate buffer at a molar ratio of 1:1 and final concentration of chitosan at 200 μ g/ml. The crosslinking agents of 0.2 mM 1-Ethyl-3-[3- dimethylaminopropyl]carbodiimide hydrochloride (EDC) and 0.5 mM *N*-hydroxysulfosuccinimide (sulfo-NHS) were added to the mixture, and then stirred for 24 h at 4°C. The next day, the solution were injected into 10K MWCO slide-A-Lyzer Dialysis Cassettes (Pierce) to remove uninterested molecules based on the instruction from company for 48 hours. (indicated as Ab-Chi). A second strategy of Ab conjugation with chitosan Nps is also performed and the water soluble crosslinking agent Bis[sulfosuccinimidyl] suberate (BS³) were used. A 30 fold

molar excess of the crosslinker BS³ solution compare to the protein was added to the sample solutions which containing a molar ratio 1:1 of IgG solution and chitosan solution which at final concentration of 200 μ g/ml. In this case, water soluble chitosan hydrochloride were used (Novamatrix, Protasan up CL114). This reaction mixture were then incubated for 30 mins at room temperature and then followed by 7K MWCO zeta spin desalting columns (Pierce) (indicated as Ab-WSC). Before synthesis of siRNA/chitosan Nps, different ratio of prepared IgG conjugated chitosan solution (10%, 20%, and 30%) were mixed with either 200 μ g/ml chitosan solution dissolved in 0.2 M sodium acetate buffer or 200 μ g/ml water soluble chitosans. Also, Mannosylated-chitosan solution were also prepared before synthesis with siRNA. This synthesis procedure was reported in Tae Hee Kim et al. [209] Briefly, mannopyranosylphenylisothiocyanate (Sigma-Aldrich) was dissolved in 1ml DMSO and then added to 60mg Chitosan (Novamatrix, Protasan up CL114) in 1ml miliQ water, and the solution was stirred for 24 hours at room temperature. Isopropanol solution was added to chitosan solution to precipitate the mannosylated-chitosan and followed by repeated centrifugation and wash. The collected precipitations were dried in high vacuum, and concentration of 200 μ g/ml mannosylated-chitosan was prepared before siRNA synthesis (indicated as M-WSC). Concentration of different chitosan solution at 200 μ g/ml was separately prepared and 20 μ l of 20 μ M iNOS-siRNAs were added to 1ml chitosan solution while stirring and remain at room temperature for 1 hour.

5.2.2 Transmission Electron Microscopy

All samples were imaged using a FEI Tecnai T20 transmission electron microscope operated at 200kV. One drop of chitosan Nps dispersed solution deposited onto a mesh copper grid coated with amorphous carbon and allowed to settle at room temperature for 2 mins. Negative staining was subsequently performed by swishing through 2% uranyl acetate droplet before imaging.

5.2.3 Size and Surface Charge of Nanoparticles

The size and zeta potential of the nanoparticles was analyzed using Zetasizer Nano ZS. Both size and zeta potential were measured in triplicate. Measurements were set at 173 degree and a temperature of 25 degree. The sample solution was placed in disposable cuvettes or zeta potential capillary cells respectively for size or zeta potential measurements. The z-average hydrodynamic diameter indicated size of the nanoparticles and calculated based on the viscosity and refractive index of water. The zeta potential was quantified based on the principle of phase analysis light scattering.

5.2.4 Gel Retardation Assay

Poly(l-aspartic acid) (PAA) displacement assay was conducted to detect the integrity of siRNA conjugated chitosan Nps. Polyanion PAA (Santa Cruz Biotechnology) were used to displac negatively charged siRNA from positively charged chitosan. Nanoparticles were incubated with or without PAA at concentration of 5mg/ml. A1 to 4 volumetric

ratio between PAA and nanocomplexes was used, and then they were incubated at 37 °C for 30mins. 50ul of sample solutions containing 0.532µg of siRNAs were placed into each wells of 10% Mini-PROTEIN TBE poly-acrylamide gels. Electrophoresis was then performed at 100V for approximately 100 mins. The gel was then transferred to SYBR gold nucleic acid staining solution for 30 mins and visualized using GBox imager.

5.2.5 Toxicity Studies

Toxicity of siRNAs and different designed Chitosan Nps in macrophages cultures were detected based on the morphology of the murine bone marrow-derived macrophages (BMDM). Macrophages were cultured in 24-wells plate and maintained as described in 6.2.1 section. They were incubated at both high concentration (5µl of 20µM siRNA with 6.5µl of Lipofectamine 2000 per well) and low concentration (2µl of 20µM siRNA with 2.5µl of Lipofectamine 2000 per well) of siRNAs and siRNAs without transfection reagent, as well as different chitosan Nps for 4 hours. Macrophages were observed and imaged using Olympus IX 81 inverted microscope.

5.3 Results

5.3.1 Chitosan Nanoparticles Morphology

To optimize siRNAs conjugated chitosan Nps, the molecular weight (MW), degree of deacetylation (DD), pH, and N/P ratio (or weight ratio) as important criteria were considered in the design of nanoparticles formation. Many successful siRNA conjugated

chitosan Nps have shown that chitosan with MW at range of 60 to 170kDa and higher DD value between 75%-90% would produce the Nps with reasonable size and surface charge. It also remains the stability of siRNAs during the distribution in bio-environment and allows the up-taking of different cell types without rapid degradation. In our experiment, all four chitosan nanocomplexes were formed using chitosan at the range mentioned above. Additionally, an weight ratio approximately at 37.5 was also predetermined according to earlier publications and used in our study. [210] The morphologies of four different chitosan Nps are illustrated in Figure 5.1. Both Chi/siRNAs Nps and M-WSC/siRNAs Nps showed a smooth surface of nanocomplexes with spherical-like shapes. In the case of two Ab conjugated chitosan Nps, the Nps predominantly exhibited a less smooth surface.

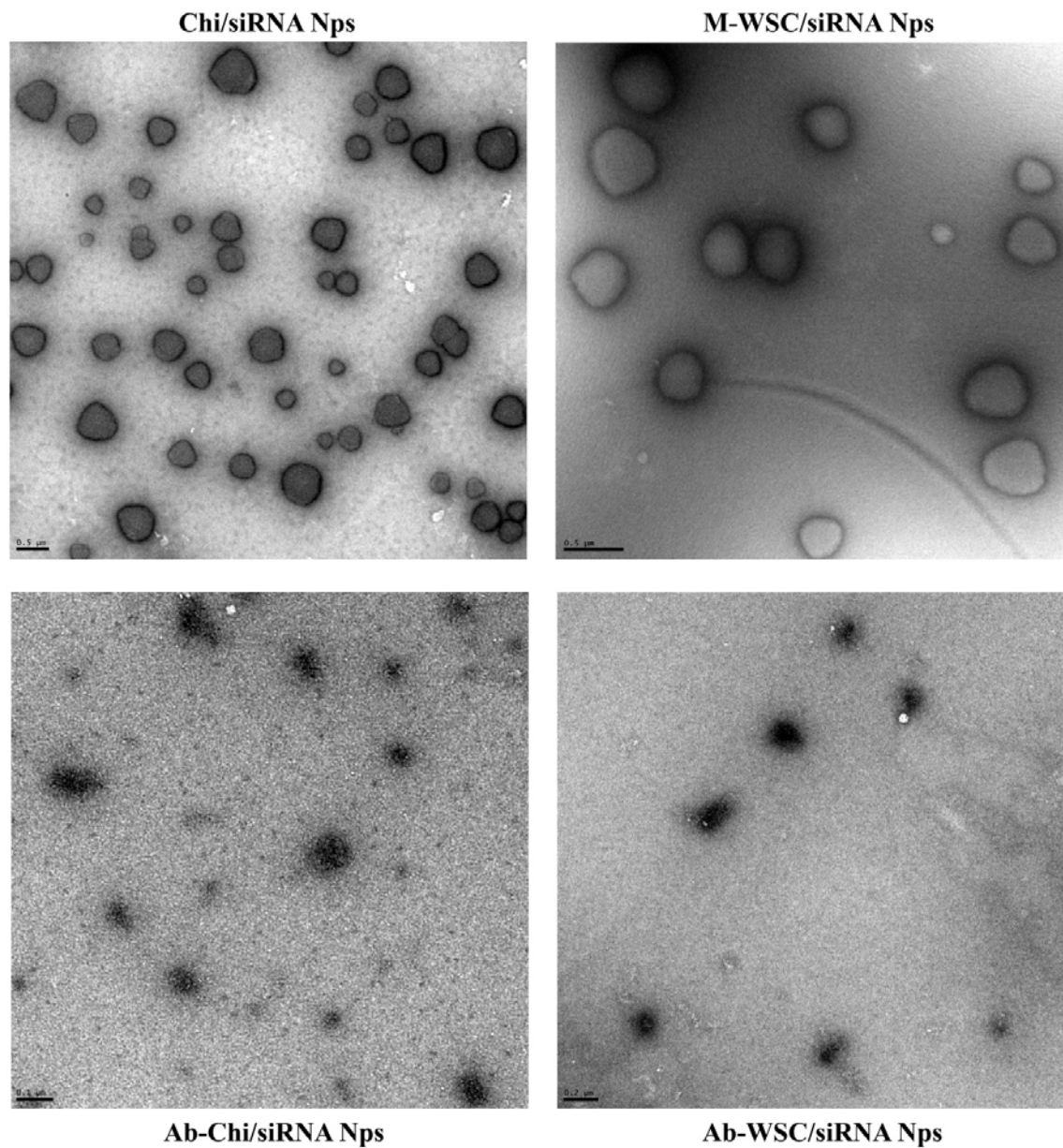


Figure 5.1 Transmission electron microscopy images of different siRNAs conjugated chitosan Nanoparticles. The scale bar for Chi/siRNA Nps and M-WSC/siRNA Nps is 0.5 μ m, and for Ab-Chi/siRNA Nps and Ab-WSC/siRNA Nps is 0.2 μ m.

5.3.2 Particle Size and Surface Charge

Size distribution and surface charge analysis was performed by DLS and shown in Table 5.1. Mean particle size of Chi/siRNAs Nps were measured as 272.2 \pm 8.13 nm, and 266.57 \pm 8.66 nm for M-WSC/siRNAs. The size of Ab conjugated chitosan Nps with different Ab ratio were also tested and showed that 10% Ab-Chi/siRNAs Nps have an average hydrodynamic diameter 295.53 \pm 6.47nm, 350.58 \pm 9.63nm for 20% Ab-Chi/siRNAs Nps, and 385.73 \pm 4.78nm for 30% Ab-Chi/siRNAs Nps. A slightly increased particle size was observed. A much larger size of Ab-WSC/siRNA Nps was detected when using BS³ conjugation methods to link Ab with chitosan. Different Ab ratios have also been performed and showed similar particle size, only 20% Ab displayed here corresponding to later study results. Three nanoparticles (Chi/siRNAs Nps, M-WSC/siRNAs Nps, Ab-Chi/siRNAs) have slightly different particle size, but no detectable statistical difference. In addition, TEM images (Figure 5.1) shown the various sizes of chitosan Nps, the smaller particle size was considered due to the lower molecular weight of chitosan and larger particle size was formed by relatively higher molecular weight chitosan.

Table 5.1 Size distribution and surface charge of different siRNAs conjugated chitosan Nps.

Name	Size (nm)	Zeta potential ζ(mV)
Chi/siRNA Nps	272.2+/- 8.13	23.63+/-0.18
M-WSC/siRNA Nps	266.57+/-8.66	35.13+/-2.19
10% Ab-Chi/siRNA Nps	295.53+/-6.47	24.33+/-0.73
20% Ab-Chi/siRNA Nps	350.58+/-9.63	21.93+/-0.61
30% Ab-Chi/siRNA Nps	385.73+/-4.78	17.77+/-0.18
20% Ab-WSC/siRNA Nps	580.73+/-18.37	11.27+/-0.81

During our studies, zeta potential analysis suggested that all nanocomplexes were positively charged. M-WSC/siRNA Nps have a higher zeta potentials than other siRNA loaded chitosan Nps, showing these Nps were more stable in suspension. In contrast, 20% Ab-WSC/siRNA Nps had a very low zeta potential approximately at 11.27+/-0.81mv. The synthesis procedures and/or instinct properties of these Nps needs further optimization and investigation. Other chitosan Nps possess an approximately 25mV zeta potentials. They are at a good stability conditions. Moreover, low zeta potential in Ab-Chi/siRNA Nps with higher Ab ratio were also observed, indicating the poor stability of 30% Ab-Chi/siRNA Nps compared to 10% Ab-Chi/siRNA Nps.

5.3.3 Binding Affinity Between siRNAs and Chitosan Nanoparticles

Electrophoretic mobility tests were performed to evaluate the chitosan and siRNA complexation efficiencies. siRNA must be stable in a bio-environment and can avoid digestion or degradation by various nucleases in order to have maximal activity for specific gene knockdown. The negatively charged siRNAs was synthesized with chitosan and formed nanoparticles to protect the siRNAs from degradation. Therefore, they would not easily separate from the nanoparticles and migrated down during electrophoresis. Co-administration of polyanions PAA can be used as a competitor to displace the siRNA from chitosan nanocomplexes. According to our results in Figure 5.2, the free siRNAs without chitosan Nps protection migrated down and showed detectable bands. Moreover, in all three chitosan nanocomplexes, the addition of PAA also results in the moving of siRNAs, and the bands showed in the figure indicated that siRNAs were displaced and move out the particle complexes as free siRNAs condition. All three chitosan nanocomplexes without incubation of PAA show any sign of siRNAs bands and demonstrating the fully protection of chitosan Nps to siRNAs and their stability.

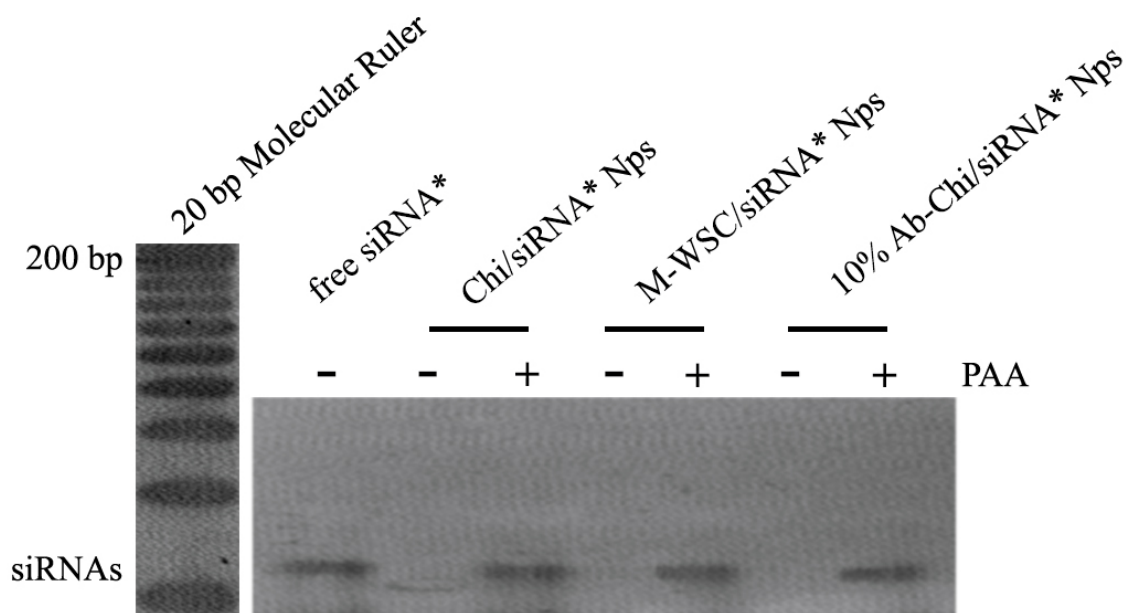


Figure 5.2 Gel retardation assay indicating the integrity of chitosan nanoparticles.

5.3.4 Low Cytotoxicity of Chitosan Nanoparticles

After 4 hours incubation at high concentration and low concentration of siRNAs and different chitosan Nps, murine bone-marrow derivatived macrophages expressed different morphology. The healthy status of macrophages without any treatment were also inspected. There is obvious sign of detachment of the cells and dramatically decrease of cell amount after high concentration of siRNAs incubation. For low concentration of siRNAs treatment, some of cell cytoplasmic vacuolation and granularity were observed. It is due to the slight toxin appeared in the present of lipid based reagents in the serum contained medium during transfection. In the contrast, there is no sign of deterioration of cells without transfection reagents. Very few granularities in the medium were also found

in three different chitosan nanopartilces, but majority of the cells remain their shape and appearance.

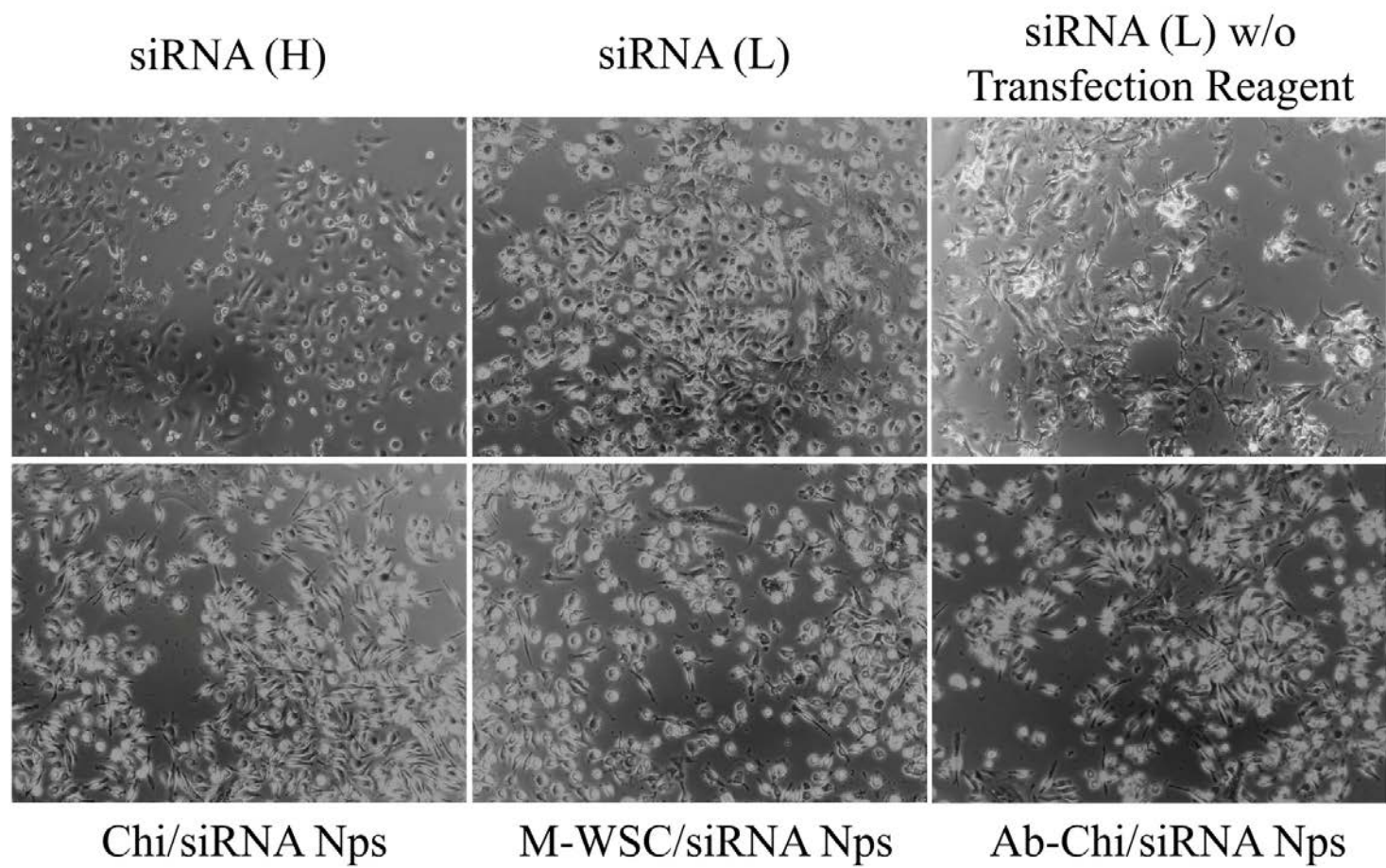


Figure 5.3 Morphology images of macrophages after treatment of siRNAs (at both high and low concentration) and different siRNA conjugated chitosan Nanoparticles (including Chi/siRNA Nps, M-WSC/siRNA Nps, and Ab-Chi/siRNA Nps).

5.4 Discussion

Due to the diverse nature of disease targets and bio-environments for siRNA gene silencing, there is no single ideal nanocarrier that is universally applicable. In our study, we tested the condition of SCI and developed a ligand conjugated natural polymer mediated siRNA delivery system to reduce inflammation induced secondary injury and promote the recovery of neural cells and tissues after SCI. We are searching for an optimal delivery tool that can be systematically administered safely and repeatably to the animal, and can deliver the siRNA specifically and efficiently to the targeted site. Unlike M2 anti-inflammation macrophages, M1 macrophages are pro-inflammation, and it can produce many pro-inflammatory molecules, especially a high level of NO production which subsequently result in the cellular death and tissue damage at spinal cord. Thus, these M1 macrophages were considered as our cellular targets in this study. Since the surface marker expressed differently in pro- and anti - inflammation macrophages after SCI, we exploited an antibody strategy to target specific macrophages in order to enhance the therapeutic outcomes.

Natural polymer chitosan was used in this study especially due to its biocompatibility, less cytotoxicity as well as convenient and reproducible synthesis procedures with siRNAs. Many publications have shown its safe and successful outcomes when delivering siRNAs. Our data has shown some observed toxic events when apply siRNA with lipid based transfection agents, but rarely detected in the cells with chitosan Np application.

Most importantly, the various possibility of chitosan modification and conjugation can avoid the intrinsic limitations of this polymer and improve its potential applications. We first focused on conjugating antibodies with chitosan polymers for targeting and considered two possible IgG incorporation methods in both acidic and neutral conditions. One approach is using combination of EDC and sulfo-NHS to react the carboxyl group of antibody with amine group of chitosan. In a whole antibody molecule, the Fr region (amine group) of antibody usually present as the antigen binding sites in the common applications. Thus, other approach we designed is using BS³ to conjugate amine group of antibody with amine group of chitosan. EDC and NHS conjugation reaction requires a pH conditions at range of 4.5~7.2 to be efficient, which is correspond to the acidic condition during the dissolution of the chitosan. On the other hand, the novel BS3 conjugation method needs an almost neutral condition to react; therefore, we prepared water soluble chitosan solutions for this case.

Although chitosan Nps with a higher Ab ratio showed gradually enlarged particle size and reduced zeta potentials, this did not mean that there was a direct correlation between size and zeta potentials. Zeta potentials depend on the level of electrolyte pH, flocculation, instability, and temperature and so on. For example, the good dispersion stability is usually with high positive (or negative) level zeta potential at very low pH or high pH, the pH between 4 and 7.5 is the range has been indicated can initiate the instability of suspension. The higher the zeta potential either negatively or positively, the stronger the repulsion between colloids to overcome the van der waal attraction. Therefore, they are more electrically stabilized. In contrast, the colloids in suspension with low zeta potentials are susceptible to agglomerate or sediment so that they are easily

to form a larger particle size. In our case, a larger particle size was observed in the chitosan Nps with increased Ab portion as well as Ab linked chitosan Nps using BS3 conjugation method. This is most likely due to the less stable condition of nanoparticles.

The selection and volume of chitosan used during nanoparticle synthesis can lead to a large structural and functional versatility for this material. During the synthesis process with nucleic acids, many parameters were determinant factors for the successful siRNAs delivery by chitosan Nps. For example, body distribution of nanoparticles after IV injection is highly influenced by their interaction with the biological environment, and this especially dependent on the physicochemical properties, such as the surface charge of the nanoparticle. The efficient delivery of siRNAs is also strongly depended on what kind of bio-environment they are delivered to and the size of the nanoparticles. These are closely related to the efficiency of cellular uptakes. Nanoparticles larger than 5nm in diameter do not readily cross the capillary endothelium. On the other hand, the enhanced vascular permeability in the liver, spleen, and some tumors permits the macromolecules and nanoparticles up to approximately 200nm in diameter to cross, it is known as the enhanced permeation and retention effect. The size of nanoparticles that is bigger than 500nm was reported easier for the recognition of macrophages and completion of phagocytosis. The degree of polymerization of chitosan (DP_n) as well as the fraction of N-acetylated units (F_A) were reported to be important associated with gene silencing efficiency as well. For example, gene silencing is most efficient when chitosan with intermediate chain lengths, that is, DP(n) approximate between 100 and 300 were used. [121]

The size, zeta potentials and stability of siRNA/Chitosan Nps are critical during siRNAs delivery and also depends on various parameters. Molecular weight of chitosan close related to the size of chitosan Nps, the size is decreased as the molecular weight increased. 10kDa chitosan was proven to produce a 3500nm size of particles. A range between 65 to 170kDa chitosan can produce 200 to 300nm diameter of nanoparticles. [210] Our data are consistent with the results in these earlier studies. The nanoparticle size of approximately 270~290nms were observed by TEM and analyzed using zetasizer when chitosan with similar molecular weight were used. In contrast, zeta potentials will slightly increase as molecular weight increases at a range of 65kDa to 170kDa. [210] In the study of nanoparticle stability, lower molecular weight of 10kDa fail to complex and compact siRNA into stable particles and a higher molecular weight (>60kDa) is required to form a stable nanoparticles. [212]

The DD value designated as the percentage of deacetylated primary amine groups along the molecular chain, which subsequently determines the positive charge density of the chitosan. Higher DD results in increased positive charge enabling a greater siRNA binding capacity. A relatively low DD value can decrease the charge of zeta potentials. In our cases, no retardation effect or unstability of siRNA conjugated chitosan Nps were observed during gel retardation study. It is because of the selected chitosan with MW between 65 to 170kDa and DD value of 75-85% were used.

The N/P ratio between chitosan and siRNAs represented as the ratio of a mass per charge of chitosan 167.88(when 84% DD is used) to a mass per phosphate of 325Da siRNAs, this relationship can also be simply described as weight ratio. They are also very

important component to modulate the size, zeta potential, and stability of nanoparticles. An w/w ratio of 37.5 (approximately N/P ratio of 54 to 59) was considered in our study based on previous successful protein silencing. [210] They showed that this range of N/P ratio can balance the toxicity and stability of chitosan materials during siRNA delivery.

Chitosan mediated siRNAs delivery is in a charge density-dependent manner and charge density strongly depends on the pH, or we can say a protonation level. The charge density of the delivery vehicle significantly impacts its interaction with components of the bloodstream and siRNA bindings. The comparative positive value of surface charge of the chitosan/siRNA complexes increased with increasing concentration of chitosan at a constant siRNA concentration. This net positive charge of the particles was desirable to prevent particle aggregation and promote electrostatic interaction with the overall negative charge of the cell membrane. It could probably explain why a higher Ab ratio, such as 30% Ab-Chi/siRNA Nps probably with less charge level, showed a less stable situation (indicated by a lower level of zeta potential). In the study of macrophage uptake, some findings also indicated that highly charged particles can lead to complement activation of macrophages, whereas near-neutral particles show reduced phagocytic uptake.

In summary, different parameters, such as molecular weight, DD value, N/P ratio, and pH level, are tightly related to the size, charge density, and stability of siRNA conjugated chitosan Nps. These characteristics of the nanoparticles can further impact the transfection and gene silencing efficiency. We successfully synthesized different chitosan Nps with reasonable size and zeta potentials value and minimized cytotoxicity based on

the earlier results established by many researchers. Especially, we developed and compared the properties of different ligands mediated chitosan Nps for macrophages subsets targeting. Additionally, we are first introduce a new Ab conjugation method with chitosan materials, in despite of the stability of Ab-WSC/siRNA Nps required further improvment.

CHAPTER SIX
PREVENTING CELL DEATH
AFTER SPINAL CORD INJURY VIA TARGETED SIRMAS DELIVERY

6.1 Introduction

6.1.1 Macrophages Polarization and Their Role in Spinal Cord Injury

Macrophages mediate a large scale of biological responses and play a key role in the immune systems. Modulation of macrophages to achieve an optimal host response could be crucial in the treatment of SCI. Recently, many groups reported the polarization of macrophages can influence neural behavior after SCI. Macrophages can perform distinctive functions by expressing either pro- or anti- inflammatory characteristics which depended on the stimuli received by the micro-environment. Classically or pro-inflammatory-activated macrophages upregulate the level of pro-inflammatory cytokines and designated as M1 macrophages. On the other hand, alternatively activated M2 macrophages, are associated with an anti-inflammatory profile and are crucial in tissue remodeling after inflammation, especially for axonal regeneration. [213] Granulocyte-macrophage colony-stimulating factor (GM-CSF) and macrophage colony-stimulating factor (M-CSF) are commonly used for different phenotypic and functional changes in macrophage lineage populations. Generally, the polarization of M1 macrophages

can be activated by GM-CSF with combination of LPS and IFN γ , and M2 macrophages can be primed by M-CSF with addition of interleukin-4 (IL-4) or IL-13 for M2a subset, combination of immune complexes and LPS for M2b subset, and IL-10 or transforming growth factor- β (TGF- β) for M2c subset of M2 macrophages. [214]

Many findings have been shown the phenomenon of macrophages polarization and its presence after SCI, [213,215,216] with a long lasting expression of M1 macrophages at damaged spinal cord tissue. The exacerbated secondary injury conditions after primary injury might due to this high level residence of pro-inflammatory macrophages. The hallmark of activated M1 macrophages is the upregulation of iNOS mRNA and its proteins expression at the earlier stage of SCI. [213]

The detecting techniques of western blotting, polymerase chain reaction (PCR), and immunohistochemical analysis are commonly used to trace the expression of iNOS. Some studies reported that the iNOS mRNA occurred at 3-12 hours after SCI and gradually decreased afterwards using PCR analysis. Immunohistochemical study shown the similar outcomes and suggested that iNOS positive cells peaked at 24 hours and declined to none expression within 3 days after injury. [217] The sum of earlier established study reveals that the ideal determination and analysis time for iNOS expression is between 12 and 24 hours after SCI, which will applied to our study.

Macrophages in the injured spinal cord origin from resident microglia and peripheral monocytes derived infiltrating macrophages. M1 macrophages trafficked through adjacent arachnoid and pia mater of the spinal cord to the injured site while M2 macrophages infiltrated through the brain-ventricular choroid plexus. [218] Compare to

the resident microglia, the infiltrated macrophages contributed to the phagocytosis, but not efficiently phagocytosing damaged and degenerated cells and debris in CNS as microglia in the early stage. However, they are the predominant cells associated with chemokins and many pro-inflammatory cytokines production, and has been identified to responding to the demyelination and axons degenerating, contributing to the secondary injury in spinal cord. [219] Therefore, bone marrow-derived macrophages were selected for our in vitro studies due to the nature of these macrophages and their susceptibility to be polarized by stimuli.

6.1.2 Route of Administration for SiRNAs Delivery

Unfortunately, siRNAs associated delivery systems possessed some limitations during in vivo applications, such as insufficient biodistribution. Therefore, the route of siRNA administration is critical during the application and also responsible for the dosage of siRNAs applied, the efficiency of tissue distribution, as well as the potential side effects. The different routes of administration of siRNA were investigated by many research groups to reveal the possible tissues that received siRNA corresponding to the administration. Intravenous administration route results in the accumulation of siRNAs in the kidney and pole/lumen of the proximal tubules, as well as urine due to the rapid excretion. Shawn D. et. al also detected the siRNAs uptake in the liver, pancreas, spleen and bone marrow using both hydrodynamic and standard IV. Intraperitoneal administration resulted in the siRNAs expression occurred in the spleen, liver and bone

marrow. Similar organs uptake, such as spleen, bone marrow as well as colon were also observed following rectal administration. [220]

The drug delivery to CNS is more complicated than other organs due to the issue of blood-brain or spinal cord barriers. The optimal administration to bypass this issue is through direct intrathecal or intraventricular injection to CNS. To effectively detect the biodistribution of siRNAs, dye-labeled siRNAs were often used through directly visualization of fluorescence signals in different tissues. Luo et. al has reported that fluorescence signal can be detected in the spinal cord and dorsal root ganglia after intrathecal delivery of siRNAs with transfection reagent. [221] The intrathecal injection can prevent certain degree of siRNA degradation which frequently occurred in the blood stream via serum protein. Even though the CNS environment contain less nuclease compared to plasma and many other tissues, the assisted delivery strategies are still critical for successful siRNAs delivery to CNS because it not only can improve transfection efficiency, but also provide various functions by simply modification of the carriers. For example, conjugating the targeting motif to drug carriers and delivering them to specific cell types or tissues for optimized siRNA uptakes in certain organs. [222]

6.1.3 Nanoparticels Targeting Strategies to Macrophages via Fc Receptor

Recently, many reports indicated that the limitation of onsite of siRNAs delivery could jeopardize its potential treatment. Therefore, our gear was directed to the development of targeting strategies in order to achieve more efficient protein silencing. Since the

targeting strategies can be potentially applied to many disease-causing cells and tissues, a various functional add-ons, such as antibodies, aptamers, and peptides were widely used to guide its conjugated nanocomplexes to the desired cells or tissue sites. In addition, these ligands can be characterized with therapeutic, diagnostic, or barrier-avoiding properties to fulfill multivalent functionalities. Antibodies (Abs) have been commonly and successfully used as escort molecules for the targeted delivery of nanoparticles, and many are either proved by FDA or under development in clinical applications. This antibody mediated targeting approach is based on the association of the ligands with the receptors and receptor-mediated endocytosis, which usually considered as active targeting. In siRNAs studies, the targeted delivery provides the potential for efficient siRNA transfection into specific type of cells and avoiding nonspecific binding.

Since mononuclear phagocyte was characterized of engulfing apoptotic cells, pathogens, and even microparticels via phagocytosis and destroy them, the passive targeting approaches can be used in the context of drug delivery to macrophages. It is close related to the intrinsic physicochemical properties of the carrier. Sometimes, nanoparticles can passively accumulate at inflamed sites because of the enhanced permeation and retention (EPR) effect. [223] However, in order for macrophages to uptake the desired therapeutics delivered by these nanoparticles, we can either use passive targeting approaches by modulating the physical properties of the nanoparticles or use a ligand associated active targeting strategies by selectively identify the surface marker of the macrophages. It has been postulated that both anionic and cationic charged particle and nanoparticle with size larger than 100nm are readily opsonized by the macrophages which is mainly resided in the liver and spleen. [223] Schafer et al. studied different particles uptake including

poly(methylmethacrylate), poly(alkylcyanoacrylate), and human serum albumin particle in human macrophages. The results indicated that nanoparticles made from the same material but of larger diameter were easier for phagocytosis. [224] In phagocytes, endocytosis can be initiated by small particulate complexes formation, and phagocytosis can be initiated by a larger aggregates. Thus, the vital methodological tool to internalize the nanoparticles to specific macrophages is to use the active targeting via specific antibody-antigens reactions.

Active targeting are commonly accomplished by modifying of the surface of nanoparticles via a targeting motif, a ligand with selective affinity, and can interact with specific receptors in certain cell types. Nanoparticles used for macrophage-targeted delivery can be associated with various receptors such as Fc receptors, mannose, galactose, and sialic acid specific lectin-based receptors, lipoprotein receptors, and scavenger receptors. [223] The activation, recognition, endocytosis, secretion activities of the macrophage depend on the surface receptors. Synthetic functionalized mannosyl ligands has been revealed to conjugate with various drug carriers: liposomes, chitosan, and gelatin nanoparticles in such way to increase the interaction with macrophages than unmodified nanoparticles. The macrophages uptake via Fc Receptors provide key role in active phagocytosis and endocytosis. Many studies reported that immunoglobulin and monoclonal antibody or its Fc fragment incorporated nanocomplexes present much higher binding and internalization by macrophages via Fc receptor-mediated endocytosis. Nano-delivery small molecules therapeutics were widely use for macrophage targeting in various pathologic conditions including mycobacterium tuberculosis, endotoxin-induced

lung inflammation, parasitic infection, as well as HIV/AIDS. Many of them are mediated through Fc receptors, and its associated drug delivery system is well developed. This mechanism of macrophage uptake is called antibody dependent cellular phagocytosis (ADCP). Briefly, IgG molecules that is specific for certain surface receptor of antigens can bind to these pathogens with their fragment antigen binding region (Fab region) which contains amine group, then their fragment crystallizable *region* (Fc regions) exposed to phagocytes in order to induce phagocytosis. The low affinity properties of Fc receptors can reduce the possible binding to antibody and agglutination when there is no present of antigen. [225,226]

A detailed understanding of the functionality and property of these Fc receptors is critical during the application. Subfamilies of Fc receptors can be classified according to variable affinity and can also be classified based on the activating and inhibitory properties. It is very important to balance the expression between activating and inhibitory Fc receptors for normal immune responses. There are some similarities of Fc γ R_s expression between human and mouse species, but do exist many differences which can complicate the clinical application. For example, mouse macrophages always express relative high levels of Fc γ RI receptors at normal conditions, but the level of Fc γ RI receptors expressed low, and high in inflamed human macrophages. The classification of similarity and difference between human and mouse was summarized in Table 6.1.

Table 6.1 Summary of Human and Mouse Fc Receptors.

Human	Fc γ RI (CD64)	Fc γ RIIA (CD32A)	Fc γ RIIB (CD32B)	Fc γ RIIC (CD32C)	Fc γ RIIIA (CD16A)	Fc γ RIIIB (CD16B)
Mouse	Fc γ RI	Fc γ RIII	Fc γ RIIB		Fc γ RIV	
Major Function	Activation	Activation	Inhibition	Activation	Activation	Activation?

Although our study focused on murine macrophages, the terms associated for human Fc receptors are used in the here.

Some experiment further indicated functionality of Fc receptors by blocking different classes of FcRs. The results showed a significant reduction of ADCP when block all three Fc Receptors with F(ab')₂ fragments. Interestingly, the decreased ADCP was not observed when only blocking FcRI receptors (CD64), indicating that Fc receptor mediated phagocytosis only involved with Fc γ RII and Fc γ RIII (CD16 and CD32). [227] Furthermore, some results also indicated that blockage of either FcRII or FcRIII receptor didn't remarkably influence the phagocytosis, but significant effected by the blockage of both receptors. This suggested that either of these two low-affinity Fc receptors is capable of functioning independently to initiate phagocytosis. [228] Therefore, the study of nanoparticle uptake by macrophages through phagocytosis can focus on either Fc γ RII or Fc γ RIII receptors, or both.

6.1.4 Targeting Macrophages in Spinal Cord

The subsets of macrophages were revealed a markedly different biofunctional role in immune system as mentioned earlier, there is no doubt that discrimination between M1 and M2 macrophages also strongly influence the targeting strategies to the macrophages. Many researchers focused on targeting tumor-associated macrophages for cancer treatment. These macrophages were favor the tumor growth via angiogenesis and metastasis, and they are usually consider as a M2-similar macrophages which particularly indicated by Arginase-1 and CD206-mannose receptor expression. However, the role of M2 macrophages in different bioenvironment could results in a completely opposite outcome. In the case of spinal cord injury, the M2 macrophages can produce neurotrophic factors and promote the nerve outgrowth in either developing or mature neurons after SCI. [229] On the other hand, pro-inflammatory M1 macrophages can produce various cytokine such as TNF- α and NO and play an pivotal role in secondary injury. Therefore, the inhibitory molecules generated from M1 macrophages could be an important target in drug delivery to treat neural trauma and disease.

The expression level of the receptors can be alternated depending on the changes in bioenvironment. The differentially higher expression of Fc receptors on the surface of macropahges was found in many rheumatoid arthritis studies, and also found in the case of SCI. Since inflammatory macrophages at rheumatoid arthritis joint over-expressed CD-64, CD64-directed immunotoxins has been reported to be useful for screening, diogonose or even treatment for rheumatoid arthritis. [230]

The surface markers after spinal cord injury were characterized as CD86, CD16/32 positive M1 macrophages and CD206 positive M2 macrophages. [213] In the case of multiple sclerosis, surface marker CD40, CD86, CD64 and CD32 were overexpressed by activated microglia and macrophages throughout demyelination. [231] There is a significant increased M1 macrophages were observed at first day after SCI, however, the M2 macrophages featured with IL-4 receptor α chain and CD206-mannose receptor surface markers start upregulation from day 3 and significant increased at day 7. [218] This timeline is cohesive with the results demonstrated by Kristina Kigerl et al and Kyoung-Jin Min et al . [213,232] The expression of CD16, CD32, and CD64 in different macrophage populations has also been indicated to correlated with phagocytic activity and phagocytosis efficacy.[233](Also see 6.1.3) Therefore, Fc receptors mediated M1 macrophage targeting can be a potential strategy in SCI study.

6.2 Materials and Methods

6.2.1 Cell Culture

Bone marrow-derived macrophages (BMDM) from C57BL/6 mice were purchased from cell biologics LLD which purified by positive selecting CD11b using flow cytometry and were maintained in cell medium with Dulbecco's modified Eagle medium/F12, 10 mM L-glutamine, supplemented with 10% fetal bovine serum, 100 U/ml penicillin, and 100 μ g/ml streptomycin in the presence of GM-CSF (5ng/ml) or M-CSF(2500U/ml). The macrophage were seeded in 12- well or 24-well tissue culture plates and allowed to adhere for 24 hour at 37°C in humidified atmosphere containing 5% CO₂.

6.2.2 Light Microscopic Studies on M1 and M2 Macrophages Morphology

Macrophages incubated with GM-CSF were polarized to M1 macrophages by challenging with combination of LPS (Sigma) and IFN γ (B&D Research) at higher concentration of 1 μ g/ml LPS+200 ng/ml IFN γ or at lower concentration of 100ng/ml LPS+20ng/ml IFN γ for 12 hours. Also, macrophages incubated with M-CSF were treated with IL-4 for 12 hours to activate M2 macrophages. The control group is prepared by GM-CSF and without stimulation of any cytokines. The morphology of macrophages was imaged using Olympus IX 81 inverted microscope.

6.2.3 In Vitro Experiment

For siRNA experiment, the siRNA was mixed with desired volume of Lipofectamine 2000 transfection reagent based on the instruction from the companies. Macrophages cultured in serum free medium were then incubated with 2 μ l of 20 μ M siRNAs per well for 48 hours (or 4 hours for comparison) before challenged with medium containing 100ng/ml LPS and 20ng/ml IFN γ for 12 hours. To screening most efficient iNOS siRNAs, macrophages were also received the same siRNA treatment but stimulated with higher concentration of insults, that is, 1 μ g/ml LPS with 200ng/ml IFN γ . The target sequences of siRNA as listed here were used for screening. GAAACGUUAUCAUGAAGAU (siRNA1), CAUGGGAGCCACAGCAAUA (siRNA2), GGAGAUGGUCCGCAAGAGA (siRNA3) and GAUUUAGAGUCUUGGUGAA (siRNA 4). In addition, three different siRNA/chitosan Nps were used as treatments during the experiment, which are

Chi/siRNA Nps, M-WSC/siRNA Nps, and Ab-Chi/siRNA Nps. Pre-prepared siRNA conjugated chitosan solution at concentration of 2 μ l of 20 μ m siRNAs was added to each well containing serum free medium for 4 hours before low concentration of LPS/ IFN γ challenge. For all experiment, cells were incubated in fresh medium for 12 hours between treatment and challenge procedures. In negative control groups, scrambled siRNAs (will not results in the specific degradation of iNOS mRNA) were synthesized with chitosan, instead of iNOS targeted siRNAs.

6.2.4 Transfection Efficiency

Bone-marrow derivate macrophages were cultured in a 12-wells dish at density of 1*10⁶. Three different chitosan Nps were prepared as described 5.2.1section with exceptional of DY547 conjugated siRNAs (customized by GE Dharmacon, CO) were used with sense sequences DY547-CAUGGGAGCCACAGCAAUAUU and antisense 5'-PUAUUGCUGUGGCUCCCAUGUU siRNAs with transfection reagents or siRNA conjugated chitosan Nps were incubated for 4 hours before imaging. The fluorescence signals and macrophage morphology was imaged by Olympus IX 81 inverted microscope. The overlapping of fluorescence and light microscopic images for each groups also performed to indicate the level of macrophage uptake.

6.2.5 Western Blot Analysis of Gene Silencing

The cells were treated and challenged as described in 6.2.3 section. Subsequently, each group of macrophages was incubated in ice-cold RIPA buffer (Pierce, Thermo Fisher

Scientific Inc, IL) containing 25mM Tris-HCl (pH 7.6), 150mM NaCl, 1% NP-40, 1% sodium deoxycholate, 0.1% SDS, and keep on ice for 5 mins. Macrophage lysate were gently collected using cell mini scraper and centrifuged for 15mins at 14000rpm at 4°C. Then supernatant were quantified by BCA protein assay kit (Pierce), and equal amount of the proteins from different samples were loaded in 7.5% sodium dodecyl sulphate (SDS)-polyacrylamide gels and transferred to a PVDF membrane. Membrane were incubated in blocking buffer containing 1X Tris Buffered Saline with Tween® 20 (TBST, Cell Signaling Technology, Inc.) and 5% w/v nonfat dry milk for 1 hour at room temperature. Immunoblotting was processed with incubating membrane with mouse specific primary antibody iNOS (#2982, Cell Signaling Technology, Inc.) and β -Actin Antibody (#4967, Cell Signaling Technology, Inc.) overnight at 4°C. Then, membrane was gentle agitated in blocking buffer containing anti-rabbit IgG, HRP-linked Antibody (#7074, Cell Signaling Technology, Inc.) for 1 hour at room temperature and developed in LumiGLO solution for 1 min at room temperature. The bands of interest were detected by Syngene GBox imager and the quantization of interest band was analyzed using Image J software.

6.2.7 NO Assay

The macrophages were incubated with siRNA with or without transfection reagent for 48 hours. Also, all four siRNA/chitosan Nps were also performed as treatment groups and incubated for 4 hours before LPS and IFN γ challenge. In two cases of Ab conjugated chitosan nanocomplexes, different level of Ab (10%, 20%, and 30%) incorporated with

chitosan were also analyzed. Cells after received different treatments were then incubated in fresh medium for 12 hours before stimulated by 1 μ g/ml LPS and 200ng/ml IFN γ for 12 hours. Different samples were immediately collected and separately detect the values of nitrate (NO₃⁻) and nitrite (NO₂⁻) levels based on Nitric Oxide Assay Kit (Pierce).

6.2.8 In Vivo Experiment

All aspects of animal care and treatment were carried out according to the guidelines of Purdue Animal Care and Use Committee (PACUC). Female BALB/c mice with weight approximate 25g were used in this study. Spinal cord injury was induced similar to the surgical procedures described at 4.2.3 section with exception that clip compression was used to spinal cord instead of forcep compression. The prepared chitosan solution described at 5.2.1section was centrifuged for 15 mins at 4 °C. The pellet was then diluted using RNase free water and prepared as 10 μ g siRNAs in 10 μ l chitosan Nps suspension. All siRNAs treatments were conducted by injecting 10 μ l solution to spinal cord via hamilton syringe with 30 Gauge needles for 10 mins.

6.2.9 Western Blot Analysis for Spinal Cord Extracts.

Mouse were deeply anesthetized, euthanized, and kept on ice at 24 hours after SCI. The injured spinal cord segments (0.5cm long) were rapidly removed and freeze in the dry ice. Before use, the frozen tissue were weighted and placed into vial with Triple-Pure, High Impact Zirconium Beads (1.5mm) and lysis buffer which containing RIPA buffer,

1x Halt Protease and phosphatase Inhibitor Cocktail, and 1x EDTA (Pierce). The samples were then homogenized using BeadBug Microtube Homogenizer (Benchmark). The homogenate was centrifuged at 10,000 g for 5 mins at 4°C. The protein concentration of tissue lysates was then determined with a BCA Protein Assay Kit (Pierce). 50ul aliquots were subjected to 4–20% polyacrylamide gel, and the proteins were electrophoretically transferred to PVDF membrane filters. The membrane then were blocked with 5% nonfat milk in TBST for 1 hour at room temperature. After washing, the membrane were incubated with primary antibody solution containing iNOS, α -tubulin (1:1000, Cell signaling), Bcl-2 (1:200), and Bax (1:100) (Santa Cruz Biotechnology, Inc) separately overnight at 4°C. Next day, the membrane were washed for 3 times with TBST and probed with HRP conjugated secondary antibody for 1 hour at room temperature. Then, it is followed by the incubation of LumiGLO solution for 1 min at room temperature. The membrane was exposed to Syngene GBox imager and the density of the immunoreactive bands was quantified using ImageJ software.

6.2.10 Statistical Analysis

All data are shown with standard error of the mean (\pm SEM). The data was determined as normal distribution based on the level of skew and kurtosis less than 2 and 9. Tukey's HSC multiple comparisons tests were used. Significance was determined by a P-value \leq 0.05.

6.3 Results

6.3.1 Divergent Morphologies of M1 and M2 Macrophages

In our results, we demonstrated that the activation of polarized macrophage is accompanied with the alternation in macrophage morphology. According to our results in Figure 6.1, the control group without any cytokine stimulation expressed a spindle-look or rounded shape of cells, and the induction of IL-4 results in a more long elongated shape of M2 macrophages. These extended shaped M2 macrophages also showed an enhanced adherence properties compared to M1 macrophages. Moreover, the stimulation of LPS+IFN γ results in more flattened round appearance as well as outspread cytoplasm in M1 macrophages. In addition, a higher concentration of LPS+IFN γ is with similar but more enhanced results.

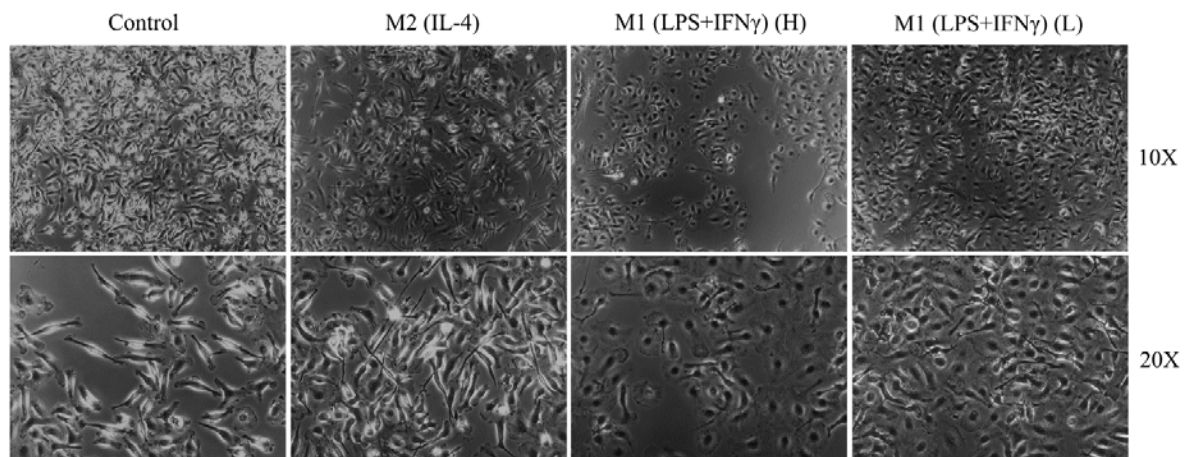


Figure 6.1 The macrophage morphology of inactivated macrophages (control), activated M2 macrophages, and activated M1 macrophages. Control group did not receive any cytokine activation. M2 macrophages were activated by IL-4 shown as M2(IL-4), and M1 macrophages were stimulated by either high concentration of LPS+IFN γ or low concentration of LPS+IFN γ , indicating by M1 (LPS+IFN γ) (H) and M1 (LPS+IFN γ) (L) respectively.

6.3.2 Efficient Transfection of SiRNAs Conjugated Chitosan Nanoparticles

The intracellular distribution of siRNA with transfection reagent, Chi/siRNA Nps, M-WSC/siRNA Nps, and Ab-Chi/siRNA Nps in the murine BMDM were imaged using fluorescence and light microscope. Customized DY547 dye conjugated with 5'end of siRNA sense strand were used to visualize the cellular uptake. In figure 6.2, DY547 signals were imaged using fluorescence microscope and expressed as the red fluorescence signals displayed in the first row.(Figure 6.2 A and B) It demonstrates the quantity and distribution of siRNAs or siRNA with chitosan complexes. The second row (Figure 6.2 C and D)

showed images of macrophages, and the third row (Figure 6.2 E and F) showed an overlapping image of these two. The results showed a comparison of the transfection efficiency between using transfection reagent (Figure 6.2 left column) and Ab conjugated chitosan Np mediated (Figure 6.2 right column) siRNA delivery. The endocytosis of Ab-Chi/siRNA Nps was dramatically higher than using transfection reagent during a 4 hours incubation time. There is approximately 60~70% DY547-labeled macrophages when using Ab-Chi/siRNA Nps delivery, comparing to 10~20% using transfection agent. However, there is no significant difference between Ab-Chi/siRNA complexes with either M-WSC/siRNA or Chi/siRNA complexes (Data not shown here).

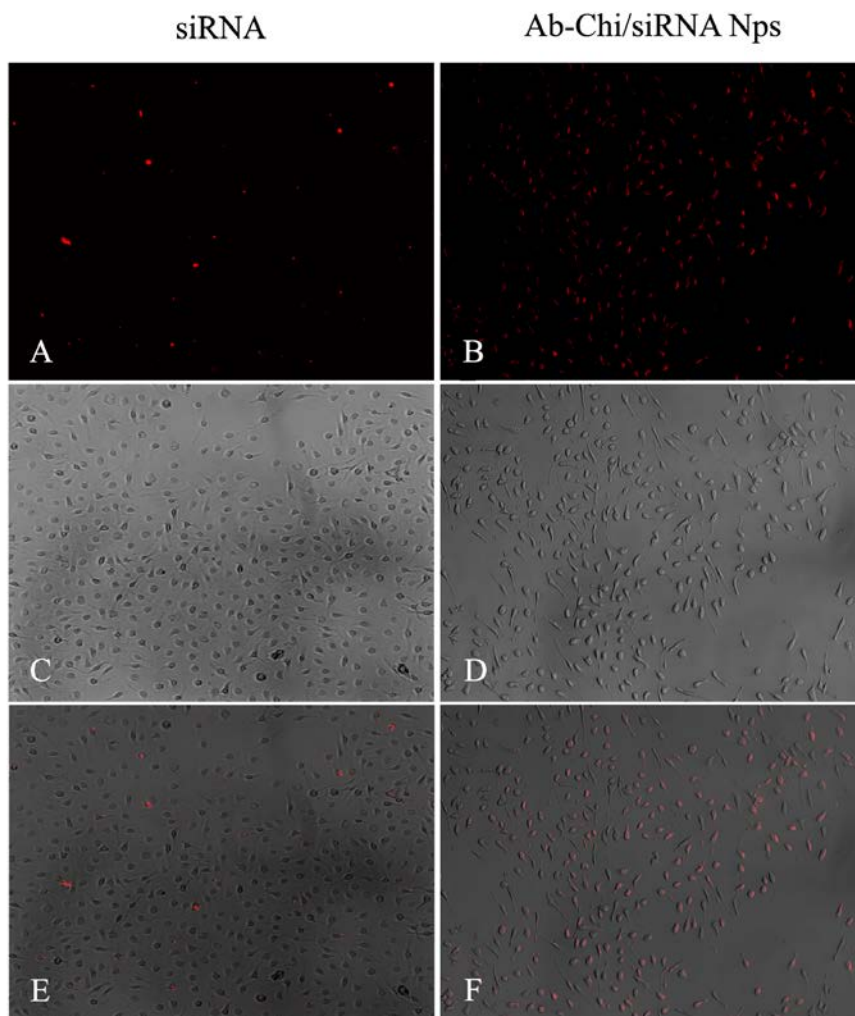


Figure 6.2 Illustration of transfection efficiency of siRNAs and siRNA conjugated Ab-chitosan Nanoparticles. A and B are fluorescence images, indicating distribution of siRNA and siRNA loaded chitosan Nps. C and D are macrophage images, and E and F are overlapping images.

6.3.3 Protein Knockdown

Following the confirmation of cellular uptake, the silencing effects of siRNA were performed using western blotting methods. We used LPS+IFN γ to initiate the activation of M1 macrophages and used IL-4 to induce M2 macrophages. The iNOS protein expressions were evaluated at the condition of activated M1 macrophages, activated M2 macrophages, and control group which is the macrophages without cytokine stimulation applied. There is no iNOS expressions were observed in either control group or IL-4 activated M2 macrophages. In contrast, there was a significant increased level of iNOS expression found after M1 macrophages activation (Figure 6.3 A), especially under the stimulation of a higher concentration of LPS+IFN γ (Figure 6.3 B). Four different siRNA sequences were applied separately for 48 hrs before LPS+IFN γ stimulation and were screened for an optimized silencing of iNOS expression. Combining low and high level of LPS+IFN γ stimulations, we conclude that the siRNA*2 showed a significant reduction of iNOS expression with $p \leq 0.001$ and $p \leq 0.01$ respectively. Although the siRNA1 also shown a dramatically reduction of iNOS protein level, the results are more variable compare to the results of siRNA*2. Therefore, siRNA*2 were used in all following experiments for further studies.

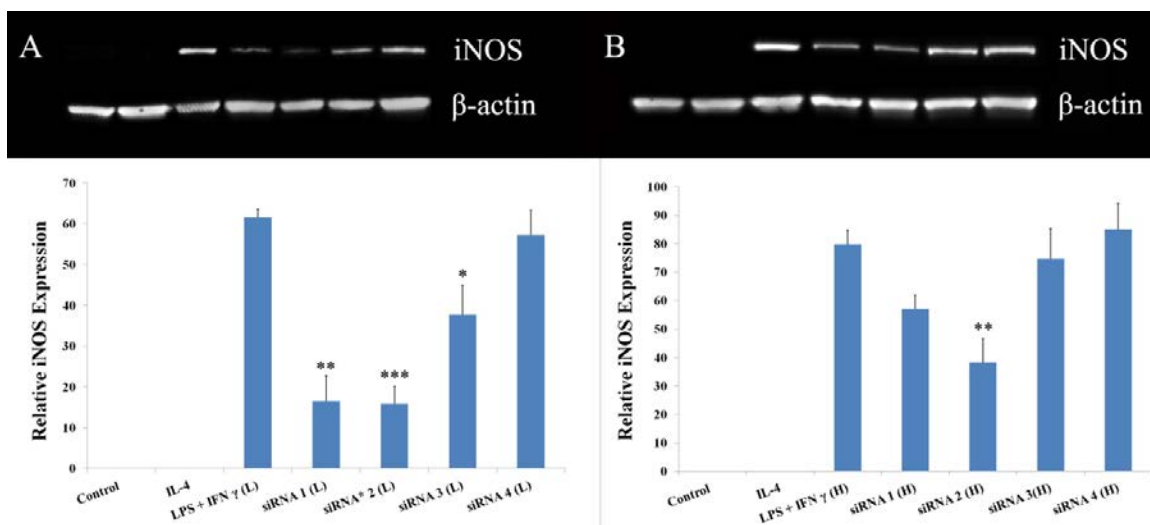


Figure 6.3 Screening of siRNAs for silencing of iNOS mRNA expression. Protein silencing efficiency of different sense and antisense strands of iNOS specific siRNAs. Control group represents the macrophages without any cytokine stimulation. IL-4 represents M2 macrophages were activated by IL-4 cytokines for 12 hours. LPS+IFN γ (H) indicated the activated M1 macrophages stimulated by 1 μ g/ml LPS +200ng/ml IFN γ , whereas LPS+IFN γ (L) indicated the activated M1 macrophages stimulated by 100ng/ml LPS +20ng/ml IFN γ for 12 hours. The target sequence of four different siRNAs was listed in 6.2.3.

As we mentioned earlier, siRNAs can be transfected into macrophages using transfection reagent, but have very limited transfection efficiency in a shorter incubation time. Most commercially available transfection reagents require days of incubation time for optimized transfection. In our study, we compared the iNOS reduction level between a 48 hours incubation and a 4 hours incubation time. The data showed that a longer incubation time results in a dramatically downregulation of iNOS expression after low level of LPS+IFN γ stimulation to M1 macrophages. Moreover, there is a significant statistical difference of iNOS expression between without (Figure 6.4 LPS+IFN γ (L)) and with pre-treatments using 48 hours incubation of siRNAs, 10%Ab-Chi/siRNA Nps, M-WSC/siRNA Nps, and Chi/siRNA Nps in activated M1 macrophages. ($p \leq 0.001$; $p \leq 0.001$; $p \leq 0.01$; $p < 0.01$ respectively shown in Figure. 6.4) It is noteworthy that there is no statistical differences were detected between siRNAs treatment for 48 hours and treatment for 4 hours, although the mean value for 4 hours incubation of siRNAs shows significant less reduction in protein silencing and showed no statistical difference compared to without treatment. The statistical differences were also observed between siRNAs treatment for 48 hours and scrambled siRNAs (N-siRNA) ($p \leq 0.001$), and similar statistical outcomes were also observed when compare targeted siRNA* with scrambled siRNAs (N-siRNA) in different siRNA conjugated chitosan nanocomplexes including 10% Ab-Chi/siRNA Nps, M-WSC/siRNA Nps, and untargeted Chi/siRNA Nps.

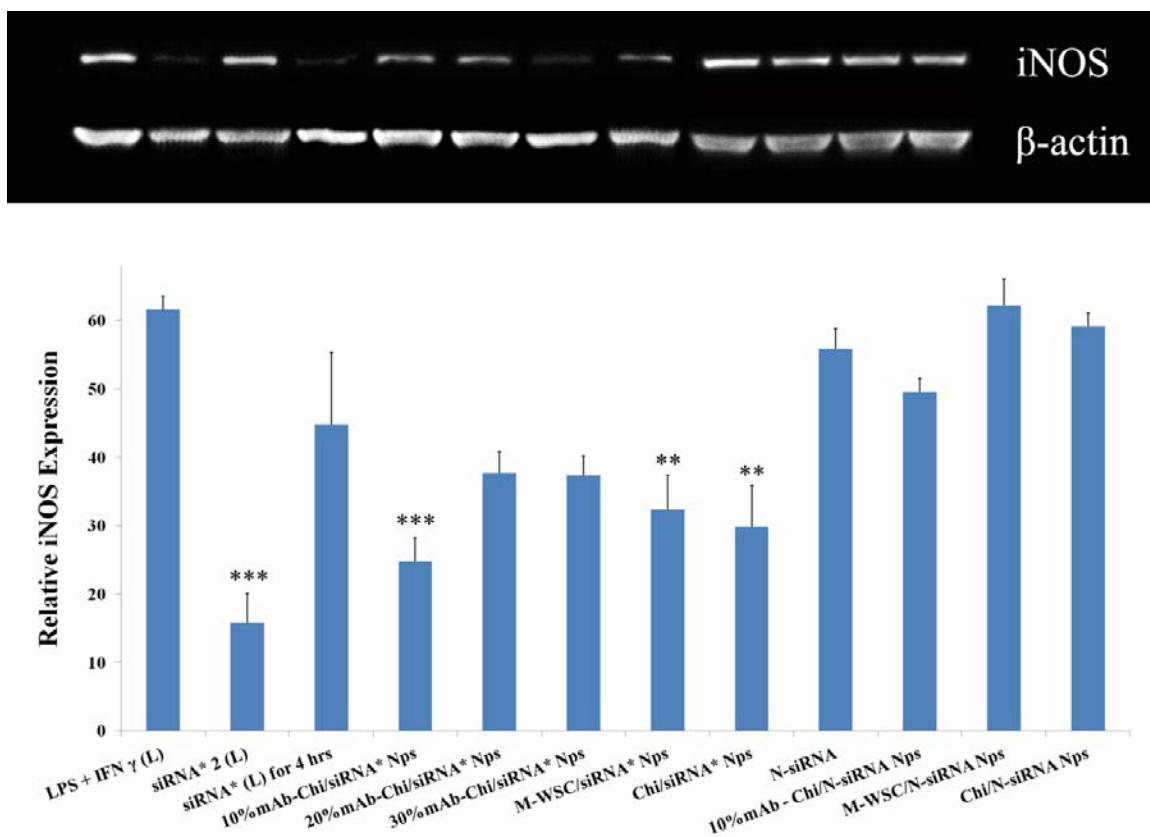


Figure 6.4 Knockdown of iNOS protein activity. All groups were challenged with low concentration of LPS+IFN γ . SiRNA*2 (L) indicated using siRNA with transfection reagent treatment for 48 hours, and a 4 hours incubation treatment time was also performed. Different Ab combination ratio range from 10% to 30% in Ab-Chi/siRNA Nps was also tested for iNOS expression. The outcomes of mannosylated chitosan and untargeted chitosan mediated siRNA treatment were presented here as well. Last four group demonstrate the same transfection reagent and chitosan Np based siRNA treatment with exception of scrambled siRNA were applied. Label siRNA* indicated the siRNAs used in all experiment was siRNA2 indicated in Figure 6.4. Label N-siRNA indicated scrambled siRNA. * $p \leq 0.05$; ** $p \leq 0.01$; *** $p \leq 0.001$.

6.3.4 NO Reduction

NO production, as a result of iNOS expression, is the direct detrimental molecules to exacerbate the primary SCI and to sabotage the neural functional recovery. The level of NO production was evaluated in a pattern as that in western blotting studies. The LPS and IFN γ stimulation was applied to all groups except for control and IL-4 initiated M2 macrophages. The results showed that all treatment groups with targeted siRNAs (siRNA*) showed a dramatically reduction of NO level. ($p < 0.001$ compare to without treatment in figure 6.5) It confirmed the silencing efficiency of siRNA*2 addressed in Figure 6.3. All the data are matching the results in protein expression study describe in 6.3.3 with exception of the similar outcomes of NO reduction for three different siRNA conjugated chitosan complexes. We also tested NO production after the treatment of siRNAs with transfection reagent and without transfection reagent. An increased NO level was observed when there is no transfection reagent applied, suggesting that the poor cellular membrane crossing of siRNA itself and failure of iNOS protein silencing. BS3 crosslinker mediated Ab conjugated chitosan Nps with a low zeta potential and larger particle size were also tested. A slightly NO reduction indicate the this synthesis method needs a further improvement in order to successfully delivery siRNA and silencing the desired mRNA expression. ($p \leq 0.05$)

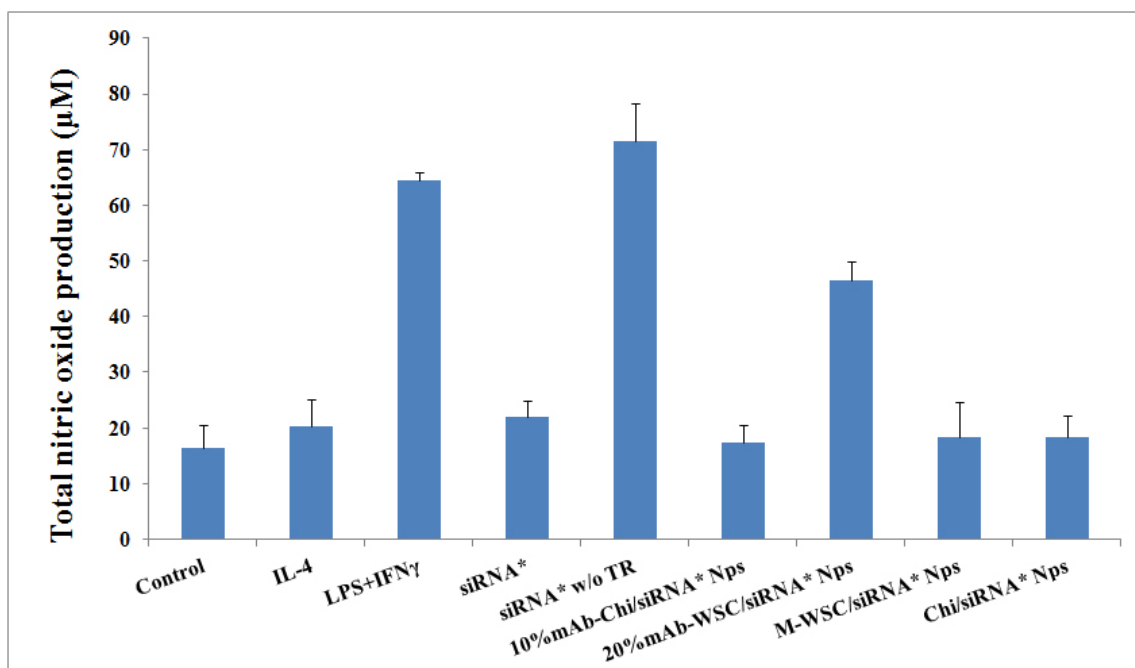


Figure 6.5 NO production of macrophages without cytokine stimulation, activated M2 macrophages stimulated by IL-4, and M1 macrophages challenged with LPS+IFN γ with and without siRNA related gene silencing treatment.

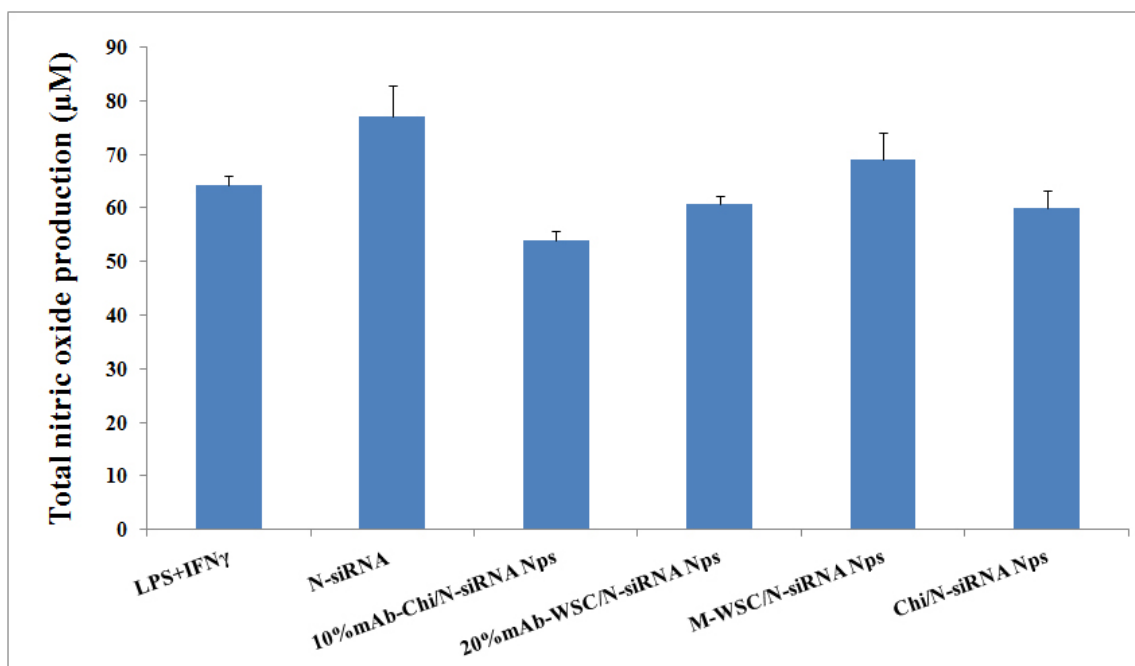


Figure 6.6 NO production using scrambled siRNAs.

In contrast, we also performed all groups with scrambled siRNA (N-siRNA), and it fail to prevent the NO production and showed no statistical difference.(See Figure 6.6)

The reduction ability of NO level using siRNA treatment with different sequences was screened before apply the experiments described at Figure 6.5. These results confirmed the knockdown ability of siRNA2 (siRNA*) as protein studies. The same NO assay also applied to evaluate the reduction level produced by two different Ab conjugated chitosan/siRNA Nps with various Ab ratio (from10%-30%). There is no statistical difference of NO level between different Ab ratio in each group. However, there is significant statistical difference between with and without chitosan/siRNA Nps treatment. ($p \leq 0.001$) (Data not shown in here)

6.3.5 Inhibition of Apoptosis Pathway after Spinal Cord Injury

To exploit the functionality of targeted chitosan Nps in SCI conditions, we induced a compression injury to spinal cord of the mice to initiate the upregulation of iNOS protein expression and NO production. In our study, not only iNOS, but also Bax and Bcl-2 protein expression were also investigated using western blotting methods at 24 hours after SCI. The upregulation of iNOS expression was observed after SCI (See Figure 6.7). Pro-apoptosis Bax level were also appreciably increased, and anti-apoptosis Bcl-2 level, in the contrary, were significantly decreased after SCI, indicating the apoptosis signaling pathway was initiated or might be propagated after injury. Two treatment groups, Ab-Chi/siRNA Nps and M-WSC/siRNA Nps, were performed to animal after SCI. Both treatment groups showed a trend of elimination of iNOS and Bax expression and

relatively increased Bcl-2 levels, especially in the case treated with Ab-Chi/siRNA Nps. (***) $p \leq 0.001$ for iNOS; ** $p \leq 0.01$ for Bax and Bcl-2) These results suggest the neuroprotective role of siRNA conjugated chitosan Nps by preventing cell apoptosis signaling pathway after spinal cord trauma.

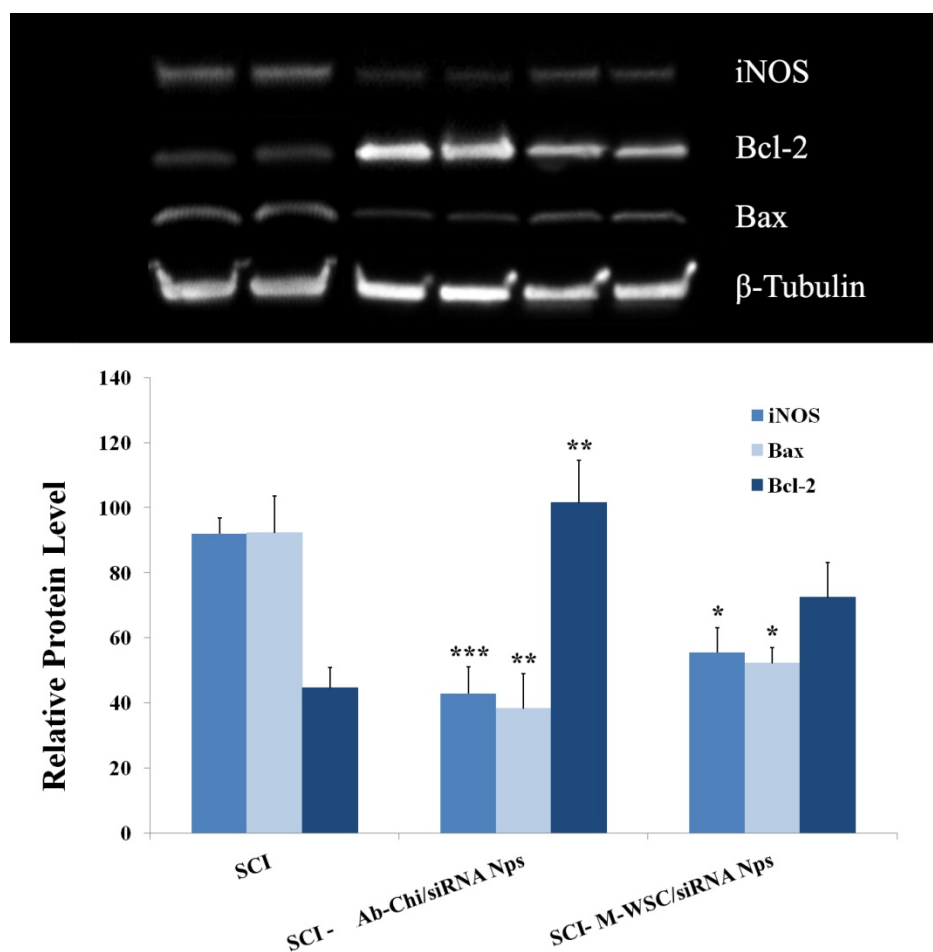


Figure 6.7 Different proteins expression level after SCI with and without treatment of different chitosan nanoparticles carried siRNAs. Ab-Chi/siRNA Nps were originally designed for M1 macrophages targeting, and M-WSC/siRNA Nps for M2 macrophages targeting. *** $p \leq 0.001$ ** $p \leq 0.01$; * $p \leq 0.05$.

6.4 Discussion

Many approaches were developed to modulate the function and secretion of macrophages to reduce the potential damage caused by secondary injury after SCI. The activation of M1 macrophages triggered by traumatic injury can initiate many pro-inflammation. Thus, preventing the proliferation of M1 macrophages or inhibiting M1 associated pro-inflammatory signaling pathways can suppress the inflammation initiated secondary injury. In our study, we targeted the hallmark expression of iNOS in M1 macrophages using siRNA gene silencing strategies and nanoscaled drug delivery systems. This work focused on targeting specific macrophages either to M1 or M2 macrophages using ligand conjugated chitosan/siRNAs Nps in SCI study. This is first time in nanoparticle targeting studies discriminating different subsets of macrophages. Since the overexpression of CD16/32 in M1 macrophages was observed at the insulted state of spinal cord, we also demonstrated the potential application of Fc receptor mediated M1 macrophages targeting. Most importantly, we indicate that this M1 macrophage targeting strategy can inhibit iNOS expression via delivery siRNAs and reduce cell damage and death after applying chitosan/siRNAs Nps by detecting apoptosis cell signaling protein marker Bax and Bcl-2 in vivo study.

There are many studies that have suggested the successful chitosan nanoparticle mediated siRNA delivery to macrophages, such as enhanced green fluorescent protein (EGFP) and TNF- α knock down in murine peritoneal macrophages. [189,196] A rabies virus glycoprotein derived short peptide was designed as a AchR targeting ligand and it can assist the delivery of TNF- α siRNA to both macrophages and microglia cells for

neuroinflammation and neuronal apoptosis reduction. [234] Different administration route of chitosan mediated nanoparticle has also been investigated for siRNA delivery to achieve potential gene silencing, for example through IP injection to macrophages, [196] and applied oral administration by modifying chitosan to mannose-incorporated trimethyl chitosan-cysteine (MTC). [235]

Due to the nature of chitosan polymers, there is no evidence of inflammatory reaction of material itself in the clinical study. However, the purity, or we may say, the low degree of acetylation of chitosan could result in an unexpected inflammation. Several publications focused on the effects of chitosan materials towards macrophage culture. The outcomes are various. Oliveira MI et al. indicated that chitosan significantly down-regulated expression of proinflammatory cytokines in macrophages, more interestingly, it also up-regulated anti-inflammatory cytokines and favors the M2 polarization. [236] These results were supported by the suppression of chitinous materials to nitric oxide production in the study of activated RAW 264.7 macrophages. [237] The mechanism of this suppression was further evaluated in other publications, and they suggested that there is a moderate activation of both iNOS and arginase in resident macrophages, but a strong expression of arginase with no altered NO production in inflammatory macrophages when treated with chitosan. Since arginase induction is responsible for proliferation of many cell lines, it has the potential to play a beneficial role in secondary injury treatment. [238] However, one paper reported that chitosan can induce apoptosis of macrophages through Fas signaling pathways. [239]

Since the iNOS is preferentially produced by classically activated proinflammatory M1 macrophages, we focused on this subset of macrophages for targeting to attenuate the iNOS expression and its consequent NO production. In addition, M1 macrophages upregulated the CD16/32, CD86, and MHCII expression after SCI. [213] Therefore, we can be able to differentiate this from anti-inflammation M2 macrophages which are designated by Arg1 and mannose receptor (CD206). The overexpression of receptors on M1 macrophages can be used as the potential target for siRNAs delivery. The increased iNOS expression starts few hours after SCI and dramatically reduced at day 3 after SCI, therefore, a time-corresponding cell surface marker expression, such as CD16/32 in M1 macrophages can be considered as mediated receptors.

Although it is known that macrophage internalization can be influenced by particle size and shape, as well as surface charge, it is still unclear about the mechanism of Nps uptake of macrophages. In general, it is believed that increased particle size (especially for nanoparticles size larger than 0.5 μ m), higher zeta potentials, or long dimension of particles can be uptaken more rapidly by macrophages compare to smaller and neutral nanoparticles. Bone marrow and circulating blood derived monocytes and resident macrophages in every organs are usually represented as Mononuclear Phagocyte System. They are mainly responsible for phagocytosis. [240] The broad spectrum of extracellular IgG molecules or IgG-coated particles can bind and interact with Fc receptors (FcRII/CD16 and or FcRIII/32) expressed on macrophage and initiate phagocytosis or Fc receptor mediated endocytosis to enhance the activity of its uptake.

Recent findings indicate that Fc γ RIIA is expressed primarily in phagocytic cells and also present in natural killer (NK) cells. Inhibitory Fc Receptor Fc γ RIIB is constitutively expressed in T and B lymphocytes as well as phagocytic cells. Macrophages and some monocytes express Fc γ RIIA, whereas Fc γ RIIB is only expressed at neutrophils. [241,242] More studies further exploit and suggested that macrophages and monocyte-derived dendritic cells and express high levels of activating Fc γ Rs and moderated level of inhibitory ones for IgG. In comparison, conventional and plasmacytoid dendritic cells mainly express the inhibitory Fc γ R. [241]

In our in vitro study, the pre-treatment approaches of siRNAs or its related drug delivery system were reported in majority of siRNAs gene silencing studies. In this bone-marrow derived macrophages study, we apply either siRNAs or different chitosan/siRNA Nps to the cells before LPS+IFN γ initiated M1 macrophage activation. Our flow cytometry results addressed both expression of CD206 and CD16/32 before activation either M1 or M2 macrophages. These results were fit with data reported by Flora Rey-Giraud et al. [243] The surface of the macrophages expressed both CD206 and CD16/32 receptors at inactivated state could lead to the successful cellular uptake of both mannosylated chitosan Nps and Ab conjugated chitosan Nps. A post-treatment was conducted during the study, however, cell viability is relatively reduced (data not shown here). Untargeted Chi/siRNA Nps also shown a significant reduction of iNOS, and it could due to the low molecular weight chitosan binds to the mannose receptors and promotes the nanoparticles internalization. [244]

We need to emphasize again that the expression of cells bearing surface receptors can be alternated, for example, accompanies with macrophage activation or spinal cord insults. The overexpression of CD16/32 after spinal cord injury can be beneficial to perform Fc receptor mediated phagocytosis and endocytosis as strategies using CD64-directed immunotoxins targeting to inflammatory macrophages at rheumatoid arthritis joint. [230]

It is noteworthy that some studies also indicated that nanoparticle taken up via mannose receptor, Fc γ receptor, or through complement receptor pathways elicit an inflammation mediated immune response. It could due the phagocytosis process associated activation of certain signaling pathway. It is not observed in our study based on the results in Figure 6.4 and 6.6, there is no trace of increased iNOS level and NO production for M-WSC/N-siRNA Nps and Ab-Chi/N-siRNA Nps treatment (using scrambled siRNAs) compared to that without treatment after LPS + IFN γ challenge. However, other cytokine production did not included in our studies. Interestingly, Ab-Chi/N-siRNA Nps treatment showed visually but not statistically down regulation of iNOS expression. This phenomenon can not be explained until very recent report (Oct,2014) published at Santegoets K.C.M et al. The studies showed that macrophages cultured with GM-CSF expressed a high level of inhibitory receptor, Fc γ RIIb, but a moderate level in the case of M-CSF cultured macrophages. This inhibitory Fc γ RIIb plays a vital role in balancing the induced inflammatory responses to prevent excessive tissue damage. More importantly, they also demonstrated that the introduction of soluble IgG immune complexes to GM-CSF macrophages can inhibited cytokine production mediated by various Toll like receptors (such as 2,3,4, 7/8) via Fc γ RIIb signaling pathways. GM-CSF macrophages challenged with LPS (trigger TLR4 signaling) can initiated high level of cytokines such

as TNF- α . After co-stimulation with IgG immune complexes, dramatically reduced level of TNF α was observed in GM-CSF macrophages whereas a slightly increase level of IL-10 was occurred in M- CSF Macrophages. IgG immune complexes treatment alone did not initiated any detectable cytokines in GM-CSF but initiate low level of cytokine in the case of M-CSF macrophages. These results can be indicated due to the overexpression of inhibitory Fc γ RIIb in GM-CSF, not in M-CSF. [245] The earlier study from this research group also showed immune complexes binding to Fc γ RIIb prevent the activation of TLR4 signaling, this study could explain the slight, but not statistical significant, reduction in iNOS level, when Ab-Chi/siRNA Nps were applied in in vitro experiment.

According to other earlier studies, the internalization by macrophages can be operated by all Fc receptors no matter they have activation or inhibition functions, but the endocytosis capacity and the route of opsonized materials are different after internalization. One investigation suggests that internalization through activating Fc γ Rs results in antigen degradation pathways and followed by the activation of T cells. On the other hand, Inhibitory Fc γ RIIB mediated macrophage internalization can transport undegraded antigen to B cells. [241] Also, it has been documented that large immune complexes or antibody-coated particles are susceptible to be uptaken via phagocytosis whereas the internalization of small immune complexes are through Fc γ R mediated endocytosis. This Fc γ R mediated endocytosis, compare to phagocytosis, require much different signal transduction mechanism which not involving Syk, SRTKs, and PI3K kinases initiated cytokine production.[246]

Moreover, our results indicated that an increased amount of Ab during nanoparticles synthesis did not result in more efficient gene silencing. 20% and 30% of Ab incorporated chitosan Nps has been shown an increased iNOS expression compare to the case using 10% Ab. The undesired concentration of antibody could affect phagocytosis. Some reports indicate that optimal phagocytosis occurred at antibody concentrations of 10-100ng/ml. A higher risk of coagulation of nanoparticles could also jeopardize the reduction in iNOS expression because Nps with higher Ab ratios have a lower zeta potentials. Most possible reason is a high Ab ratio have a lower ratio of encapsulating chitosan and limit synthesis of chitosan materials with desired amount of siRNAs.

Chitosan mediated siRNA delivery system has demonstrate the improved transfection efficiency and gene silencing results, especially showed a shorter incubation time during the treatment when compared to using lipid-based transfection reagent. The complete depletion of iNOS expression is not set as our goal. But, in many situations, extremely efficient blocking of the specific protein expression is required. The efficiency of nanoparticle delivery usually can be effected by phagosome or phagolysosomal entrapment for phagocytic cell studies or by endosome for other cells. It could be a critical point in gene delivery to avoid degradation in the compartments of phagosome or endosome. Some groups reported that TNF- α specific siRNA conjugated large nanoparticles containing polyketal PK3 and chloroquine can significantly block targeted gene expression. It is due to the characteristics of PK3 which not only protect the siRNA from serum nucleases, but most importantly, it can cause osmotic disruption of the phagosome. Therefore, the siRNA loaded nanocomplexes can be released to the cytoplasm. [247] Endosomolytic agent modified with maleic anhydride generating a pH-

sensitive maleamate bonds which can be cleaved under acidic endosome conditions in order to expose positive charged amine group and destabilized the endosome membrane for siRNAs to escape. [248,249] In addition, other agents, such as an amphipathic poly(vinyl ether), were also well developed for this purpose of application. [250] Therefore, agents used in endosome escape can also be considered to prevent phagosome or phagolysosomal entrapment in the future studies to optimize silencing efficiency.

The macrophage morphology studies showed apparent elongation or extension of M2 macrophages, and it accompanied with no detectable iNOS expression and nearly same amount of NO production when compared to control group. It matches the neuroprotection properties of M2 macrophages reported in many earlier publications. Some researchers has also confirmed our results and elaborated the shape of macrophages correlated with the macrophages polarization and M2 macrophages are not associated with the initiation of inflammation, such as M1-polarizing stimuli triggered iNOS expression. [251]

In conclusion, we introduce a siRNAs based gene silencing strategies to reduce the iNOS expression which usually triggered by activated pro-inflammatory macrophages after SCI. We successfully synthesized different ligand conjugated chitosan nanoparticles carrying siRNAs. In vitro study, all siRNA loaded chitosan Nps showed significant iNOS knockdown with low cytotoxicity and efficient transfection. We further evaluate the targeting and gene silencing effects in animal studies. The results showed an alleviation of iNOS and Bax expression which is the indicator for pro-apoptosis cell death whereas an significant upregulation of anti-apoptosis marker Bcl-2 after Ab-Chi/siRNAs Nps

treatment, indicating the efficient targeting and therapeutic effects after attenuation of iNOS level by siRNAs application.

CHAPTER SEVEN

FUTURE STUDIES

There are many potential improvements that can still be provided to Ppy platform or chitosan nanoparticles mediated drug delivery system. Either polymer based drug carriers have been shown their unique functionality during the drug delivery.

In this study, we focused on the structure, synthesis, and releasing profile for the Ppy platform to optimize localized drug release in spinal cord bio-environment. A further investigation on the 3D structure with increased drug loading capacities would possibly be a next step. The figure 7.1 shows the Ppy nanotubes that we have manufactured with a larger surface area of polymers. It could enhance the drug release because there is less possible drug entrapment due to larger areas exposure of materials. In figure 7.1, one PC-12 cell was adhesived on the surface of Ppy matrix, indicating the small size of nanotube diameter.

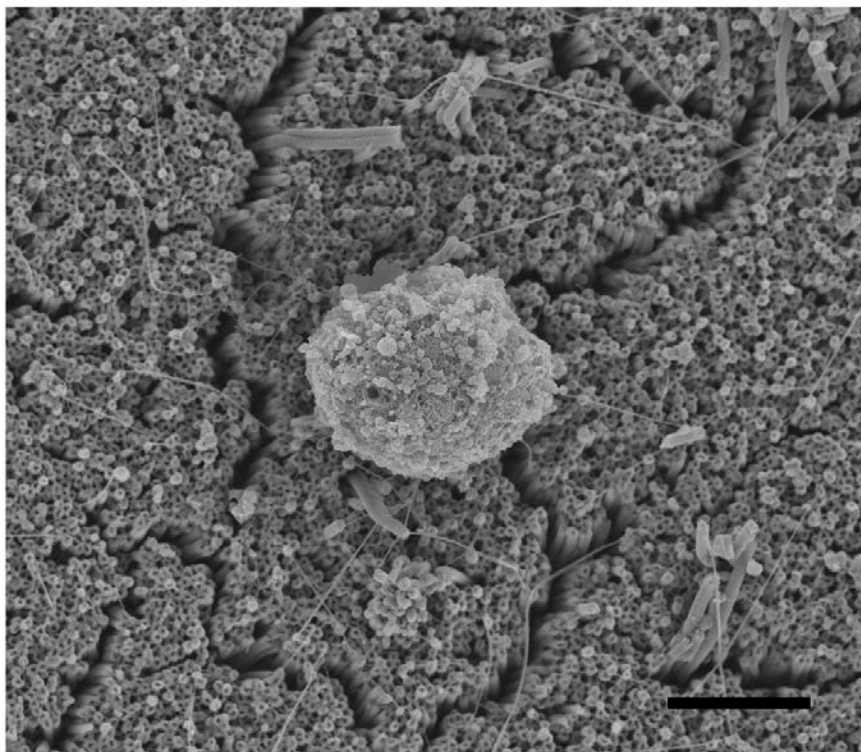


Figure 7.1 SEM image of single cell on Ppy nanotube structure. Scale bar = 5 μ m.

Parameters of the EMF generator can also be modified, such as the frequency and the coil size. We will start from a EMF stimulator with a low frequency instead of using current radiofrequency frequency. So we can further explore the cell responses to the low frequency stimulator (it has been well-established in the bio-electrical literatures) while detect the potential drug release. It could acheive a dual treatment through one application. Also, the penetration capacity of current induced by alternating electromagnetic field generator (described in 3.4 section) can also be further studied with a larger coil size and lower frequencies generator.

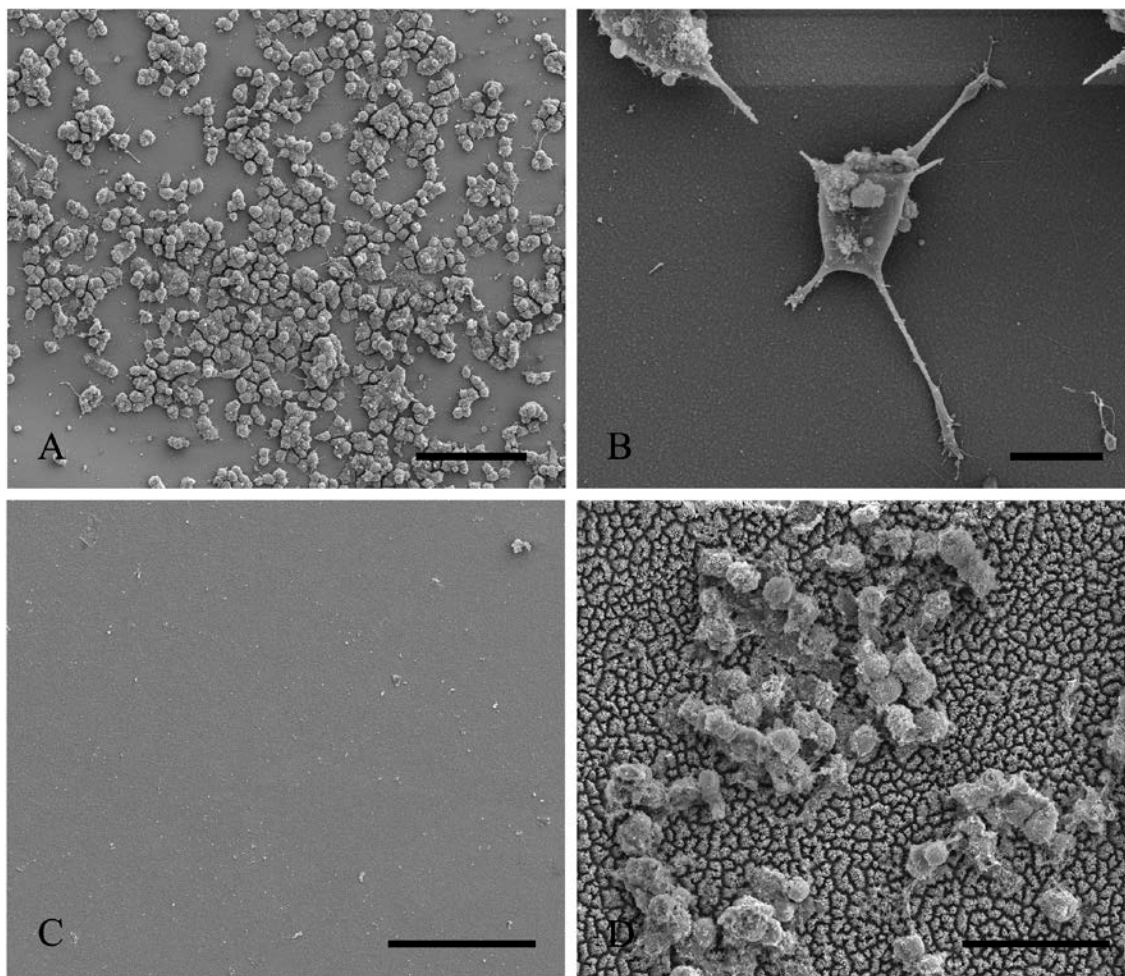


Figure 7.2 SEM images for cell adhesion on flat Ppy and Ppy Nws. Scale bar A=100 μ m; B=10 μ m; C and D=40 μ m.

Moreover, from tissue engineering perspectives, this Ppy NWs platform can be potentially developed as biocompatible or even biodegradable substrates for cell adhesion and connection. Collagen coated flat Ppy indicated the successful cell attachment see figure 7.2 A and there is apparent neurite extension. (see lower magnification figure 7.2 B) However, there is no cell adhesion that was observed for the flat Ppy without collagen substrate coating (See figure 7.2C). Interestingly, PC-12 cells successfully adhered to the PpyNWs structured platform without substrate assistance (Figure 7.2D). A further and

thoroughly studies can be performed in the future as well. Meanwhile, different drugs incorporation with this Ppy platform can also be discovered to improve neuronal recovery after SCI.

For chitosan mediated siRNAs drug delivery system, co-polymerization and different targeting motifs can be exploited as an add-on to improve the existing nanoparticles, such as assisting nanoparticles cross spinal blood barriers. Thus, a simple IV injection instead of intrathecal injection can be used. Also, the study on M1 and M2 macrophages shifting through modulating various cytokines in bio-environment could lead to a new chapter of therapeutic strategies for SCI.

BIBLIOGRAPHY

BIBLIOGRAPHY

1. Dasari, V.R., K.K. Veeravalli, and D.H. Dinh, *Mesenchymal stem cells in the treatment of spinal cord injuries: A review*. World J Stem Cells, 2014. **6**(2): p. 120-33.
2. Chen, J., et al., *Experimental Spinal Cord Injury Models*, in *Animal Models of Acute Neurological Injuries*.
3. Buki, A., et al., *Cytochrome c release and caspase activation in traumatic axonal injury*. Journal of Neuroscience, 2000. **20**(8): p. 2825-34.
4. Shields, D.C., et al., *Calpain activity and expression increased in activated glial and inflammatory cells in penumbra of spinal cord injury lesion*. J Neurosci Res, 2000. **61**(2): p. 146-50.
5. Okonkwo, D.O. and J.T. Povlishock, *An intrathecal bolus of cyclosporin A before injury preserves mitochondrial integrity and attenuates axonal disruption in traumatic brain injury*. Journal of Cerebral Blood Flow & Metabolism, 1999. **19**(4): p. 443-51.
6. Oyinbo, C.A., *Secondary injury mechanisms in traumatic spinal cord injury: a nugget of this multiply cascade*. Acta Neurobiol Exp (Wars), 2011. **71**(2): p. 281-99.
7. Hulsebosch, C.E., *Recent advances in pathophysiology and treatment of spinal cord injury*. Advances in Physiology Education, 2002. **26**(4): p. 238-255.
8. Blight, A.R. and M.P. Zimber, *Acute spinal cord injury: pharmacotherapy and drug development perspectives*. Current Opinion in Investigational Drugs. 2001. **2**(6): p. 801-8.

9. Wada, S., et al., *Apoptosis following spinal cord injury in rats and preventative effect of N-methyl-D-aspartate receptor antagonist*. PG - 98-104. J Neurosurg, 1999. **91**(1 Suppl).
10. Wrathall, J.R., Y.D. Teng, and D. Choiniere, *Amelioration of functional deficits from spinal cord trauma with systemically administered NBQX, an antagonist of non-N-methyl-D-aspartate receptors*. Exp Neurol, 1996. **137**(1): p. 119-126.
11. Görgülü, A., et al., *Superoxide dismutase activity and the effects of NBQX and CPP on lipid peroxidation in experimental spinal cord injury*. Research in Experimental Medicine, 1999. **199**(5): p. 285-293.
12. Pointillart V., et al. *Effects of nimodipine on post traumatic spinal cord ischemia in baboons*. J neurotrauma, 1993. **10**(2): p.201-213.
13. Hayes, K.C., et al., *4-Aminopyridine-sensitive neurologic deficits in patients with spinal cord injury*. Journal of Neurotrauma, 1994. **11**: p. 433-446.
14. Segal, J.L. and S.R. Brunnemann, *4-Aminopyridine alters gait characteristics and enhances locomotion in spinal cord injured humans*. J Spinal Cord Med, 1998. **21**(3): p. 200-4.
15. Grill, R., et al., *Cellular delivery of neurotrophin-3 promotes corticospinal axonal growth and partial functional recovery after spinal cord injury*. J Neurosci, 1997a. **17**(14): p. 5560-72.
16. Grill, R.J., A. Blesch, and M.H. Tuszynski, *Robust growth of chronically injured spinal cord axons induced by grafts of genetically modified NGF-secreting cells*. Exp. Neurol., 1997b. **148**: p. 444-452.
17. Jin, Y., et al., *Transplants of Fibroblasts Genetically Modified to Express BDNF Promote Axonal Regeneration from Supraspinal Neurons Following Chronic Spinal Cord Injury*. Experimental Neurology, 2002. **177**(1): p. 265-275.
18. Chico, L.K., L.J. Van Eldik, and D.M. Watterson, *Targeting protein kinases in central nervous system disorders*. Nat Rev Drug Discov, 2009. **8**(11): p. 892-909.

19. Kopp, M.A., et al., *Small-molecule-induced Rho-inhibition: NSAIDs after spinal cord injury*. Cell Tissue Res, 2012. **349**(1): p. 119-32.
20. Silveira, M. and R. Linden, *Neuroprotection by cAMP: Another brick in the wall*, in *Brain Repair*, M. Bähr, Editor. 2006, Springer US. p. 164-176.
21. Hasko, G., M.V. Sitkovsky, and C. Szabo, *Immunomodulatory and neuroprotective effects of inosine*. Trends Pharmacol Sci, 2004. **25**(3): p. 152-157.
22. Tomaselli, B., et al., *p42/44 MAPK is an essential effector for purine nucleoside-mediated neuroprotection of hypoxic PC12 cells and primary cerebellar granule neurons*. Mol Cell Neurosci, 2008. **38**(4): p. 559-68.
23. Svirskis, D., et al., *Electrochemically controlled drug delivery based on intrinsically conducting polymers*. Journal of Controlled Release, 2010. **146**(1): p. 6-15.
24. Straley, K.S., C.W. Foo, and S.C. Heilshorn, *Biomaterial design strategies for the treatment of spinal cord injuries*. J Neurotrauma, 2010. **27**(1): p. 1-19.
25. Wu, W., et al., *Neuroprotective ferulic acid (FA)-glycol chitosan (GC) nanoparticles for functional restoration of traumatically injured spinal cord*. Biomaterials, 2014. **35**(7): p. 2355-64.
26. Wang, Y.C., et al., *Sustained intraspinal delivery of neurotrophic factor encapsulated in biodegradable nanoparticles following contusive spinal cord injury*. Biomaterials, 2008. **29**(34): p. 4546-53.
27. Shi, Y., et al., *Effective repair of traumatically injured spinal cord by nanoscale block copolymer micelles*. Nat Nanotechnol, 2009. **5**(1): p. 80-7
28. Borgens, R.B., R. Shi, and D. Bohnert, *Behavioral recovery from spinal cord injury following delayed application of polyethylene glycol*. J. Exp. Biol., 2002. **205**: p. 1-12.
29. Ingram, M.D., H. Staeschea, and K.S. Ryderb, *"Activated" polypyrrole electrodes for high-power supercapacitor applications*. Solid State Ionics, 2004. **169**: p.51-57.

30. Song, H.-K. and G. T. R. Palmore, *Redox-Active Polypyrrole: Toward Polymer-Based Batteries*. Adv. Mater, 2006. **18**: p.1764–1768.
31. Yuan, X., et al., *Use of polypyrrole in catalysts for low temperature fuel cells*. Energy Environ. Sci., 2013. **6**: p. 1105-1124.
32. Tüken, T., *Zinc deposited polymer coatings for copper protection*. Progress in Organic Coatings, 2006. **55**(1): p. 60-65.
33. Yavuz, Ö., et al., *Polypyrrole composites for shielding applications*. Synthetic Metals, 2005. **151**(3): p. 211-217.
34. Ramanaviciene, A., and A. Ramanavicius, *Molecularly imprinted polypyrrole-based synthetic receptor for direct detection of bovine leukemia virus glycoproteins*. Biosens Bioelectron, 2004. **20**(6): p. 1076-82.
35. Schmidt, C.E., V.R. Shastri, and J.P. Vacanti, *Stimulation of neurite outgrowth using an electrically conducting polymer*. . Proc. Natl. Acad. Sci. U.S.A., 1997. **94**: p. 8948-53.
36. Brett Runge, M., et al., *The development of electrically conductive polycaprolactone fumarate–polypyrrole composite materials for nerve regeneration*. Biomaterials, 2010. **31**(23): p. 5916-5926.
37. Georgea, P.M., et al., *Fabrication and biocompatibility of polypyrrole implants suitable for neural prosthetics*. Biomaterials, 2005. **26**: p. 3511–3519.
38. Lee, J.Y., J.W. Lee, and C.E. Schmidt, *Neuroactive conducting scaffolds: nerve growth factor conjugation on active ester-functionalized polypyrrole*. J R Soc Interface, 2009. **6**(38): p. 801-10.
39. Nguyen, H.T., et al., *Electric field stimulation through a biodegradable polypyrrole-co-polycaprolactone substrate enhances neural cell growth*. J Biomed Mater Res A, 2014. **102**(8): p. 2554-64.
40. Forciniti, L., et al., *Schwann cell response on polypyrrole substrates upon electrical stimulation*. Acta Biomater, 2014. **10**(6): p. 2423-33.

41. Olayo, R., et al., *Tissue spinal cord response in rats after implants of polypyrrole and polyethylene glycol obtained by plasma*. J Mater Sci Mater Med, 2008. **19**(2): p. 817-26.
42. Cruz, G.J., et al., *Plasma polypyrrole implants recover motor function in rats after spinal cord transection*. J Mater Sci Mater Med, 2012. **23**(10): p. 2583-92.
43. Ateh, D.D., H.A. Navsaria, and P. Vadgama, *Polypyrrole-based conducting polymers and interactions with biological tissues*. J R Soc Interface, 2006. **3**(11): p. 741-52.
44. Dai., L., *Conducting polymer*, in *Intelligent Macromolecules for Smart Devices: From Materials Synthesis to Device Applications*.
45. Bhattacharya, A., A. De, and S. Das, *Electrochemical preparation and study of transport properties of polypyrrole doped with unsaturated organic sulfonates*. Polymer, 1996. **37**(19): p. 4375-4382.
46. Wang, P.-C. and J.-Y. Yu, *Dopant-dependent variation in the distribution of polarons and bipolarons as charge-carriers in polypyrrole thin films synthesized by oxidative chemical polymerization*. Reactive and Functional Polymers, 2012. **72**(5): p. 311-316.
47. Otero, T.F. and J.G. Martinez, *Biomimetic intracellular matrix (ICM) materials, properties and functions. Full integration of actuators and sensors*. Journal of Materials Chemistry B, 2013. **1**(1): p. 26-38.
48. Ansari, R., N.K. Fahim, and A.F. Delavar, *Removal of Nitrite Ions from Aqueous Solutions Using Conducting Electroactive Polymers*. The Open Process Chemistry Journal, 2009. **2**(1): p. 1-5.
49. Garfias-García, E., et al., *Eletrochemical Nucleation of Polypyrrole onto Different Substrates*. Int. J. Electrochem. Sci., 2010. **5**(6): p. 763-773.
50. Hepel, M. and F. Mahdavi, *Application of the Electrochemical Quartz Crystal Microbalance for Electrochemically Controlled Binding and Release of Chlorpromazine from Conductive Polymer Matrix*. Microchemical Journal, 1997. **56**(1): p. 54-64.

51. Curtin, L.S., G.C. Komplin, and W.J. Pietro, *Diffusive anion exchange in polypyrrole films*. The Journal of Physical Chemistry, 1988. **92**(1): p. 12-13.
52. Fattahi, P., et al., *A Review of Organic and Inorganic Biomaterials for Neural Interfaces*. Advanced Materials, 2014. **26**(12): p. 1846-1885.
53. Bidan, G., et al., *Incorporation of sulphonated cyclodextrins into polypyrrole: an approach for the electro-controlled delivering of neutral drugs*. Biosens Bioelectron, 1995. **10**(1-2): p. 219-29.
54. Kopecka, J., et al., *Polypyrrole nanotubes: mechanism of formation*. RSC Advances, 2014. **4**(4): p. 1551-1558.
55. Luo, X. and X.T. Cui, *Sponge-like nanostructured conducting polymers for electrically controlled drug release*. Electrochem commun, 2009. **11**(10): p. 1956.
56. Kang, G., R.B. Borgens, and Y. Cho, *Well-ordered porous conductive polypyrrole as a new platform for neural interfaces*. Langmuir, 2011. **27**(10): p. 6179-84.
57. Sirivisoot, S., R. Pareta, and T.J. Webster, *Electrically controlled drug release from nanostructured polypyrrole coated on titanium*. Nanotechnology, 2011. **22**(8): p. 085101.
58. Richardson, R.T., et al., *The effect of polypyrrole with incorporated neurotrophin-3 on the promotion of neurite outgrowth from auditory neurons*. Biomaterials, 2007. **28**(3): p. 513-523.
59. Evans, A.J., et al., *Promoting neurite outgrowth from spiral ganglion neuron explants using polypyrrole/BDNF-coated electrodes*. J Biomed Mater Res A, 2009. **91**(1): p. 241-50.
60. Thompson, B.C., et al., *Conducting polymers, dual neurotrophins and pulsed electrical stimulation--dramatic effects on neurite outgrowth*. J Control Release, 2010. **141**(2): p. 161-7.
61. Weidlich, C., K.M. Mangold, and K. Jüttner, *Conducting polymers as ion-exchangers for water purification*. Electrochimica Acta, 2001. **47**(5): p. 741-745.

62. Kang, E.T., et al., *XPS studies of proton modification and some anion exchange processes in polypyrrole*. Synthetic Metals, 1990. **39**(1): p. 69-80.
63. Pei, Q. and R. Qian, *Protonation and deprotonation of polypyrrole chain in aqueous solutions*. Synthetic Metals, 1991. **45**(1): p. 35-48.
64. Moulton, S.E., et al., *Galvanic coupling conducting polymers to biodegradable Mg initiates autonomously powered drug release*. Journal of Materials Chemistry, 2008. **18**(30): p. 3608-3613.
65. Zinger, B. and L.L. Miller, *Timed release of chemicals from polypyrrole films*. Journal of the American Chemical Society, 1984. **106**(22): p. 6861-6863.
66. Ge, D., et al., *A polypyrrole-based microchip for controlled drug release*. Electrochimica Acta, 2009. **55**(1): p. 271-275.
67. Xiao, Y., et al., *Preparation of nano-tentacle polypyrrole with pseudo-molecular template for ATP incorporation*. Journal of Biomedical Materials Research Part A, 2007. **80A**(4): p. 925-931.
68. Arbizzani, C., et al., *Polypyrrole: A drug-eluting membrane for coronary stents*. Electrochimica Acta, 2007. **52**(9): p. 3274-3279.
69. Orcajo, O., et al., *A new reflection–transmission bidimensional spectroelectrochemistry cell: Electrically controlled release of chemicals from a conducting polymer*. Journal of Electroanalytical Chemistry, 2006. **596**(2): p. 95-100.
70. Massoumi, B. and A. Entezami, *Electrochemically Controlled Binding and Release of Dexamethasone from Conducting Polymer Bilayer Films*. Journal of Bioactive and Compatible Polymers January, 2002. **17**(1): p. 51-62.
71. George, P.M., et al., *Electrically controlled drug delivery from biotin-doped conductive polypyrrole*. Adv. Mater., 2006. **18**: p. 577-581.
72. Miller, L.L. and X.Q. Zhou, *Poly(N-methylpyrrolylium) poly(styrenesulfonate) - a conductive, electrically switchable cation exchanger that cathodically binds and anodically releases dopamine*. Macromolecules, 1987. **20**(7): p. 1594-1597.

73. Leprince, L., et al., *Dexamethasone electrically controlled release from polypyrrole-coated nanostructured electrodes*. *J Mater Sci Mater Med*, 2010. **21**(3): p. 925-30.
74. Wadhwa, R., L. Carl, and C. Xinyan, *Electrochemically controlled release of dexamethasone from conducting polymer polypyrrole coated electrode*. *J. Control. Release*, 2006. **110**(3): p. 531-541.
75. Pyo, M. and J.R. Reynolds, *Poly(pyrrole adenosine 5'-triphosphate) (PP-ATP) and conducting polymer bilayers for transport of biologically active ions*. *Synthetic Metals*, 1995. **71**(1-3): p. 2233-2236.
76. Pyo, M. and J.R. Reynolds, *Electrochemically Stimulated Adenosine 5'-Triphosphate (ATP) Release through Redox Switching of Conducting Polypyrrole Films and Bilayers*. *Chemistry of Materials*, 1996. **8**(1): p. 128-133.
77. Creed, S., et al., *Towards electrochemical analgesia: acetylsalicylate delivered from polypyrrole by electroreduction*. *Journal of the Chemical Society, Chemical Communications*, 1994(19): p. 2291-2292.
78. Thompson, B.C., et al., *Optimising the incorporation and release of a neurotrophic factor using conducting polypyrrole*. *J Control Release*, 2006. **116**(3): p. 285-94.
79. Richardson, R.T., et al., *Polypyrrole-coated electrodes for the delivery of charge and neurotrophins to cochlear neurons*. *Biomaterials*, 2009. **30**(13): p. 2614-2624.
80. Li, Y. and S. Dong, *Electrochemically controlled release of adenosine 5[prime or minute]-triphosphate from polypyrrole film*. *Journal of the Chemical Society, Chemical Communications*, 1992(11): p. 827-828.
81. Zhou, Q.-X., L.L. Miller, and J.R. Valentine, *Electrochemically controlled binding and release of protonated dimethyldopamine and other cations from poly(N-methyl-pyrrole)/polyanion composite redox polymers*. *Journal of Electroanalytical Chemistry and Interfacial Electrochemistry*, 1989. **261**(1): p. 147-164.

82. Pilla, A.A., *Mechanisms and therapeutic applications of time varying and static magnetic fields.*, in *Biological and medical aspects of electromagnetic fields*, F. Barnes and B. Greenebaum, Editors. 2006, CRC: Boca Raton, FL. p. 351-411.
83. Ganesan, K., et al., *Low frequency pulsed electromagnetic field — A viable alternative therapy for arthritis.* Indian Journal of Experimental Biology (IJEB) 2009. **47**(12): p. 939-948.
84. Wu, C.-H., et al., *Trojan-Horse Nanotube On-Command Intracellular Drug Delivery.* Nano Letters, 2012. **12**(11): p. 5475-5480.
85. Ding, G.R., et al., *Extremely low frequency magnetic fields and the promotion of H₂O₂-induced cell death in HL-60 cells.* International Journal of Radiation Biology, 2004. **80**(4): p. 317-324.
86. Zmysłony, M., et al., *Effects of in vitro exposure to power frequency magnetic fields on UV-induced DNA damage of rat lymphocytes.* Bioelectromagnetics, 2004. **25**(7): p. 560-562.
87. Jajte, J., et al., *Effect of 7 mT static magnetic field and iron ions on rat lymphocytes: apoptosis, necrosis and free radical processes.* Bioelectrochemistry, 2002. **57**(2): p. 107-111.
88. Zmysłony, M., et al., *Acute exposure to 930 MHz CW electromagnetic radiation in vitro affects reactive oxygen species level in rat lymphocytes treated by iron ions.* Bioelectromagnetics, 2004. **25**(5): p. 324-328.
89. Kirtman, B., et al., *Polarization of one-dimensional periodic systems in a static electric field: Sawtooth potential treatment revisited.* The Journal of Chemical Physics, 2009. **131**(4).
90. Bishop, A. and J.E. Anderson, *NO signaling in the CNS: from the physiological to the pathological.* Toxicology, 2005. **208**(2): p. 193-205.
91. Radi, R., *Nitric oxide, oxidants, and protein tyrosine nitration.* Proc Natl Acad Sci U S A, 2004. **101**(12): p. 4003-8.

92. Liu, D., et al., *The role of reactive nitrogen species in secondary spinal cord injury: formation of nitric oxide, peroxynitrite, and nitrated protein*. J Neurochem, 2000. **75**(5): p. 2144-54.
93. Liu, D., et al., *Peroxynitrite generated at the level produced by spinal cord injury induces peroxidation of membrane phospholipids in normal rat cord: Reduction by a metalloporphyrin*. J. Neurotrauma, 2005. **22**(10): p. 1123-1133.
94. Scott, G.S., C. Szabó, and D.C. Hooper, *Poly(ADP-ribose) polymerase activity contributes to peroxynitrite-induced spinal cord neuronal cell death in vitro*. J Neurotrauma 2004. **21**(9): p. 1255-1263.
95. Xiong, Y., A.G. Rabchevsky, and E.D. Hall, *Role of peroxynitrite in secondary oxidative damage after spinal cord injury*. Journal of Neurochemistry, 2007. **100**(3): p. 639-649.
96. Genovese, T., et al., *Evidence for the Role of Mitogen-Activated Protein Kinase Signaling Pathways in the Development of Spinal Cord Injury*. Journal of Pharmacology and Experimental Therapeutics, 2008. **325**(1): p. 100-114.
97. Bhat, N.R., et al., *Extracellular Signal-Regulated Kinase and p38 Subgroups of Mitogen-Activated Protein Kinases Regulate Inducible Nitric Oxide Synthase and Tumor Necrosis Factor- α Gene Expression in Endotoxin-Stimulated Primary Glial Cultures*. The Journal of Neuroscience, 1998. **18**(5): p. 1633-1641.
98. Wang, M.-J., et al., *c-Jun N-terminal kinase and, to a lesser extent, p38 mitogen-activated protein kinase regulate inducible nitric oxide synthase expression in hyaluronan fragments-stimulated BV-2 microglia*. Journal of Neuroimmunology, 2004. **146**(1-2): p. 50-62.
99. Xu, Z., et al., *ERK1/2 and p38 mitogen-activated protein kinase mediate iNOS-induced spinal neuron degeneration after acute traumatic spinal cord injury*. Life Sciences, 2006. **79**(20): p. 1895-1905.

100. Xie, Z., C.J. Smith, and L.J. Van Eldik, *Activated glia induce neuron death via MAP kinase signaling pathways involving JNK and p38*. *Glia*, 2004. **45**(2): p. 170-179.
101. Torres, M. and H.J. Forman, *Redox signaling and the MAP kinase pathways*. *BioFactors*, 2003. **17**(1-4): p. 287-296.
102. McCubrey, J.A., M.M. LaHair, and R.A. Franklin, *Reactive oxygen species-induced activation of the MAP kinase signaling pathways*. *Antioxidants and Redox Signaling*, 2006. **8**(9-10): p. 1775-1789.
103. Guyton, K.Z., et al., *Activation of mitogen-activated protein kinase by H₂O₂. Role in cell survival following oxidant injury*. *J Biol Chem*, 1996. **271**(8): p. 4138-42.
104. Tobiume, K., et al., *ASK1 is required for sustained activations of JNK/p38 MAP kinases and apoptosis*. *EMBO reports*, 2001. **2**(3): p. 222-228.
105. Kamata, H., et al., *Reactive Oxygen Species Promote TNF α -Induced Death and Sustained JNK Activation by Inhibiting MAP Kinase Phosphatases*. *Cell*, 2005. **120**(5): p. 649-661.
106. Hou, N., et al., *Reactive Oxygen Species-Mediated Pancreatic β -Cell Death Is Regulated by Interactions between Stress-Activated Protein Kinases, p38 and c-Jun N-Terminal Kinase, and Mitogen-Activated Protein Kinase Phosphatases*. *Endocrinology*, 2008. **149**(4): p. 1654-1665.
107. Choi, B.H., et al., *Protein kinase C δ -mediated proteasomal degradation of MAP kinase phosphatase-1 contributes to glutamate-induced neuronal cell death*. *J Cell Sci* 2006. **119**: p. 1329-1340.
108. Chan, E.D. and D.W. Riches, *Potential role of the JNK/SAPK signal transduction pathway in the induction of iNOS by TNF- α* . *Biochem Biophys Res Commun*, 1998. **253**(3): p. 790-6.
109. Chan, E.D., et al., *Evaluation of the role of mitogen-activated protein kinases in the expression of inducible nitric oxide synthase by IFN- γ and TNF- α in mouse macrophages*. *J Immunol*, 1999. **162**(1): p. 415-22.

110. Chan, E.D. and D.W. Riches, *IFN-gamma + LPS induction of iNOS is modulated by ERK, JNK/SAPK, and p38(mapk) in a mouse macrophage cell line*. Am J Physiol Cell Physiol, 2001. **280**(3): p. C441-50.
111. Swantek, J.L., M.H. Cobb, and T.D. Geppert, *Jun N-terminal kinase/stress-activated protein kinase (JNK/SAPK) is required for lipopolysaccharide stimulation of tumor necrosis factor alpha (TNF-alpha) translation: glucocorticoids inhibit TNF-alpha translation by blocking JNK/SAPK*. Mol Cell Biol, 1997. **17**(11): p. 6274-82.
112. Lasa, M., et al., *Dexamethasone Causes Sustained Expression of Mitogen-Activated Protein Kinase (MAPK) Phosphatase 1 and Phosphatase-Mediated Inhibition of MAPK p38*. Mol Cell Biol, 2002. **22**(22): p. 7802-7811.
113. Medeiros, R., et al., *Connecting TNF-alpha signaling pathways to iNOS expression in a mouse model of Alzheimer's disease: relevance for the behavioral and synaptic deficits induced by amyloid beta protein*. J Neurosci, 2007. **27**(20): p. 5394-404.
114. Huo, Y., et al., *Dexamethasone inhibits the Nox-dependent ROS production via suppression of MKP-1-dependent MAPK pathways in activated microglia*. BMC Neurosci, 2011. **12**: p. 49.
115. Ozaki, T., et al., *Dexamethasone inhibits the induction of iNOS gene expression through destabilization of its mRNA in proinflammatory cytokine-stimulated hepatocytes*. Shock, 2010. **33**(1): p. 64-9.
116. Matsumura, M., et al., *Dexamethasone suppresses iNOS gene expression by inhibiting NF-kB in vascular smooth muscle cells*. Life Sciences, 2001. **69**(9): p. 1067-1077.
117. Korhonen, R., et al., *Dexamethasone Inhibits Inducible Nitric-Oxide Synthase Expression and Nitric Oxide Production by Destabilizing mRNA in Lipopolysaccharide-Treated Macrophages*. Molecular Pharmacology, 2002. **62**(3): p. 698-704.

118. Walker, G., J. Pfeilschifter, and D. Kunz, *Mechanisms of suppression of inducible nitric-oxide synthase (iNOS) expression in interferon (IFN)-gamma-stimulated RAW 264.7 cells by dexamethasone. Evidence for glucocorticoid-induced degradation of iNOS protein by calpain as a key step in post-transcriptional regulation.* J Biol Chem, 1997. **272**(26): p. 16679-87.
119. Golde, S., et al., *Decreased iNOS synthesis mediates dexamethasone-induced protection of neurons from inflammatory injury in vitro.* European Journal of Neuroscience, 2003. **18**(9): p. 2527-2537.
120. Xu, W., et al., *Increased production of reactive oxygen species contributes to motor neuron death in a compression mouse model of spinal cord injury.* Spinal Cord, 2005. **43**(4): p. 204-13.
121. Hassler, S.N., K.M. Johnson, and C.E. Hulsebosch, *Reactive oxygen species and lipid peroxidation inhibitors reduce mechanical sensitivity in a chronic neuropathic pain model of spinal cord injury in rats.* J Neurochem, 2014. **131**(4): p. 413-7.
122. Diaz-Ruiz, A., et al., *Cyclosporin-A inhibits inducible nitric oxide synthase activity and expression after spinal cord injury in rats.* Neurosci Lett, 2004. **357**(1): p. 49-52.
123. Chatzipanteli, K., et al., *Temporal and segmental distribution of constitutive and inducible nitric oxide synthases after traumatic spinal cord injury: effect of aminoguanidine treatment.* J Neurotrauma, 2002. **19**(5): p. 639-51.
124. Kwon, D.-J., et al., *Suppression of iNOS and COX-2 expression by flavokawain A via blockade of NF- κ B and AP-1 activation in RAW 264.7 macrophages.* Food and Chemical Toxicology, 2013. **58**(0): p. 479-486.
125. Satake, K., et al., *Nitric oxide via macrophage iNOS induces apoptosis following traumatic spinal cord injury.* Brain Res Mol Brain Res, 2000. **85**(1-2): p. 114-122.
126. Mukherjee, P., et al., *Development of nitric oxide synthase inhibitors for neurodegeneration and neuropathic pain.* Chemical Society Reviews, 2014. **43**(19): p. 6814-6838.

127. Hirakawa, A., et al., *Pyrrroloquinoline quinone attenuates iNOS gene expression in the injured spinal cord*. Biochemical and Biophysical Research Communications, 2009. **378**(2): p. 308-312.
128. Isaksson, J., M. Farooque, and Y. Olsson, *Improved functional outcome after spinal cord injury in iNOS-deficient mice*. Spinal Cord, 2004. **43**(3): p. 167-170.
129. Pearse, D.D., et al., *Comparison of iNOS inhibition by antisense and pharmacological inhibitors after spinal cord injury*. J Neuropathol Exp Neurol, 2003. **62**(11): p. 1096-107.
130. Maggio, D.M., et al., *Acute molecular perturbation of inducible nitric oxide synthase with an antisense approach enhances neuronal preservation and functional recovery after contusive spinal cord injury*. J Neurotrauma, 2012. **29**(12): p. 2244-9.
131. Mertas, A., et al., *N-[3-(Aminomethyl)benzyl]acetamide (1400W) as a Potential Immunomodulatory Agent*. Oxidative Medicine and Cellular Longevity, 2014. **2014**: p. 6.
132. Gwak, Y.S., et al., *Spatial and temporal activation of spinal glial cells: role of gliopathy in central neuropathic pain following spinal cord injury in rats*. Exp Neurol, 2012. **234**(2): p. 362-72.
133. Baldwin, S.A., et al., *Alterations in temporal/spatial distribution of GFAP- and vimentin-positive astrocytes after spinal cord contusion with the New York University spinal cord injury device*. J Neurotrauma, 1998. **15**(12): p. 1015-26.
134. Nesic, O., et al., *Transcriptional profiling of spinal cord injury-induced central neuropathic pain*. J Neurochem, 2005. **95**(4): p. 998-1014.
135. Wu, D., et al., *Co-expression of radial glial marker in macrophages/microglia in rat spinal cord contusion injury model*. Brain Res, 2005. **1051**(1-2): p. 183-8.

136. Li, Z., E.L. Hogan, and N.L. Banik, *Role of calpain in spinal cord injury: increased calpain immunoreactivity in spinal cord after compression injury in the rat*. *Neurochemistry International*, 1995. **27**(4-5): p. 425-432.
137. Jung, K., et al., *Upregulation of phospholipase D1 in the spinal cords of rats with clip compression injury*. *Neurosci Lett*, 2003. **336**(2): p. 126-30.
138. Chen, J., S.-Y. Leong, and M. Schachner, *Differential expression of cell fate determinants in neurons and glial cells of adult mouse spinal cord after compression injury*. *European Journal of Neuroscience*, 2005. **22**(8): p. 1895-1906.
139. Chadi, G., et al., *Experimental Models of Partial Lesion of Rat Spinal Cord to Investigate Neurodegeneration, Glial Activation, and Behavior Impairments*. *International Journal of Neuroscience*, 2001. **111**(3-4): p. 137-165.
140. Tian, D.S., et al., *Attenuation of astrogliosis by suppressing of microglial proliferation with the cell cycle inhibitor olomoucine in rat spinal cord injury model*. *Brain Res*, 2007. **1154**: p. 206-14.
141. Baloui, H., et al., *Upregulation in rat spinal cord microglia of the nonintegrin laminin receptor 37 kDa-LRP following activation by a traumatic lesion or peripheral injury*. *J Neurotrauma*, 2009. **26**(2): p. 195-207.
142. Koshinaga, M. and S.R. Whittemore, *The temporal and spatial activation of microglia in fiber tracts undergoing anterograde and retrograde degeneration following spinal cord lesion*. *J Neurotrauma*, 1995. **12**(2): p. 209-22.
143. Verdú, E., et al., *Olfactory ensheathing cells transplanted in lesioned spinal cord prevent loss of spinal cord parenchyma and promote functional recovery*. *Glia*, 2003. **42**(3): p. 275-286.
144. Matsumoto, S., et al., *The temporal profile of the reaction of microglia, astrocytes, and macrophages in the delayed onset paraplegia after transient spinal cord ischemia in rabbits*. *Anesth Analg*, 2003. **96**(6): p. 1777-84, table of contents.

145. Gomes-Leal, W., et al., *Astrocytosis, microglia activation, oligodendrocyte degeneration, and pyknosis following acute spinal cord injury*. *Exp Neurol*, 2004. **190**(2): p. 456-67.
146. Dihne, M., et al., *Time course of glial proliferation and glial apoptosis following excitotoxic CNS injury*. *Brain Res*, 2001. **902**(2): p. 178-89.
147. Zhong, Y. and R.V. Bellamkonda, *Dexamethasone-coated neural probes elicit attenuated inflammatory response and neuronal loss compared to uncoated neural probes*. *Brain Res*, 2007. **1148**: p. 15-27.
148. Fitch, M.T. and J. Silver, *Activated macrophages and the blood-brain barrier: Inflammation after CNS injury leads to increases in putative inhibitory molecules*. *Exp. Neurol.*, 1997. **148**: p. 587-603.
149. Busch, S.A. and J. Silver, *The role of extracellular matrix in CNS regeneration*. *Curr Opin Neurobiol*, 2007. **17**(1): p. 120-7.
150. Fitch, M.T. and J. Silver, *Inflammation and the glial scar: Factors at the site of injury that influence regeneration in the central nervous system.*, in *Degeneration and regeneration in the nervous system.*, N.R. Saunders and K.M. Dziegielewska, Editors. 2000, Harwood Academic Press. p. 77-92.
151. Fitch, M.T. and J. Silver, *CNS injury, glial scars, and inflammation: Inhibitory extracellular matrices and regeneration failure*. *Exp Neurol*, 2008. **209**(2): p. 294-301.
152. Fujita, K., et al., *Increase of glial fibrillary acidic protein fragments in the spinal cord of motor neuron degeneration mutant mouse*. *Brain Res*, 1998. **785**(1): p. 31-40.
153. Bracchi-Ricard, V., et al., *Inhibition of astroglial NF-kappaB enhances oligodendrogenesis following spinal cord injury*. *J Neuroinflammation*, 2013. **10**(1): p. 92.
154. Liedtke, W., et al., *GFAP is necessary for the integrity of CNS white matter architecture and long-term maintenance of myelination*. *Neuron*, 1996. **17**(4): p. 607-615.

155. Brenner, M., *Role of GFAP in CNS injuries*. Neurosci Lett, 2014. **565**: p. 7-13.
156. Jung, K., et al., *Upregulation of phospholipase D1 in the spinal cords of rats with clip compression injury*. Neurosci Lett, 2003. **336**(2): p. 126-30.
157. Li, Z., E.L. Hogan, and N.L. Banik, *Role of calpain in spinal cord injury: increased mcalpain immunoreactivity in spinal cord after compression injury in the rat*. Neurochem. Int., 1995. **27**: p. 425–432.
158. Xu, M., Y.K. Ng, and S.K. Leong, *Neuroprotective and neurodestructive functions of nitric oxide after spinal cord hemisection*. Exp Neurol, 2000. **161**(2): p. 472-80.
159. Friday, E., J. Ledet, and F. Turturro, *Response to dexamethasone is glucose-sensitive in multiple myeloma cell lines*. J Exp Clin Cancer Res, 2011. **30**: p. 81.
160. Kitajima, T., et al., *A novel mechanism of glucocorticoid-induced immune suppression: the inhibition of T cell-mediated terminal maturation of a murine dendritic cell line*. J Clin Invest, 1996. **98**(1): p. 142-7.
161. Murray, C.L., D.T. Skelly, and C. Cunningham, *Exacerbation of CNS inflammation and neurodegeneration by systemic LPS treatment is independent of circulating IL-1beta and IL-6*. J Neuroinflammation, 2011. **8**: p. 50.
162. Ruiz, L.M., et al., *Dexamethasone Inhibits Apoptosis of Human Neutrophils Induced by Reactive Oxygen Species*. Inflammation, 2002. **26**(5): p. 215-222.
163. Sanner, B.M., et al., *Effects of glucocorticoids on generation of reactive oxygen species in platelets*. Steroids, 2002. **67**(8): p. 715-9.
164. Lingaiah, H.B., R. Thamaraiselvan, and B. Periyasamy, *Dexamethasone induced alterations in lipid peroxidation, antioxidants, membrane bound ATPase in wistar albino rats*. International Journal of Pharmacy & Pharmaceutical Sciences, 2012. **4**.

165. Kraaij, M.D., et al., *Dexamethasone increases ROS production and T cell suppressive capacity by anti-inflammatory macrophages*. *Molecular Immunology*, 2011. **49**(3): p. 549-557.
166. Wang, L., K.J. Colodner, and M.B. Feany, *Protein Misfolding and Oxidative Stress Promote Glial-Mediated Neurodegeneration in an Alexander Disease Model*. *The Journal of Neuroscience*, 2011. **31**(8): p. 2868-2877.
167. Muntane, G., et al., *Glial fibrillary acidic protein is a major target of glycoxidative and lipoxidative damage in Pick's disease*. *J Neurochem*, 2006. **99**(1): p. 177-85.
168. Morgan, T.E., et al., *Increased transcription of the astrocyte gene GFAP during middle-age is attenuated by food restriction: implications for the role of oxidative stress*. *Free Radic Biol Med*, 1997. **23**(3): p. 524-8.
169. Theriault, E., et al., *Connexin43 and astrocytic gap junctions in the rat spinal cord after acute compression injury*. *J Comp Neurol*, 1997. **382**(2): p. 199-214.
170. Yang, P., et al., *Expression of nestin and glial fibrillary acidic protein in injured spinal cord of adult rats at different time*]. *Zhongguo Xiu Fu Chong Jian Wai Ke Za Zhi*, 2005. **19**(6): p. 411-5.
171. Fitch, M.T. and J. Silver, *Glial Cells, Inflammation, and CNS Trauma: Modulation of the Inflammatory Environment After Injury Can Lead to Long-Distance Regeneration Beyond the Glial Scar*, in *CNS Regeneration (Second Edition)*, J.H.K.H. Tuszynski, Editor. 2008, Academic Press: San Diego. p. 59-94
172. Myer, D.J., et al., *Essential protective roles of reactive astrocytes in traumatic brain injury*. *Brain*, 2006. **129**(Pt 10): p. 2761-72.
173. George, E.R., et al., *Failure of methylprednisolone to improve the outcome of spinal cord injuries*. *Am Surg*, 1995. **61**(8): p. 659-63; discussion 663-4.
174. Lee, H.C., et al., *Pitfalls in treatment of acute cervical spinal cord injury using high-dose methylprednisolone: a retrospect audit of 111 patients*. *Surg Neurol*, 2007. **68 Suppl 1**: p. S37-41; discussion S41-2.

175. Pointillart, V., et al., *Pharmacological therapy of spinal cord injury during the acute phase*. Spinal Cord, 2000. **38**(2): p. 71-6.
176. Bracken, M.B., *High dose methylprednisolone must be given for 24 or 48 hours after acute spinal cord injury*. Bmj, 2001. **322**(7290): p. 862-3.
177. Bracken, M.B., *Steroids for acute spinal cord injury*. Cochrane Database Syst Rev, 2012. **1**: p. Cd001046.
178. Kuchner, E.F., R.R. Hansebout, and H.M. Pappius, *Effects of dexamethasone and of local hypothermia on early and late tissue electrolyte changes in experimental spinal cord injury*. J Spinal Disord, 2000. **13**(5): p. 391-8.
179. Lewin, M.G., R.R. Hansebout, and H.M. Pappius, *Chemical characteristics of traumatic spinal cord edema in cats. Effects of steroids on potassium depletion*. J Neurosurg, 1974. **40**(1): p. 65-75.
180. Dorsett, Y. and T. Tuschl, *siRNAs: applications in functional genomics and potential as therapeutics*. Nat Rev Drug Discov, 2004. **3**(4): p. 318-29.
181. Reischl, D. and A. Zimmer, *Drug delivery of siRNA therapeutics: potentials and limits of nanosystems*. Nanomedicine, 2009. **5**(1): p. 8-20.
182. Kilic, E., et al., *Role of Nogo-A in neuronal survival in the reperfused ischemic brain*. J Cereb Blood Flow Metab, 2010. **30**(5): p. 969-984.
183. Otsuka, S., et al., *Delayed intrathecal delivery of RhoA siRNA to the contused spinal cord inhibits allodynia, preserves white matter, and increases serotonergic fiber growth*. J Neurotrauma, 2011. **28**(6): p. 1063-76.
184. Qu, Y., et al., *Silencing ephrinB3 improves functional recovery following spinal cord injury*. Mol Med Rep, 2014. **9**(5): p. 1761-6.
185. Ando, T., et al., *Photomechanical wave-driven delivery of siRNAs targeting intermediate filament proteins promotes functional recovery after spinal cord injury in rats*. PLoS One, 2012. **7**(12): p. e51744.
186. Tao, X., et al., *Role of telomerase reverse transcriptase in glial scar formation after spinal cord injury in rats*. Neurochem Res, 2013. **38**(9): p. 1914-20.
187. Wong, J.W.J., *Knocking Down Glycosaminoglycan Synthesis*. The Journal of Neuroscience, 2008. **28**(11): p. 2688-2689.

188. Lee, J.Y., et al., *Matrix Metalloproteinase-3 Promotes Early Blood-Spinal Cord Barrier Disruption and Hemorrhage and Impairs Long-Term Neurological Recovery after Spinal Cord Injury*. Am J Pathol, 2014.
189. Howard, K.A., et al., *RNA interference in vitro and in vivo using a novel chitosan/siRNA nanoparticle system*. Mol Ther, 2006. **14**(4): p. 476-84.
190. Koping-Hoggard, M., et al., *Chitosan as a nonviral gene delivery system. Structure-property relationships and characteristics compared with polyethylenimine in vitro and after lung administration in vivo*. Gene Ther, 2001. **8**(14): p. 1108-21.
191. Ruan, G.X., et al., *Hepatic-targeted gene delivery using cationic mannan vehicle*. Mol Pharm, 2014. **11**(10): p. 3322-9.
192. Ji, A.M., et al., *Functional gene silencing mediated by chitosan/siRNA nanocomplexes*. Nanotechnology, 2009. **20**(40): p. 405103.
193. Fernandes, J.C., et al., *Low molecular weight chitosan conjugated with folate for siRNA delivery in vitro: optimization studies*. Int J Nanomedicine, 2012. **7**: p. 5833-45.
194. Kong, F., et al., *Phosphorylatable short peptide conjugated low molecular weight chitosan for efficient siRNA delivery and target gene silencing*. Int J Pharm, 2012. **422**(1-2): p. 445-53.
195. Lee, J., et al., *T cell-specific siRNA delivery using antibody-conjugated chitosan nanoparticles*. Bioconjug Chem, 2012. **23**(6): p. 1174-80.
196. Howard, K.A., et al., *Chitosan/siRNA nanoparticle-mediated TNF-alpha knockdown in peritoneal macrophages for anti-inflammatory treatment in a murine arthritis model*. Mol Ther, 2009. **17**(1): p. 162-8.
197. Malmo J, et al., *Nanoparticle Mediated P-Glycoprotein Silencing for Improved Drug Delivery across the Blood-Brain Barrier: A siRNA-Chitosan Approach*. PLoS ONE, 2013. **8**(1): p. e54182.
198. Mittnacht, U., et al., *Chitosan/siRNA nanoparticles biofunctionalize nerve implants and enable neurite outgrowth*. Nano Lett, 2010. **10**(10): p. 3933-9.

199. Cho, Y., R. Shi, and R.B. Borgens, *Chitosan produces potent neuroprotection and physiological recovery following traumatic spinal cord injury*. J Exp Biol, 2010. **213**(9): p. 1513-1520.
200. Zhang, J., C. Tang, and C. Yin, *Galactosylated trimethyl chitosan-cysteine nanoparticles loaded with Map4k4 siRNA for targeting activated macrophages*. Biomaterials, 2013. **34**(14): p. 3667-77.
201. Gao, J.-Q., et al., *Gene-carried chitosan-linked-PEI induced high gene transfection efficiency with low toxicity and significant tumor-suppressive activity*. International Journal of Pharmaceutics, 2010. **387**(1–2): p. 286-294.
202. Gaspar, V.M., et al., *Biofunctionalized nanoparticles with pH-responsive and cell penetrating blocks for gene delivery*. Nanotechnology, 2013. **24**(27): p. 275101.
203. Dehousse, V., et al., *Comparison of chitosan/siRNA and trimethylchitosan/siRNA complexes behaviour in vitro*. Int J Biol Macromol, 2010. **46**(3): p. 342-9.
204. Katas, H. and H.O. Alpar, *Development and characterisation of chitosan nanoparticles for siRNA delivery*. Journal of Controlled Release, 2006. **115**(2): p. 216-225.
205. Sato, T. and Y. Matsuda, *Macromolecular Assemblies in Solution: Characterization by Light Scattering*. Polym. J, 2009. **41**(4): p. 241-251.
206. Andersen, M.O., et al., *Delivery of siRNA from lyophilized polymeric surfaces*. Biomaterials, 2008. **29**(4): p. 506-12.
207. Mao, H., et al., *Chitosan-DNA nanoparticles as gene carriers: synthesis, characterization and transfection efficiency*. J Controlled Release, 2001. **70**(3): p. 399-421.
208. Techaarpornkul, S., et al., *Chitosan-Mediated siRNA Delivery In Vitro: Effect of Polymer Molecular Weight, Concentration and Salt Forms*. AAPS PharmSciTech, 2010. **11**(1): p. 64-72.

209. Kim, T.H., et al., *Mannosylated chitosan nanoparticle-based cytokine gene therapy suppressed cancer growth in BALB/c mice bearing CT-26 carcinoma cells*. Mol Cancer Ther. , 2006. **5**(7): p. 1723-32.
210. Liu, X., et al., *The influence of polymeric properties on chitosan/siRNA nanoparticle formulation and gene silencing*. Biomaterials, 2007. **28**(6): p. 1280-8.
211. Malmo, J., et al., *siRNA delivery with chitosan nanoparticles: Molecular properties favoring efficient gene silencing*. J Control Release, 2012. **158**(2): p. 261-8.
212. Koping-Hoggard, M., et al., *Improved chitosan-mediated gene delivery based on easily dissociated chitosan polyplexes of highly defined chitosan oligomers*. Gene Ther, 2004. **11**(19): p. 1441-52.
213. Kigerl, K.A., et al., *Identification of two distinct macrophage subsets with divergent effects causing either neurotoxicity or regeneration in the injured mouse spinal cord*. J Neurosci, 2009. **29**(43): p. 13435-44.
214. Wu, A.C., et al., *Unraveling macrophage contributions to bone repair*. BoneKEy Rep, 2013. **2**.
215. David, S. and A. Kroner, *Repertoire of microglial and macrophage responses after spinal cord injury*. Nat Rev Neurosci, 2011. **12**(7): p. 388-99.
216. Kuo, H.-S., et al., *Acid Fibroblast Growth Factor and Peripheral Nerve Grafts Regulate Th2 Cytokine Expression, Macrophage Activation, Polyamine Synthesis, and Neurotrophin Expression in Transected Rat Spinal Cords*. The Journal of Neuroscience, 2011. **31**(11): p. 4137-4147.
217. Satake, K., et al., *Nitric oxide via macrophage iNOS induces apoptosis following traumatic spinal cord injury*. Brain Res Mol Brain Res, 2000. **85**(1-2): p. 114-22.
218. Shechter, R., et al., *Recruitment of Beneficial M2 Macrophages to Injured Spinal Cord Is Orchestrated by Remote Brain Choroid Plexus*. Immunity, 2013. **38**(3): p. 555-569.

219. Greenhalgh, A.D. and S. David, *Differences in the Phagocytic Response of Microglia and Peripheral Macrophages after Spinal Cord Injury and Its Effects on Cell Death*. The Journal of Neuroscience, 2014. **34**(18): p. 6316-6322.
220. Larson, S.D., et al., *Effectiveness of siRNA uptake in target tissues by various delivery methods*. Journal of Surgical Research, 2007. **137**(2): p. 189-190.
221. Luo, M.C., et al., *An efficient intrathecal delivery of small interfering RNA to the spinal cord and peripheral neurons*. Mol Pain, 2005. **1**: p. 29.
222. Santel, A., et al., *A novel siRNA-lipoplex technology for RNA interference in the mouse vascular endothelium*. Gene Ther, 2006. **13**(16): p. 1222-34.
223. Jain, S. and M.M. Amiji, *Macrophage-Targeted Nanoparticle Delivery Systems*, in *Multifunctional nanoparticles for drug delivery applications: imaging, targeting, and delivery nanoparticles for drug delivery applications: imaging, targeting, and delivery*.
224. Schäfer, V., et al., *Phagocytosis of nanoparticles by human immunodeficiency virus (HIV)-infected macrophages: a possibility for antiviral drug targeting*. Pharm Res, 1992. **9**(4): p. 541-546.
225. Ahsan, F., et al., *Targeting to macrophages: role of physicochemical properties of particulate carriers—liposomes and microspheres—on the phagocytosis by macrophages*. Journal of Controlled Release, 2002. **79**(1–3): p. 29-40.
226. Angyal, A., et al., *CD16/32-specific biotinylated 2.4G2 single-chain Fv complexed with avidin–FITC enhances FITC-specific humoral immune response in vivo in a CD16-dependent manner*. International Immunology, 2010. **22**(2): p. 71-80.
227. Ashraf, S.Q., et al., *Humanised IgG1 antibody variants targeting membrane-bound carcinoembryonic antigen by antibody-dependent cellular cytotoxicity and phagocytosis*. Br J Cancer, 2009. **101**(10): p. 1758-1768.

228. Munn, D.H., M. McBride, and N.K. Cheung, *Role of low-affinity Fc receptors in antibody-dependent tumor cell phagocytosis by human monocyte-derived macrophages*. *Cancer Res*, 1991. **51**(4): p. 1117-23.
229. Hirai, T., et al., *The prevalence and phenotype of activated microglia/macrophages within the spinal cord of the hyperostotic mouse (twy/twy) changes in response to chronic progressive spinal cord compression: implications for human cervical compressive myelopathy*. *PLoS One*, 2013. **8**(5): p. e64528.
230. Van Vuuren, A.J., et al., *CD64-directed immunotoxin inhibits arthritis in a novel CD64 transgenic rat model*. *J Immunol*, 2006. **176**(10): p. 5833-8.
231. Vogel, D.Y., et al., *Macrophages in inflammatory multiple sclerosis lesions have an intermediate activation status*. *Journal of Neuroinflammation*, 2013. **10**: p. 35-46.
232. Min, K.-J., et al., *Spatial and temporal correlation in progressive degeneration of neurons and astrocytes in contusion-induced spinal cord injury*. *Journal of Neuroinflammation*, 2012. **9**(1): p. 1-13.
233. Leidi, M., et al., *M2 macrophages phagocytose rituximab-opsonized leukemic targets more efficiently than m1 cells in vitro*. *J Immunol*, 2009. **182**(7): p. 4415-22.
234. Kim, S.S., et al., *Targeted delivery of siRNA to macrophages for anti-inflammatory treatment*. *Mol Ther*, 2010. **18**(5): p. 993-1001.
235. He, C., et al., *Multifunctional polymeric nanoparticles for oral delivery of TNF-alpha siRNA to macrophages*. *Biomaterials*, 2013. **34**(11): p. 2843-54.
236. Oliveira, M.I., et al., *Chitosan drives anti-inflammatory macrophage polarisation and pro-inflammatory dendritic cell stimulation*. *Eur Cell Mater*, 2012. **24**: p. 136-52; discussion 152-3.
237. Hwang, S.M., et al., *Chitinous materials inhibit nitric oxide production by activated RAW 264.7 macrophages*. *Biochem Biophys Res Commun*, 2000. **271**(1): p. 229-33.

238. Porporatto, C., et al., *Chitosan induces different l-arginine metabolic pathways in resting and inflammatory macrophages*. Biochemical and Biophysical Research Communications, 2003. **304**(2): p. 266-272.
239. Mori, T., et al., *Mechanism of macrophage activation by chitin derivatives*. J Vet Med Sci, 2005. **67**(1): p. 51-6.
240. Murray, P.J. and T.A. Wynn, *Protective and pathogenic functions of macrophage subsets*. Nat Rev Immunol, 2011. **11**(11): p. 723-37.
241. Guillelliams, M., et al., *The function of Fc[gamma] receptors in dendritic cells and macrophages*. Nat Rev Immunol, 2014. **14**(2): p. 94-108.
242. Rosales, C. and E. Uribe-Querol, *Fc receptors: Cell activators of antibody functions*. Advances in Bioscience and Biotechnology, 2013. **4**: p. 21-33.
243. Rey-Giraud, F., M. Hafner, and C.H. Ries, *In Vitro Generation of Monocyte-Derived Macrophages under Serum-Free Conditions Improves Their Tumor Promoting Functions*. PLoS ONE, 2012. **7**(8): e42656.
244. Shibata, Y., W.J. Metzger, and Q.N. Myrvik, *Chitin particle-induced cell-mediated immunity is inhibited by soluble mannan: mannose receptor-mediated phagocytosis initiates IL-12 production*. J Immunol, 1997. **159**(5): p. 2462-7.
245. Santegoets, K.C.M., et al., *Fc Gamma Receptor IIb on GM-CSF Macrophages Controls Immune Complex Mediated Inhibition of Inflammatory Signals*. PLoS ONE, 2014. **9**(10): e110966.
246. Huang, Z.Y., et al., *Differential kinase requirements in human and mouse Fc-gamma receptor phagocytosis and endocytosis*. J Leukoc Biol, 2006. **80**(6): p. 1553-62.
247. Lee, S., et al., *Solid polymeric microparticles enhance the delivery of siRNA to macrophages in vivo*. Nucleic Acids Res, 2009. **37**(22): p. e145.
248. Kirby, A.J. and P.W. Lancaster, *Structure and efficiency in intramolecular and enzymic catalysis. Catalysis of amide hydrolysis by the carboxy-group of substituted maleamic acids*. Journal of the Chemical Society, Perkin Transactions 2, 1972(9): p. 1206-1214.

249. Rozema, D.B., et al., *Endosomolysis by Masking of a Membrane-Active Agent (EMMA) for Cytoplasmic Release of Macromolecules*. *Bioconjugate Chemistry*, 2002. **14**(1): p. 51-57.
250. Wakefield, D.H., et al., *Membrane Activity and Transfection Ability of Amphipathic Polycations as a Function of Alkyl Group Size*. *Bioconjugate Chemistry*, 2005. **16**(5): p. 1204-1208.
251. McWhorter, F.Y., et al., *Modulation of macrophage phenotype by cell shape*. *Proceedings of the National Academy of Sciences*, 2013. **110**(43): p. 17253-17258.

VITA

VITA

Wen Gao was born and raised in Beijing, China. Wen completed her undergraduate in Xian International Studies University in 2006. After graduate, she was employed as Project Assistant for Exhibitions and Conventions. In 2009, She came to United State and pursue her study in science. She enrolled in the graduate program in Department of Basic Medical Sciences at Purdue University and joined to Dr. Richard Borgens lab in Center for Paralysis Research. Her research concentration is on nanotechnology and polymer science in drug delivery for spinal cord injury treatment. Up to this date, Wen is working together with her advisor and colleagues on several patent disclosures based on her research of interest. She expects to graduate at Purdue and earn her Ph.D degree in Basic Medical Science in December 2014.